Stellingen

1. Kennis van de vorm en het verloop van het stromingsprofiel van de continue fase is overbodig voor het bepalen van de scheidingsrendement van de separator wanneer de af te scheiden deeltjes een vaste daal- of stijgsnelheid t.o.v. de continue fase hebben.
(Dit proefschrift, appendix B)

2. Hoewel theoretisch het scheidingsrendement van plaatseparatoren met vlakke platen hoger is dan met gegolfde platen (dit proefschrift, paragraaf 3.3), zal in de praktijk de voorkeur uitgaan naar het gebruik van gegolfde platen (dit proefschrift, paragraaf 7.1.1).

3. De stelling van Mark P. Freeman* dat de Coriolis-kracht de scheiding van twee vloeistoffen nooit bevordert, is niet juist.
(Dit proefschrift, paragraaf 5.6)
* *In: G. Hetsroni, Handbook of Multi Phase Systems, pag. 9-105.*

4. Aangezien een centrifuge zowel delen heeft die een scheidende werking hebben als delen die een mengende werking hebben, kan niet voorspeld worden hoe de centrifuge zich gedraagt wanneer de eigenschappen van het te behandelen mengsel onbekend zijn.

5. Indien je vrouw secretaresse is van de vakgroep waarin je werkt, doe je meer administratief werk zelf om bij je collega's de indruk te vermijden dat je door deze situatie bevoordeeld wordt.

6. Indien racisten en politiek radicalen een vezelplaat zouden bestuderen, moeten ook zij kunnen bedenken dat een samenleving die uit uniforme, gelijkgerichte mensen bestaat snel uit elkaar valt.

7. Bij de regel over het minimum aantal personen dat in een auto moet zitten om over een carpoolstrook te mogen rijden, zou de bestuurder alleen meegerekend mogen worden indien deze niet louter chauffeur is.

8. Zodra een accu geïntroduceerd wordt die de prestaties van auto's met een elektromotor vergelijkbaar maakt met de prestaties van auto's met een benzinemotor, zullen de laatstgenoemde net zo snel van de markt verdrongen worden, als de langspeelplaat dat werd door de compact disk.

9. Gezien de functie van de 'bad-slipper' had men deze beter 'bad-gripper' kunnen noemen.

10. Als uiteindelijk alles onderzocht is, zal er gezocht worden naar het nog niet onderzochte op een manier zoals er nu gezocht wordt naar het perpetuum mobile.

11. De toevoeging van 'plat is prachtig' aan de spreuk 'small is beautiful' heeft voor mijn vrouw en mij meer betekenis dan beschreven door Otto van de Vijver in het NRC Handelsblad dd. 29-07-'93.

12. Door de toenemende drukte op de wegen zou het nuttig zijn landkaarten te maken waarbij de afstand op de kaart overeenkomt met de werkelijke reistijd, zogenaamde reistijdwegenkaarten, waardoor de kortste route op de kaart de snelste weg is. Doordat de drukte op de wegen varieert door o.a. de spitsuren, is het aan te bevelen een set reistijdwegenkaarten te maken, vergelijkbaar met de getijdenkaarten bij de scheepvaart.

Delft, 16 mei 1994 Robert Plat

TR diss
2371

Gravitational and centrifugal oil-water separators with plate pack internals

Gravitational and centrifugal oil-water separators with plate pack internals

PROEFSCHRIFT

ter verkrijging van de graad van doctor
aan de Technische Universiteit Delft,
op gezag van de Rector Magnificus, Prof. ir. K.F. Wakker,
in het openbaar te verdedigen ten overstaan van een commissie,
door het College van Dekanen aangewezen,
op maandag 16 mei 1994 te 13.30 uur

door

Robert PLAT

HBO-ingenieur petroleum- en gastechnologie

geboren te Bergen op Zoom

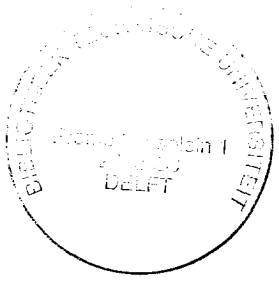

Dit proefschrift is goedgekeurd door de promotoren:
Prof.ir. J.J. van der Vuurst de Vries
Prof.dr.ir. J. de Graauw

en de toegevoegd promotor:
Dr.ir. W.M.G.T. van den Broek

Published and distributed by:

Delft University Press
Stevinweg 1
2628 CN Delft

Telephone +31 15.783254
Telefax +31 15.781661

CIP-DATA KONINKLIJKE BIBLIOTHEEK, DEN HAAG

Plat, Robert

Gravitational and centrifugal oil-water separators with plate pack internals / Robert Plat. - Delft : Delft University Press. - Ill.
Thesis Technische Universiteit Delft. - With ref. - With summary in Dutch.
ISBN 90-6275-985-8
NUGI 841
Subject headings: gravitational separators / centrifugal separators / waste water treatment.

© Copyright: Delft University of Technology

All rights reserved.
No part of the material protected by this copyright notice may be reproduced or utilized in any form or by any means, electronic or mechanical, including photo-copying, recording or by any information storage and retrieval system, without permission from the publisher.

Printed in The Netherlands

Voor Marijke

Voor mijn ouders en broer

The research described in this thesis was performed at the Dietz Laboratory of the Faculty of Mining and Petroleum Engineering, Delft University of Technology, Mijnbouwstraat 120, 2628 RX Delft, The Netherlands.

Parts of the research were supported by the special DUT fund for Ph.D. projects ('Onderzoekbeleidsruimte'), by Alfa Laval Industries, by Burgess-Manning Europe and by the Faculty of Mechanical Engineering & Marine Engineering.

Contents

1. Introduction

1.1	Scope for oily-water treatment	1
	1.1.1 Marine oil pollution	1
	1.1.2 Legislation	2
	1.1.3 Economical aspects	3
1.2	Oil-water mixtures	3
1.3	State of the art	4
	1.3.1 Category 1 separators	4
	1.3.2 Category 2 separators	6
	1.3.3 Comparison of the common separators	7
1.4	Areas of interest	10
1.5	Scope of the present study	10
1.6	Outline of the thesis	11
	References	11

2. The effect of gravity and centrifugal forces on the behaviour of oil droplets in water

2.1	Introduction	13
2.2	Shape regimes for droplets in free motion	14
2.3	Gravitational forces	16
2.4	Centrifugal forces	16
2.5	Coriolis forces	17
2.6	Shear forces and droplet rotation	18
2.7	Brownian motion	20
2.8	Particle-interface coalescence	22
2.9	Particle-particle coalescence	25
2.10	Break-up of droplets	25
2.11	Electrical effects	27
2.12	Discussion and conclusions	27
	References	28

3. Gravity oil-water plate separators

3.1	Introduction	31
3.2	The path of an oil droplet in water	32
	3.2.1 Horizontal skimmer separator (settling tank)	32
	3.2.2 Plate separators with flat plates	34

3.2.3 Flow velocity profiles 35
3.2.4 Separation efficiency and particle size 37
3.3 Plate separators with corrugated plates 42
3.4 Inclination of plate packs 46
3.5 Oil concentration and particle size 47
3.6 Discussion and conclusions 48
References 48

4. Gravity plate separators: numerical simulations and laboratory experiments
4.1 Introduction 49
4.2 Numerical simulations 49
4.2.1 Flow profiles 49
4.2.2 Separation efficiency 50
4.3 Experimental verification 54
4.3.1 Introduction 54
4.3.2 Flow velocity profiles 55
4.3.3 Oil-water separation efficiency experiments 57
4.4 Conclusions 63
References 63

5. Plate packs for rotating separators
5.1 Introduction 65
5.2 Centrifugation 66
5.3 The parallel plate centrifuge and the parallel channel centrifuge 68
5.4 Characteristics of plate packed centrifuges 70
5.4.1 Dimensions of the parallel plate centrifuge and the parallel channel centrifuge 70
5.4.2 Channel shape of a parallel plate centrifuge (PPC) 72
5.4.3 Channel shape of a parallel channel centrifuge (PCC) 74
5.5 Hydrodynamic aspects of plate packed centrifuges 74
5.5.1 Path and velocity of an oil droplet 74
5.5.2 Flow velocity and residence time of the continuous phase 76
5.6 Direction of rotation 78
5.7 Separation efficiency 79
5.8 Bending of the plates 80
References 80

6. Simulations and experiments with plate packed centrifuges
6.1 Introduction 81
6.2 Numerical simulations 81
6.2.1 Simulation programs for the PPC and the PCC 81
6.2.2 The model 82
6.2.3 Results of the PPC and PCC simulations 88
6.3 Experimental verification 94
6.4 Conclusions 102

7. Discussion and conclusions

7.1 Evaluation of the experiments 103
7.1.1 Estimation of the dominant mechanisms 103
7.1.2 Plate pack dimensions 108
7.1.3 Uneven flow distribution 111
7.1.4 Separation outside the pack of plates 111
7.1.5 Measurement inaccuracies 112
7.2 Conclusions 113
References 115

Appendix A Derivation of the terminal rising velocity 119

Appendix B Derivation of the general separation efficiency function 121

Appendix C Experimental set-up 125
C.1 In-line oil-water mixing 125
C.2 In-line droplet size measurement 126

Appendix D The disc stacked centrifuge 129
D.1 Principles 129
D.2 Experimental 131

Appendix E Results of the simulations with plate packed centrifuges 133

List of symbols 151

Summary 155

Samenvatting 157

Nawoord 159

Curriculum vitae 161

Chapter 1

Introduction

1.1 Scope for oily-water treatment

1.1.1 Marine oil pollution

Discharge of oily water into the environment results in oil contamination of the soil, ground water, surface waters, rivers and seas. Lighter oil fractions may evaporate and contaminate the atmosphere. To protect the environment, the total amount of oil discharged must be kept to a minimum. The source of marine oil pollution can roughly be divided into four categories [3]:

- The atmosphere: caused by incomplete combustion of fossil fuels. This is a very diffuse source and can be controlled by modification of combustion installations and the use of catalytic converters.

- Land run-off: spillage on land and inland waters, discharged into the sea via rivers and dumping of harbour sludge.

- Shipping: caused by the discharge of ballast and tank cleaning water and bilge water.

- The offshore industry: caused by the discharge of water produced together with oil and gas and of drill cuttings covered with oil-based mud.

These sources do not include accidental spills and unauthorized discharges.

It is not easy to determine the dose/effect relationship of the various types of oil contamination under different conditions and in a wide range of ecosystems present in the North Sea. Different oil types vary in chemical composition and potential toxicity. Aromatic compounds which are soluble are presumed to be the most toxic oil compounds [3]. Although environmental aspects of oily waste water discharges from offshore installations have been dealt with in many reports, the total effect of this source of pollution is hard to determine. It is not always clear which part of the oil pollution is caused by the discharge of waste water and which part by the discharge of oil-contaminated solids, i.e. drill cuttings with oil-based mud.

After treatment, production water and other oily waste water is discharged into the sea. A part of the oil still present in the discharged water rises to the surface and forms slicks.

Another part stays in the water column and a part is adsorbed by solids in the water column and eventually sinks to the seabed.

The amount of oil remaining in the water column is rapidly diluted and because of the small size of the droplets, this oil is readily accessible for biological degradation. Biodegradation is the main factor in the breakdown of oil in the water column. As crude oil is a natural material which enters the sea in many parts of the world from natural seeps in the seabed, micro organisms have developed which can break it down. Biodegradation can only take place at the oil-water interface. It is a slow process which depends on the type of oil, the temperature and the oxygen available. When enough oxygen is present, 0.5 grams oil per m^2 oil-water interface can be oxidised per day by bacteria [2]. Rising oil droplets and emulsified oil in the water column hardly have any toxic effects because they are rapidly diluted and degraded. As long as the oil concentration is lower than 0.1 g/m^3 ($\approx$0.1 ppm) and the oil is weathered, most organisms can co-exist with hydrocarbons [4].

The oil adhering to suspended solids settles on the seabed. Most of the oil then stays locked into the sediments, with only a small portion, approximately 5% [2], accessible for dispersion. For this reason the effects can be compared with the effects caused by the discharge of solids contaminated with oil. Oil present in sediments will degrade only slowly. Effects caused by this type of oil accumulation are generally confined to an area within 500 m of a platform, depending on the characteristics of the oil, the oceanographic conditions of the area and the total amount of discharged waste water.

Apart from free, emulsified and dispersed oil, (treated) waste water also contains dissolved hydrocarbons, such as polycyclic aromatics. These can accumulate in living organisms and cause diseases.

1.1.2 Legislation

Legislation with regard to the discharge of oil into the sea is currently being pursued in an international context. For the oil industry, the most important convention for their offshore activities is the Paris Convention, covering regulations for discharges from both offshore and onshore operations in and around the North Sea. The Paris Convention for the 'Prevention of Marine Pollution from Land Based Sources' seeks to control pollution from all countries bordering the North East Atlantic Ocean.

An important aspect of the Paris Convention is that for the discharge of oily water from platforms a limit of 40 ppm monthly average has been agreed. Regular monitoring of the water discharge from the platform has to be carried out by the operator; at less frequent intervals visits are made and samples taken by government inspectors. Monitoring of sea water and the sea-bed around the major platforms to a distance of some kilometres away is carried out by government marine research laboratories.

1.1.3 Economical aspects

Research into more efficient de-oiling techniques contributes to reduced pollution by oil. From a practical point of view the offshore industry sets certain specifications for de-oiling equipment. Because of the limited load and deck space of a platform, it has to be compact and relatively light. The equipment must be able to de-oil large volumes of water without becoming clogged and with a minimum amount of maintenance. Depleting oil and gas reservoirs cause increasing production of water, requiring higher separator capacities. Produced water can be re-injected into the reservoir. Obviously, re-injected oily water does not contribute to pollution, but still needs to be de-oiled to prevent plugging of the reservoir pores near the injection well.

1.2 Oil-water mixtures

Oil can be present in waste water as a segregated phase, or in solution. Free oil readily rises to the surface to form slicks. Oil-water mixtures may be true solutions, emulsions, or dispersions. The major difference between solutions and dispersions and/or emulsions is that in case of a solution only one liquid phase exists, whereas dispersions and emulsions are made up of two immiscible phases, one existing in the form of droplets distributed throughout the other phase.

A dispersion is thermodynamically unstable and, if left alone, will in time separate into two liquid layers (oil and water). The separation is brought about by oil droplets coming into contact with each other due to the density difference between the two liquid phases and differences in the velocity of upward movement, followed by coalescence. This process continues until the two phases are completely separated into two layers arranged in accordance with the densities of the liquids. Each layer will be a solution containing a very small amount of the other phase.

An emulsion is a heterogeneous two-phase mixture but, in this case, coalescence of the dispersed (droplet) phase is suppressed, usually by the presence of a third component; an emulsifying agent. Thus, the mixture is stabilized and gravity separation does not take place. The system is only quasi-stable, because some inter-droplet coalescence does take place. However, this proceeds so slow that for practical purposes the mixture may be considered stable. The oil only separates when the emulsifying agent has been de-activated or broken down due to oxidation, thermal decomposition or by the action of a demulsifier. Under these conditions the emulsion will convert into an oil-in-water dispersion and then separates.

In practice, when oil and water are mixed, oil droplets are formed in a range of sizes. These may span a wide range from one to several hundreds of microns. It is obvious that not all droplets in the original mixture behave in the same way and that it may take a long time before all droplets have coalesced again. It is common practice to define dispersions that readily separate as *primary dispersions*, and those with fine droplets and long separation

times as *secondary dispersions*. The distinction between primary and secondary dispersions is therefore made on droplet size and separation behaviour.

1.3 State of the art

The removal of oil from water can be based on different principles, for each of which many types of equipment are currently available. The simplest processes are based on gravity separation, but highly complex ones also exist. Oil-water separators can be divided into two main categories:

- Category 1: comprises separators which are able to remove free oil, dispersed oil and part of the emulsified oil. Due to density differences between oil and water, the oil droplets rise to the surface. The rising velocity of a small oil droplet is proportional to the square of its diameter. The driving force can be either gravitational or centrifugal.

- Category 2: comprises separators which are also able to remove dissolved oil. Working principles of separators of this category are based on micro filtration, adsorption, extraction, and (bio-)chemical decomposition.

1.3.1 Category 1 separators

On oil and gas platforms the most frequently used separators of category 1 are:

- skimmer tanks,
- plate separators,
- flotation units,
- hydrocyclones,
- centrifuges.

1.3.1.1 The skimmer tank

The skimmer tank is the simplest and most frequently used separator and it is often applied for pre-treatment. Separation takes place on account of the density difference between oil and water. Between the floating oil layer and the water an emulsion layer can be present. The floating oil is skimmed off the surface.

A skimmer tank is relatively cheap and provides a simple way to remove free oil and, if the residence time is long enough, part of the dispersed oil, too. Disadvantages are:

- long residence time required,

- large vessel dimensions,
- heavy weight of the vessel.

The separation efficiency is determined by the surface area and not by the height of the tank.

1.3.1.2 The plate separator

A plate separator consists of a tank or vessel with a pack of parallel equidistant plates through which the oily water is led. The rising oil droplets coalesce on the underside of the plates where they can slip through oil flow channels and rise to the surface. To enhance the removal of the collected oil, the pack of plates is usually placed at an angle with the horizontal. This prevents an oil build-up between the plates. The plate separator is more compact compared to the skimmer tank and is therefore important for the offshore industry. Free oil and primary dispersions can easily be treated. The plates can either be flat or corrugated and can be made of polyester, teflon or stainless steel, depending on the specific purpose. Polyester plates are the cheapest, but a high aromatics content and high operating pressures can affect this material.

1.3.1.3 The flotation unit

Flotation is based on the injection of fine gas bubbles into the oily water (e.g. air, nitrogen or natural gas) to which oil droplets adhere. Due to the resulting reduced density and increased diameter, the oil droplets with adhering gas bubbles will rise more readily to the surface. The process of flotation consists of four basic steps [7]:

- bubble generation in oily water,
- contact between a gas bubble and an oil droplet,
- attachment of the oil droplet to the gas bubble,
- rising of the gas-oil combination to the surface where it can be removed by skimming.

There are four common methods of bubble generation:

- the dissolution of gas from a supersaturated solution (dissolved-gas flotation),
- mechanical mixing of gas and liquid (dispersed-gas flotation),
- direct gas injection by means of a sparger (induced-gas flotation),
- gas generation by electrolysis (electro-flotation).

The method of bubble generation is important. It determines the bubble size. Decrease of the bubble size increases the removal efficiency, because the surface activity of bubbles increases as the bubble size decreases.

Since both oil and gas are less dense than water, they both tend to rise to the surface. Gas bubbles are generally larger than oil droplets (usually larger than 100 microns in the case of dispersed gas flotation and 50 microns for dissolved gas flotation, while dispersed oil droplets in waste water are usually smaller than 30 microns) and the density difference between gas

and water is much larger than between oil and water. Therefore, gas bubbles rise more rapidly than oil droplets and overtake them. This leads to the possibility of bubble-droplet contact. The contact efficiency is determined by the design of the separator and the characteristics of the waste water. In a dissolved-gas flotation unit bubble-droplet contact can also occur when oil droplets act as nuclei for the generation of gas bubbles from solution.

Oil droplets with a minimum size of 10 to 15 microns can be removed by gas flotation. This method is often used for very dilute dispersions for which gravity settling is not efficient. Separation can be improved by the use of demulsifiers, poly-electrolytes and flocculation agents.

1.3.1.4 The hydrocyclone

In a hydrocyclone separation is achieved by generating centrifugal forces that are orders of magnitude higher than the forces available in conventional gravity-based separation equipment. The waste water is forced into circular motion by tangential injection of the liquid into the cylindrical or funnel-shaped hydrocyclone. The lighter oil droplets are forced towards the central core. The coalesced oil droplets are removed through a narrow orifice in the centre of the inlet head. The water leaves the hydrocyclone as a continuous phase from the downstream end.

Advantages of a hydrocyclone are that it is a relatively small and light separator and that this separation method is practically insensitive to platform motion. However, sometimes after-treatment is needed to obtain a sufficiently low oil concentration.

1.3.1.5 The centrifuge

A centrifuge consists of a mechanically driven rotating bowl in which the oily water is accelerated and subsequently separated into an oil and a water phase. As centrifugal forces can be several thousands times larger than the gravitational force, the separation velocity of the droplets is much higher. Very efficient and effective separation can be achieved. Residence times are in the order of one second. Centrifuges are often provided with internals. These internals prevent turbulence and increase the effective surface area. They have the same function as the plates of a plate separator [5]. Usually, these internals consist of a stack of conical discs. A novel type of internal, the *parallel plate pack*, is proposed in this thesis.

1.3.2 Category 2 separators

On oil and gas platforms the most frequently used category 2 separators are coalescers and membrane filters. Some other category 2 separators are active carbon adsorption units, freon extraction units and biological treaters. These are seldom applied on oil and gas platforms. We will therefore limit ourselves to some remarks on coalescers and membrane filters.

1.3.2.1 The coalescer

The coalescer consists of a vessel with a bed of porous material or a screen. The porous material often consists of glass fibres or sand. For the material of the bed, a large surface-area to bulk-volume ratio is required to allow the dispersed oil to coalesce. Hence, the porous material acts as a converter, causing smaller droplets to coalesce and form larger droplets. Separation takes place in a settling zone downstream of the bed.

A coalescer is a simple and compact separator. However, depending on the waste water characteristics clogging can occur.

1.3.2.2 The membrane filter unit

For this type of separation a membrane is used as a filter medium. Membrane filtration can be divided into three groups, depending on the pore size of the membrane [9]:

- reversed osmosis: 0.0001 to 0.01 μm,
- ultra filtration: 0.001 to 0.1 μm,
- micro filtration: 0.05 to 4 μm.

For separation of oil-in-water emulsions, micro filtration is the most suitable method [9]. The pore size of the micro filtration membrane allows only water molecules and dissolved particles to pass.

Membrane filter modules may consist of flat membranes, spirally wound membranes or tubular membranes. A special type of the tubular membrane is the hollow fibre. The tubular type is best suited for treating large amounts of oily waste water, because the membrane surface can be cleaned more easily.

Pre-treatment is not strictly necessary. If the waste water has a high solids concentration, it is advisable to place a coarse filter at the inlet. Free, dispersed and part of the emulsified oil can easily be removed by this type of separator. A membrane filter unit is compact and relatively light. A disadvantage is that membranes need to be replaced quite often, depending on the waste water characteristics. Regular maintenance is required.

1.3.3 Comparison of the common separators

All category 1 separators are based on the equation for the rising velocity of oil-droplets derived from Stokes' law [6]:

$$v_t = \frac{\Delta\rho \; g \; D^2}{18 \; \mu} \qquad \textbf{(1-1)}$$

where v_t is the rise velocity,
$\Delta\rho$ is the density difference between oil and water,

g is the gravitational acceleration (≈ 9.81 m/s^2),
D is the diameter of the oil droplet,
μ is the dynamic viscosity of water.

In the case of centrifugal forces, g should be replaced by $a = \omega^2 r$, where ω is the angular velocity and r is the distance from the axis of rotation. In a centrifuge, a can be up to 10,000 times g, resulting in a corresponding increase of v_t.

In a flotation unit, the effective difference between the densities of the droplet-bubble combination and water ($\Delta\rho_e$), as well as the effective diameter of the droplet-bubble combination D_e, are increased.

The separator surface area A (perpendicular to the direction of g or a) is one of the most important parameters determining the separation efficiency. The plates of a plate separator and the internals of a centrifuge are designed to increase the effective surface area (A_e).

	$\Delta\rho_e/\Delta\rho$	a/g	D_e/D	A_e/A
Skimmer tank	1	(1)	1	1
Plate separator	1	(1)	1	10 - 100
Flotation unit	2 - 20	(1)	2 - 10	1
Coalescer	1	(1)	10 - 1,000	1
Hydrocyclone	1	100 - 1,000	1	1
Centrifuge	1	1,000 - 10,000	1	5 - 20

Table (1-1) Six separators most frequently used in the oil field and the relative magnitude of their characteristic parameters (approximate values).

Table (1-1) gives a summary of the common separators and the relative magnitude of the characteristic parameters. The viscosity of water μ can only be decreased by increasing the temperature of the water. This results in an increase of v_t; higher temperatures can also lead to more unstable emulsions.

Table (1-2) gives some characteristics of five of the most frequently used separators; all data relate to a capacity of 120 m^3 per hour. The skimmer tank is left out because this separator is only used for pre-treatment. Relevant data about the (porous-media) coalescer could not be obtained. In the table, D_c is the critical (oil) droplet diameter (also called *cut-off diameter*), which is the maximum diameter of the droplets present in the separator's effluent. Droplets larger than D_c will be removed. C_{out} is the expected oil-concentration in the effluent.

	Plate Separator	Flotation Unit	Hydro-cyclone	Centrifuge	Membrane Filter
Required Deck Space [m^2]	13.5	20	8	10	9
Weight [tonnes]	40	38	9	8	13
Pre-treatment Required	no	no	no	no	yes
After-treatment Required	(yes)	(yes)	(yes)	no	no
D_c [μm]	30 - 50	20 - 30	15 - 25	1 - 3	< 1
C_{out} [ppm]	30 - 100	20 - 80	20 - 70	< 10	< 10
Costs [kUS$]	200	250	400	1900	2500
Source	Skimovex	Skimovex	Vortoil	Alfa Laval	[8]

Table (1-2) Comparison of five separators for 120 m^3 per hour ($\approx$ 18,000 bbl/day)

It is clear that, although a plate separator and a flotation unit are both relatively cheap compared to the rest, they are both heavy and bulky and cannot always reach the target of 40 ppm, set by the Paris Convention.

A hydrocyclone is more expensive than a flotation unit or a plate separator, but performs better. The use of demulsifiers and after-treatment is sometimes necessary to obtain an acceptable degree of separation. A hydrocyclone requires far less deck space than the other four separators and is also the lightest.

From table (1-2) it can be seen that performance and costs are proportional to a certain extent. The membrane filter unit and the centrifuge both give very good performance -less than 10 ppm oil in the treated water- but they are both far more expensive than the other separators. Pre-treatment is not required, although it is advisable to use a coarse filter upstream of the membrane unit. Such a filter is often built-in in this unit.

It should be noted that the costs given in this table are the costs of the equipment only. The costs for installation, operation and maintenance vary considerably. For example, for a flotation unit weekly maintenance is required, while a centrifuge needs maintenance only about four times a year (total cost for 1 year: $ 12500). How often filter membranes need to be replaced depends on the waste water characteristics. Besides replacement of the membranes, cleaning is required. A plate separator needs to be cleaned only twice a year. For a complete cost comparison, information is required about oily-water characteristics,

throughput, available (deck) space, maximum deck load and location.

From table (1-2) it is clear that the centrifuge and the membrane filter unit are among the best separators. They can meet the Paris Convention requirements, give good performance, and are quite light. The main disadvantage of the centrifuge is its price. The main disadvantage of the membrane filter unit is - apart from the cost - the frequent occurrence of clogging.

1.4 Areas of interest

Plate separators are among the most applied separator types in the oil industry. Numerous types of different manufacturers are on the market today. A number of different plate shapes is available, from simply flat to complicated corrugated structures. From the vast body of available literature on the subject, a few aspects attract attention about plate separators. Firstly, the relation between separation efficiency and plate shape is not clear. Secondly, there appears to be a critical value for the droplet diameter, whereby smaller droplets cannot be separated at all by a plate separator. The phenomenon 'Brownian motion' is said to be the cause of that. However, consistent values were not given.

In contrast with plate separators, centrifuges are less frequently used for oily-water treatment. This is not only because of their relatively high costs but also because sometimes problems occur, resulting in an unsatisfactory separation efficiency, probably due to break-up of oil-droplets and/or oil build-up in the flow distributor of the centrifuge.

The configuration of the internals is of major importance for the separation performance. The position of the oil-water interface is also crucial: many problems are due to its improper adjustment. The position of this interface depends on the densities of oil and water and on the flow-rate. While the densities of the two phases generally do not vary much, the flow-rate sometimes does, causing a drastic decrease of the separation efficiency. Some types are provided with a system to control the back pressure of one or both of the outlets, thereby improving this situation to some extent.

1.5 Scope of the present study

The purpose of this study is to investigate existing plate packs for both gravitational and centrifugal separators by modelling and experimentation, with the aim of determining an optimum configuration. A generally applicable separation efficiency function has been derived which is valid for gravity separators as well as centrifuges. For gravity plate separators, a pack of corrugated plates does not appear to give a better performance than a comparable pack of flat plates. For centrifugal separators, performance of the type that

employs a pack of fan-shaped plates proved to be superior to those with a stack of conical discs.

1.6 Outline of the thesis

Chapter 2 gives an overview of the mechanisms that control the behaviour of oil droplets in water in a gravitational or a centrifugal field. For each mechanism an attempt has been made to determine its effect.

Chapter 3 deals with the theoretical performance of different gravity plate separators. The path of an oil droplet in water flowing between two plates has been determined for plug flow as well as parabolic flow profiles. The separation efficiency as a function of droplet size is derived for all laminar flow profiles.

Chapter 4 gives results of simulations and experiments with gravity plate separators for the purpose of verifying the theory discussed in chapter 2.

Chapter 5 introduces the basics of centrifugal separators. Subsequently the plate pack centrifuge is described. Equations for modelling the pack, the flow and the droplet path are given.

Chapter 6 shows results of simulations and experiments with plate pack centrifuges. Although the theory developed in chapter 5 does not cover all facets of the process, the results of the experiments indicate that actual performance can be predicted fairly accurately.

The thesis ends with a discussion of the results obtained and a list of conclusions in chapter 7.

References

[1] Berg, P.Y. van den: Modification design for a disc stacked centrifuge for the treatment of oily water, graduation report for College for petroleum and gas technology, Marine environmental sciences, Den Helder, carried out at Delft university of technology, Faculty of mining and petroleum engineering, April 1990.

[2] E&P Forum: Submission on the North Sea of offshore oil and gas industry, The international conference on the protection of the North Sea, june 1984, Bremen.

[3] Kuiper, J.: Effects of oil pollution in the North Sea, North Sea Monitoring 88.3, November 1988.

[4] Milne, K. and Greene, G.: An evaluation of the performance and costs of waste water treatment technologies for offshore oil and gas production, Environmental Protection Service, july 1985, Ottawa.

[5] Plat, R. and Broek, W.M.G.T. van den: New centrifuge design leads to more efficient de-oiling of produced water, In: Weijnen, M.P.C. and Drinkenburg, A.A.H. (eds.), Precision process technology, Kluwer Academic Publishers, 1993.

[6] Plat, R. and Broek, W.M.G.T. van den: New plate pack design leads to increased separation efficient of a centrifuge, Paper presented at the 66th Annual Technical Conference of the Society of Petroleum Engineers, Dallas, October 1991.

[7] Plat, R. and Broek, W.M.G.T. van den: Towards more compact and efficient de-oiling equipment, Paper presented at the 22th Annual Offshore Technology Conference of the Society of Petroleum Engineers, Houston, May 1990.

[8] Workshop: Energiebesparing met membranen, NOVEM bv., Utrecht, March 11th, 1993.

[9] Workshop: Industriële besparingstechnologieën, Ministerie v. Economische Zaken, June 25th, 1993.

Chapter 2

The effect of gravity and centrifugal forces on the behaviour of oil droplets in water

2.1 Introduction

The basic function of all oil-water separators is to force the dispersed droplets, which are present in the continuous phase, to move to an interface. Usually, this interface is the boundary between the continuous phase and a phase with the same composition as the droplets. The latter is often called the droplets' bulk phase. When a droplet moves towards the interface and makes contact with it, a film of the continuous phase will initially keep the droplet separated from its bulk phase. Then, when rupture of the film takes place, the contents of the droplet is transferred into its bulk phase. The process of forming and rupturing of the film and the transfer of the contents of the droplet into its bulk phase is called coalescence. A droplet is separated from the continuous phase when it is completely coalesced.

Consequently, separation can be divided into two main processes. Firstly, the process of moving of dispersed droplets towards the interface and, secondly, the process of coalescence. The way these processes take place is influenced by different forces acting on the two phases and by the physical properties of these phases.

This chapter describes factors which can influence one or both processes. Firstly, the shapes of droplets under various circumstances are considered. Subsequently, different forces which may act on the dispersed or continuous phase are discussed. Finally, interfacial phenomena are described. Where possible, an attempt is made to determine the relative importance of the different factors for gravity and centrifugal separation, respectively.

Most of the theory described in this chapter is valid for any immiscible liquid-liquid mixture. This thesis, however, deals particularly with de-oiling of waste and production water with oil concentrations below 2000 ppm (1 ppm $\approx 10^{-3}$ kg/m^3). Therefore water is assumed to be the continuous phase, while oil is the dispersed part of the mixture. Droplet sizes are always given as diameters of spherical droplets.

2.2 Shape regimes for droplets in free motion

The shapes of droplets rising or falling freely in an infinite medium under the influence of gravity are generally grouped under the following three categories [8]:

1. Spherical,
2. Ellipsoidal,
3. Spherical-cap/ ellipsoidal-cap.

The shape of a droplet depends on the ratio between inertia and viscous forces (Reynolds number) and on the ratio between gravity and interfacial forces (Eötvös number). Clift et al. [8] mapped the three categories (or regimes) by plotting the droplet Reynolds number,

$$Re = \frac{\rho D_e v_t}{\mu} \tag{2-1}$$

versus the Eötvös number,

$$Eo = \frac{g \Delta\rho D_e^2}{\sigma} \tag{2-2}$$

with a fluid property group, the Morton number,

$$M = \frac{g \mu^4 |\Delta\rho|}{\rho^2 \sigma^3} \tag{2-3}$$

as parameter [8, 10]. Here, v_t is the terminal rising or falling velocity of the droplet, which is discussed later. D_e is the equivalent diameter, or the diameter of a sphere with equal volume V $\{D_e = (6V/\pi)^{1/3}\}$. Unsubscripted symbols refer to properties of the continuous phase. The regime map given by Clift et al. [8] is shown in figure (2-1). Each liquid-liquid (or gas-liquid) system corresponds to a distinct value of M. Droplets and bubbles are spherical if either interfacial forces or viscous forces are dominant over gravity and inertia forces.

In a gravitational field at 20°C in water, a 500 μm oil droplet (ρ_o=900 kg/m^3, σ=0.01 N/m) will have Re=6.81 and Eo=2.45 10^{-2}. Hence, according to figure (2-1) the shape of this droplet can be considered spherical. Droplets smaller than 500 μm have lower values of Re and Eo and can also be considered to be spherical. Droplets substantially larger than 500 μm will deform. Generally, oil droplets in water and in a gravitational field which are larger than 500 to 1500 μm (depending on temperature, densities and interfacial tension), will not be spherical.

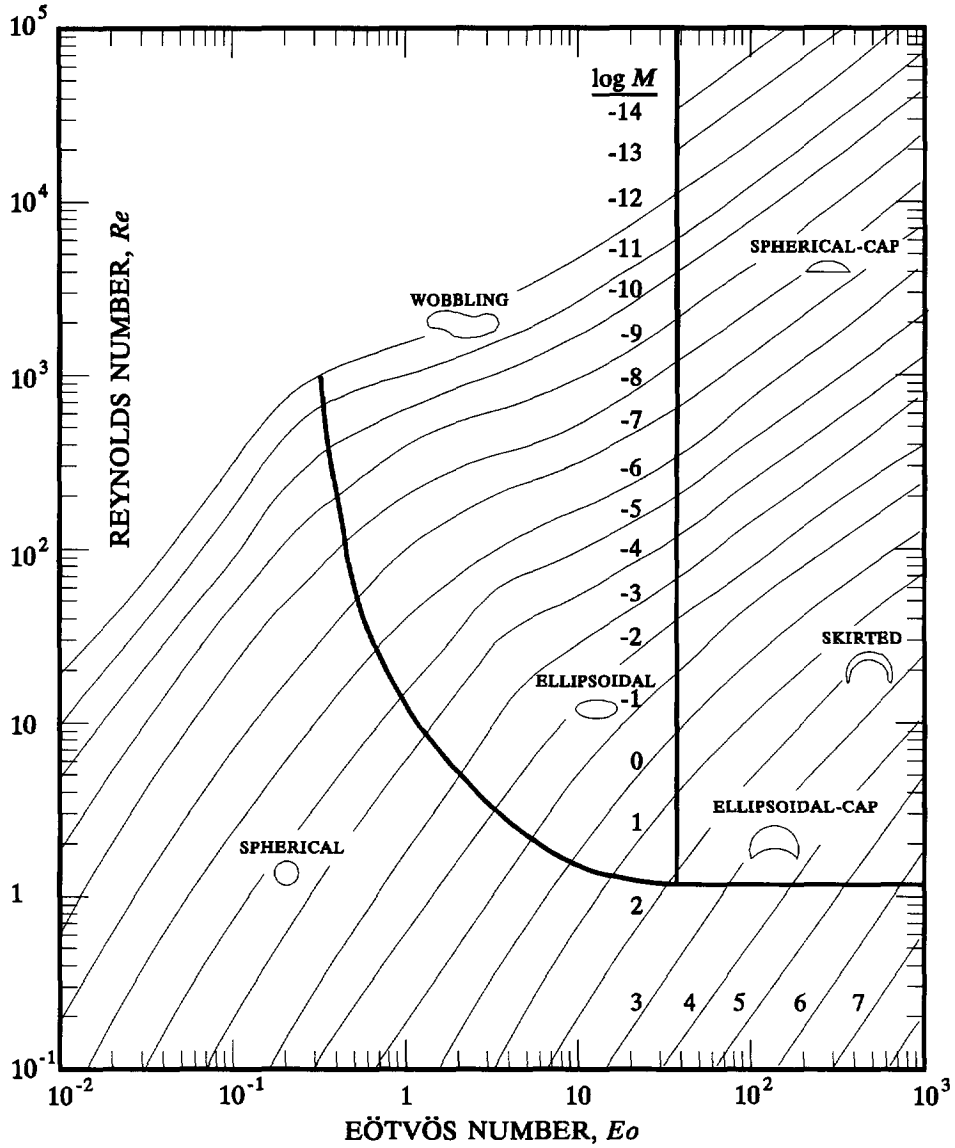

Figure (2-1) Shape regimes for bubbles and drops in unhindered gravitational motion through liquids. From: Clift, Grace and Weber: Bubbles, drops and particles, 1978.

A similar analysis can be made for droplets in a centrifugal force field. In centrifugal oil-water separators the acceleration field due to rotation is approximately 5000 times the acceleration of gravity. In centrifuges, droplets smaller than 20 to 60 μm can be considered spherical.

2.3 Gravitational forces

Gravitational forces cause a droplet of oil in water to rise to some interface where the oil can be collected. A free droplet will move by a buoyant force:

$$F_b = \frac{\pi}{6} D^3 (\rho_w - \rho_o) g \tag{2-4}$$

This motion gives rise to a resistance force. For $Re < 0.3$ [10] this force is, according to Stokes' law:

$$F_S = 3 \pi \mu v D \tag{2-5}$$

The droplet accelerates due to F_b. Hence, v increases until F_b balances F_S, from which point the droplet has a constant velocity, called the terminal rising (or falling) velocity v_t. Appendix A gives the derivation of the rising velocity as a function of time as well as the terminal rising velocity. According to equation (2A-7) a 200 μm oil droplet (ρ_o=900 kg/m^3), at 20°C in water, will have a velocity of 0.99 v_t after about 0.01 second (for any value of g). Thus, the terminal rising velocity is attained practically instantaneously for droplets smaller than 200 μm in either gravity separators or centrifuges. For oil droplets in water v_t is given by:

$$v_t = \frac{(\rho_w - \rho_o) g D^2}{18 \mu} \tag{2-6}$$

This equation is only valid for rigid spheres. The terminal velocities of clean liquid droplets are somewhat higher, due to internal circulation within the droplets [8]. On the other hand, surface contaminants reduce internal circulation [8]. According to Warshay et al. [18], droplet terminal velocities can be calculated with reasonable accuracy from the rigid-sphere equations for Reynolds numbers up to 10.

2.4 Centrifugal forces

Also centrifugal forces can be used to accelerate the droplets. The acceleration of gravity, g, is constant. The acceleration in a centrifugal field is not constant. It is given by:

$$a_c = \omega^2 r \tag{2-7}$$

Note that since a_c is acting in the direction of r and is a function of r, the droplets never achieve a true terminal velocity. In practice, however, for sufficiently small droplets the

droplet velocity is close to the value of the local terminal velocity.

The buoyant force on an oil droplet in water in a centrifugal force field is:

$$F_b = \frac{\pi}{6} D^3 (\rho_w - \rho_o) a_c \qquad (2\text{-}8)$$

while the drag force corresponds to equation (2-5). This yields for the terminal radial velocity in a centrifugal field:

$$v_{tr} = \frac{(\rho_w - \rho_o) \omega^2 r D^2}{18 \mu} \qquad (2\text{-}9)$$

which is directed towards, and is perpendicular to, the axis of rotation.

Instead of centrifugal acceleration, the term *g*-factor is often used. The *g*-factor is defined as a multiple of the acceleration of gravity. With the centrifugal acceleration of $\omega^2 r$, the *g*-factor G is given by:

$$G = \frac{\omega^2 r}{g} \qquad (2\text{-}10)$$

The *g*-factor for a centrifuge, as used in the chemical and oil industry, can be up to 10000 (or even larger); v_{tr} can therefore also be 10000 times as large as in a gravity separator. This results in much shorter settling times, even for very small droplets.

2.5 Coriolis forces

In a rotating system, radially moving particles are subject to an apparent tangential force, called Coriolis force. Consider a rotating bowl filled with water, with an oil droplet at a certain distance r from the centre of rotation. Assume solid body rotation (i.e. the water moves with the same angular velocity as the centrifuge). The water has a tangential velocity of:

$$v_\omega = \omega r \qquad (2\text{-}11)$$

The droplet has a radial velocity according to equation (2-9). The Coriolis force acting on the droplet is [2]:

$$F_{cor} = 2 m v_{tr} \omega \qquad (2\text{-}12)$$

Hence, with equation (2-5) this will result in a tangential velocity relative to the bowl of:

$$v_{cor} = \frac{2\ m\ v_{tr}\ \omega}{3\ \pi\ \mu_w\ D} = \frac{\rho_o\ (\rho_w - \rho_o)\ \omega^3\ r\ D^4}{162\ \mu_w^2} \qquad (2\text{-}13)$$

The ratio between v_{cor} and v_{tr} describes the influence of the Coriolis force, and is given by:

$$\frac{v_{cor}}{v_{tr}} = \frac{F_{cor}}{F_b} = \frac{\rho_o\ \omega\ D^2}{9\ \mu_w} \qquad (2\text{-}14)$$

At 20 °C in water, in a centrifuge (ω=800 rad/s), a 5-μm oil droplet (ρ_o=900 kg/m^3) will have v_{cor}/v_{tr}=0.002. The same situation for D=50 μm yields: v_{cor}/v_{tr}=0.2 . Hence, the Coriolis force can be neglected for relatively small droplets.

2.6 Shear forces and droplet rotation

In case of a velocity gradient in the continuous phase, droplets tend to rotate. This rotation, termed 'top spin', has been investigated by Clift et al. [8]. Figure (2-2) shows schematically a sphere undergoing top spin in an unbounded liquid with velocity v_F at its centre with uniform velocity gradient:

$$G_S = \frac{dv_F}{dy} \qquad (2\text{-}15)$$

The angular velocity Ω of the droplet can be estimated reasonably well by [8]:

$$\Omega = \tfrac{1}{2} G_S \qquad (2\text{-}16)$$

Due to the rotation, a lift force F_L occurs (figure (2-2)). It is given by [8]:

$$F_L = 1.615\ \mu\ D\ v_R\ \sqrt{Re_{G_s}} \qquad (Re_{G_s} < 0.1) \qquad (2\text{-}17)$$

where v_R is the droplet velocity relative to the fluid measured on the streamline through the centre, and

$$Re_{G_s} = \frac{\rho\ G_S\ D^2}{\mu} \qquad (2\text{-}18)$$

For $Re_{G_s} > 0.1$, no correlations were found for Ω or F_L. If $Re_G > 6$, a droplet rotates unsteadily and the wake is oscillatory [8]. High shear forces may induce break-up of droplets (see: section 2.10).

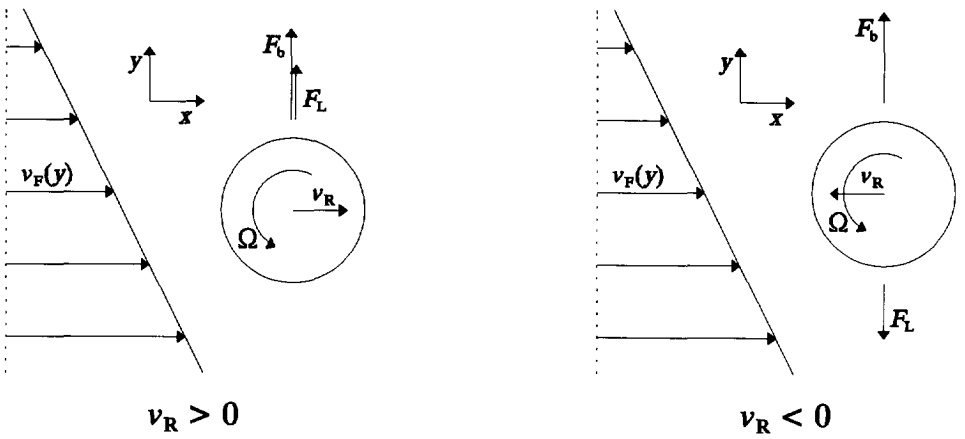

Figure (2-2) Sketch of a spherical droplet rotating in a fluid; **left**, when the droplet moves faster than the continuous phase, and **right**, when the droplet lags behind the continuous phase.

From figure (2-2) it can be seen that, depending on v_R, the lift force F_L acts in the same or in the opposite direction as the buoyant force F_b or at an angle θ with respect to F_b, depending on the type of separator (see chapter 3). This will cause an increase or a decrease of v_t. An important factor is therefore:

$$\frac{F_L}{F_b} \approx \frac{3.1\ v_R\ G_S^{\frac{1}{2}}\ \mu^{\frac{1}{2}}\ \rho_w^{\frac{1}{2}}\ \cos\theta}{(\rho_w - \rho_o)\ g\ D} \qquad \text{(gravity separation)} \qquad \textbf{(2-19)}$$

or:

$$\frac{F_L}{F_b} \approx \frac{3.1\ v_R\ G_S^{\frac{1}{2}}\ \mu^{\frac{1}{2}}\ \rho_w^{\frac{1}{2}}\ \cos\theta}{(\rho_w - \rho_o)\ \omega^2\ r\ D} \qquad \text{(centrifugal separation)} \qquad \textbf{(2-20)}$$

which gives the relative importance of F_L.

It was also found [8] that, if there are no forces acting from the outside (e.g. gravity), the droplet centre moves with the velocity which the continuous phase would have at that point in the absence of the droplet. Hence, v_R will be zero it that case. However, if the oily water flow in a gravity separator is directed upwards or downwards under an angle γ with the horizontal then, due to gravity, v_R will be:

$$v_R = v_t \sin\gamma \qquad \textbf{(2-21)}$$

where γ is positive when the flow is directed upwards, and negative when it is directed downwards. Equation (2-19) is then given by:

$$\frac{F_L}{F_b} \approx \frac{0.172\ G_S^{\frac{1}{2}}\ \rho_w^{\frac{1}{2}}\ D\ \sin\gamma\ \cos\theta}{\mu^{\frac{1}{2}}} \qquad \text{(gravity separation)} \qquad (2\text{-}22)$$

or in the case of a centrifuge:

$$\frac{F_L}{F_b} \approx \frac{0.172\ G_S^{\frac{1}{2}}\ \rho_w^{\frac{1}{2}}\ g\ D\ \sin\gamma\ \cos\theta}{\omega^2\ r\ \mu^{\frac{1}{2}}} \qquad \text{(centrifugal separation)} \qquad (2\text{-}23)$$

Consider a 200 μm oil droplet, rotating in a gravitational field in water at 20 °C with G_S=5 s^{-1}. According to equation (2-22), F_L/F_b=0.078 sinγ cosθ. In a horizontal separator when γ=0 the ratio F_L/F_b is zero, but for $|\gamma| > 0$ the lift force could have some effect.

Assume that in a centrifuge with ω=750 rad/s and r=0.1 m, a 5 μm oil droplet (ρ_o= 900 kg/m^3) rotates by shear rate G_S=50000 s^{-1}. Then, according to equation (2-23), F_L/F_b=3.35 10^{-5} sinγ cosθ. Thus, in a centrifuge F_L can be neglected.

2.7 Brownian motion

Brownian motion is the motion of small particles in a liquid or a gas as a result of the thermal energy of the molecules of the continuous phase. This thermal energy is equal to the average kinetic energy, which is $^3/_2 kT$. Einstein and Von Smoluchowsky derived the mean distance q travelled due to Brownian motion by a particle suspended in a liquid, as a function of time t (valid down to times of approximately 10^{-5} s) [3]:

$$q = \sqrt{\frac{2\ k\ T\ t}{\pi\ \mu\ D}} \qquad (2\text{-}24)$$

Because the motion is erratic, q can be in any direction. In a gravity separator the residence time t_r can be 10 minutes. Hence, at 20 °C in water, a 10 μm oil droplet (ρ_o=900 kg/m^3) will migrate on average 12 μm by Brownian movement. According to equation (2-6) the corresponding terminal rising velocity is: $v_t \approx 5.5$ μm/s. Consequently, the travelled distance by gravity is: $s = t_r v_t \approx 3300$ μm. This indicates that for oil droplets with diameters of 10 μm or larger, Brownian motion does not have a significant effect on the path of the droplet. However, droplets of 1 μm diameter in the same situation move (according to equation (2-24)) 39 μm, but have a terminal rising velocity of only 0.055 μm/s. This yields for the travelled distance: $s \approx 33$ μm, which is somewhat smaller than its corresponding q. Hence,

the path of an oil droplet in a gravitational field becomes significantly more affected by Brownian motion if its diameter decreases and becomes much smaller than, say, 10 μm.

The same calculation can be carried out for droplets in a centrifugal acceleration field. Figure (2-3) shows the relation between q and s as a function of the droplet size for gravity and centrifugal forces. The following values of the parameters were taken: ρ_0=900 kg/m^3, μ=0.001 Ns/m^2 and T= 293 K. Further, for gravity t_r=600 s and for centrifugal forces t_r=1 s and G=6000. From the graph it can be observed that Brownian motion has more influence in gravity separators than in centrifuges.

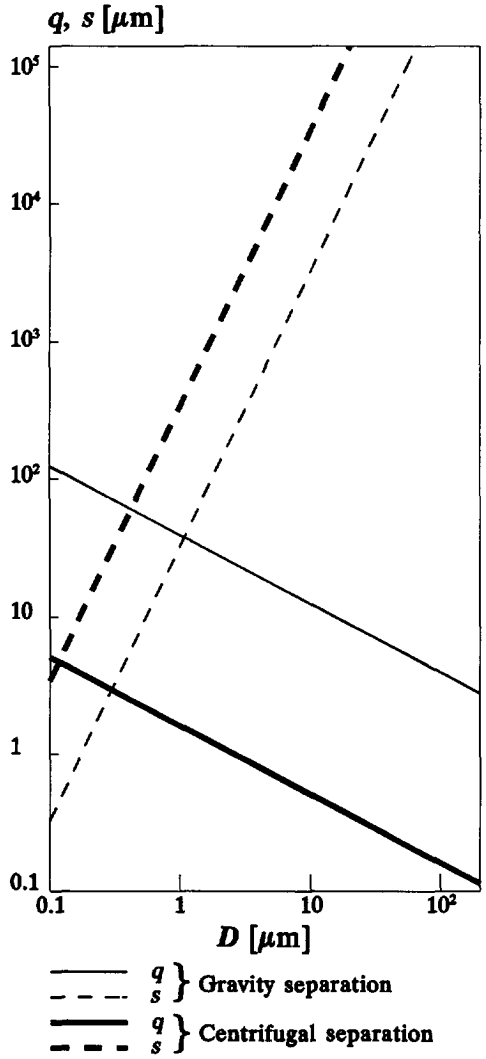

Figure (2-3)
Comparison between distance travelled by Brownian motion q and by gravity s.

It must be emphasized that the calculations and conclusions in this section are purely theoretical. The theory includes neither the effect of collision nor break-up of suspended droplets. However, due to Brownian motion, suspended droplets are continuously colliding with each other. Repulsive forces, on the other hand, help to keep the suspension dispersed. The ultimate effect of Brownian motion is therefore uncertain; it has been ignored in the theory and the simulations described in the following chapters.

2.8 Particle-interface coalescence

The second phase in the separation process is the process of coalescence. In the past, a number of experimental and theoretical studies have been carried out on the phenomenon of coalescence of a single droplet at a flat or deformable interface. Most authors of the reviewed literature assume that the coalescence process takes place through five consecutive stages. These are:

1. The approach of the droplet to the interface, resulting in deformation of both the droplet and the interface.
2. Damped oscillation of the droplet at the interface.
3. The formation of a film of the continuous phase between the droplet and its bulk phase.
4. Drainage, rupture and removal of the film.
5. Transfer of the content of the droplet into its bulk phase.

Of these stages, film drainage appears to be the controlling factor. From visual observations it was established that steps 1, 2, 3 and 5 occur extremely fast [5]. Furthermore, it was noted that a droplet situated at the interface between two liquid phases may coalesce completely or it may coalesce partially, producing a second -smaller- droplet which behaves in a similar manner as its parent droplet.

The factors that most affect the drainage and rupture process are [12]:

1. Droplet size.
2. Distance of fall or rise of the droplet to the interface.
3. Curvature of the interface.
4. Density difference between the phases.
5. Phase viscosity ratio.
6. Interfacial tension.
7. Temperature.
8. Vibrational effects.
9. Electrical effects (see section 2.10).
10. The presence of electrical double layers.
11. The presence of a third component.

Several authors derived, mathematically as well as experimentally, correlations between the rate of coalescence and one or more of the factors given above. The results of the different studies sometimes conflict. For instance, some authors found that an increase of droplet size leads to an increase of the coalescence time t_c, while others found no effect or even the opposite one. The extremes are: $t_c \propto D^{-1}$ [6] and $t_c \propto D^{1.46}$ [12].

The correlation found by Jeffreys [12] reads:

$$\frac{\sigma\, t_c}{\mu\, D} = 1.32 \cdot 10^5 \left(\frac{\Lambda}{D}\right)^{0.18} \left(\frac{D^2\, |\Delta\rho|\, g}{\sigma}\right)^{0.32} \qquad (2\text{-}25)$$

where Λ is the distance of fall. This is the distance from the interface where the droplet is released in their experimental set-up. Although equation (2-25) is not suitable for our purposes, it predicts that: $t_c \propto D^{1.46}$ and $t_c \propto g^{0.32}$.

Gillespie and Rideal [9] derived an equation for t_c, considering a flat interface and an approaching droplet, assuming that within a very small area the droplet surface can be considered to be flat. They found:

$$t_c = \frac{\mu\, |\Delta\rho|\, g}{400\, \sigma^2} \frac{D^5}{2^5} \left(\frac{1}{h_R^2} - \frac{1}{h_0^2}\right) \qquad (2\text{-}26)$$

where h_0 is the thickness of the film at the moment the droplet initially comes to rest on the interface and from when time starts. The thickness of the film is h_R at time t_c when the film ruptures. They also derived that $h_0^2 \propto D^4$, $h_0^2 \propto g$, $h_R^2 \propto D^4$ and $h_R^2 \propto g$. Hence, $t_c \propto D$ and $t_c \propto g^0$. To test their derivations, they studied experimentally the coalescence times of water droplets at a benzene-water interface. The results of these experiments are displayed in figure (2-4).

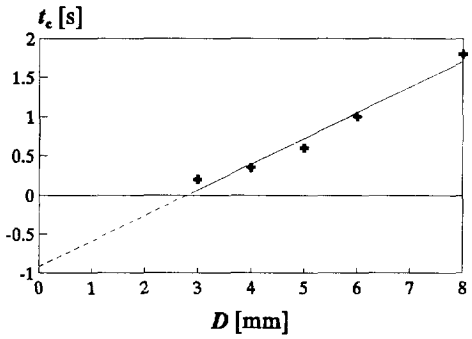

Figure (2-4)
Variation of coalescence time as a function of droplet size at a benzene-droplet interface (From: Gillespie et al. The coalescence of droplets at an oil-water interface, 1955).

According to equation (2-26), a straight line through the experimental points should intersect $t_c = D = 0$. Hence, a calculation of t_c for small droplets does not give realistic values, only the insight into trends may be useful.

In their attempt to derive an equation for t_c, Charles and Mason [6] considered a curved surface which approaches a plane interface with a certain velocity so that the liquid in between is squeezed out. They found:

$$t_c = \frac{\mu}{|\Delta\rho|\, g\, D} \ln\frac{h_0}{h_R} \qquad (2\text{-}27)$$

and assumed that h_0/h_R is constant. Hence, $t_c \propto D^{-1}$ and $t_c \propto g^{-1}$. Equation (2-27) is only applicable to small droplets which are not able to affect the interface and can be considered as rigid spheres. Some results of experiments carried out by Charles and Mason are displayed in figure (2-5).

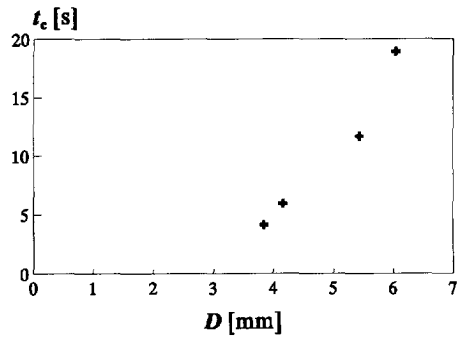

Figure (2-5)
Variation of coalescence time as a function of droplet size at a benzene-droplet interface (From: Charles et al. The coalescence of liquid droplets with flat liquid-liquid interfaces, 1960).

Although the experimental set-up was nearly the same as the one Gillespie and Rideal used, the values of t_c are much larger than those observed by the latter.

Because equations (2-25), (2-26) and (2-27) differ widely and none of the authors give satisfactory values for h_0 and h_R, carrying out calculations without further research will give unreliable results. However, the experiments justify the conclusions that for droplets above about 0.5 mm, the coalescence time increases with increasing droplet diameter. Below that diameter it is questionable whether coalescing rates can be predicted. In spite of the fact that small droplets can be assumed to be spherical, the mathematically derived equations for t_c do not involve the effects of all the factors mentioned at the beginning of this section. Moreover, experimental results with droplets below 1 mm diameter were not found. Finally, the effect of g is not clear. Equations (2-25), (2-26) and (2-27) give $t_c \propto g^{0.32}$, $t_c \propto g^0$ and $t_c \propto g^{-1}$ respectively.

Jeffreys [12] reported that there are some conflicting articles on the effects of vibration on coalescence times. However, a majority of the conclusions found in the literature reports that vibration tends to stabilize emulsions. This means that vibration must be excluded from separators. In the case of centrifuges, it is probably important that rotating parts are balanced as accurately as possible.

The presence of electrical double layers increases the coalescence time [12]. These double layers tend to retard the flow of the draining film. It was also found that coalescence times of small droplets are not more affected than those of large ones.

The effects of electric fields on the process of coalescence is discussed in section 2.11.

The presence of a third component may accelerate or retard the rate of coalescence [12]. Generally, solids promote coalescence, while a surfactant reduces drainage rates of the film.

2.9 Particle-particle coalescence

Due to experimental difficulties, relatively little work has been reported on the coalescence of pairs of droplets [12]. In the literature only a few equations were found which are derived from mathematical models. The simplest case, where the droplets are assumed to be rigid and of equal size, was first considered by McAvoy and Kintner [14]. They derived:

$$t_c = \frac{3\ \pi\ \mu\ D^2}{4\ F} \ln\frac{h_0}{h_R} \qquad \textbf{(2-28)}$$

where h_0 and h_R are the distances between the droplet surfaces at the moment the droplets come initially to rest, and at the moment of film rupture, respectively. F is a force as a result of gravity, fluid flow or electrical charges. In the case of gravity, equation (2-28) yields:

$$t_c = \frac{9\ \mu}{2\ |\Delta\rho|\ g\ D} \ln\frac{h_0}{h_R} \qquad \textbf{(2-29)}$$

which is nearly equal to equation (2-27). Values for h_0 and h_R were not given. The effect of particle-particle coalescence is therefore uncertain. For a relatively low oil concentration the effect will probably be negligible, because the average distance between the droplets is then large with respect to their diameters.

2.10 Break-up of droplets

Shear flow causes a droplet to rotate and to deform. If the velocity gradients are large enough, interfacial forces will no longer be able to keep the droplet intact, causing rupture into two or more smaller particles. Gravity settlers are designed to have low velocities throughout the apparatus. Hence, Reynolds numbers are low. No serious break-up occurs, thus separation performance is not affected. However, an oil-water mixture in the inlet part of rotating separators (called: accelerator) is exposed to high shear forces. Here the mixture is accelerated from zero to its angular velocity.

In the past much research has been carried out on the behaviour of droplets in agitated systems. No work was found concerning accelerators in centrifuges, just work about other rotating systems. For a mixer with rotating discs the maximum stable droplet size is given by Strand et al. [17]:

$$D_{max} = C_1 \left(\frac{\sigma}{\rho}\right)^{0.6} e^{-0.4} \qquad \textbf{(2-30)}$$

They found C_1 in the region 0.4-0.6 for organic droplets and 0.8-1.2 for water droplets. The

droplet.

- Shear forces probably have a negligible effect on the path of an oil droplet, but must be considered when a separator is designed in which relatively high shear rates are expected.
- The effect of Brownian motion can generally be neglected.
- The effect of coalescence time could be important in some cases for the separation efficiency.
- Substantial break-up of droplets will not occur in gravity separators, but will probably occur in the accelerator of a centrifuge, causing alteration of the influx droplet size distribution.
- Due to the high conductance of water, electric fields do not affect the droplet path.

References

[1] Allan, R.S., Charles, G.E. and Mason, S.G.: J. of Coll. Sc., **16**, 1961, 150-171.

[2] Alonso, M. and Finn, E.J.: Fundamentele natuurkunde (Deel 1: Mechanica), Elsevier, Amsterdam, 1983.

[3] Alonso, M. and Finn, E.J.: Fundamentele natuurkunde (Deel 6: Statistische Fysica), Elsevier, Amsterdam, 1979.

[4] Baird, M.H.I. and Lane, S.J.: Drop size and hold-up in a reciprocating plate extraction column, Chem. Eng. Sc., **28**, 947-957.

[5] Bohnet, M.: Trennen nicht mischbarer flüssigkeiten, Chemie Ingenieur Technik, **48**, März 1976, Nr.3, 177-264.

[6] Charles, G.E. and Mason, S.G.: The coalescence of liquid drops with flat liquid-liquid interfaces, J. of Coll. Sc., **15**, 1960, 236-267.

[7] Chen, H.T. and Middleman, S.: Drop size distribution in agitated liquid-liquid systems, AIChE journal, **13**, 1967, 989-995.

[8] Clift, R., Grace, J.R. and Weber, M.E.: Bubbles, drops, and particles, Academic Press, New York, 1978.

[9] Gillespie, T. and Rideal, E.K.: The coalescence of drops at an oil-water interface, Trans Faraday Soc., **52**, 1956, 173-183.

[10] Hetsroni, G.: Handbook of multiphase systems, Hemisphere Publishing Corporation, 1982.

[11] Hinze, J.O.: Fundamentals of the hydrodynamic mechanism of splitting in dispersion processes, AIChE Journal Vol. 1, **3**, 1955, 289-295.

[12] Jeffreys, G.V., Davies, G.A.: Coalescence of liquid droplets and liquid dispersion, in: Hanson, C., Recent advances in liquid-liquid extraction, University of Bradford, U.K., Pergamom Press, 1971.

[13] Kolmogorov, A.N.: The break-up of droplets in a turbulent stream, Directorate of Scientific Information Service, DRB Canada, 6-1956, T 210 R, Translated from: Dok. Akad. Nauk., **66**, 5-1949, 825-828.

[14] McAvoy, R.M. and Kintner, R.C.: Approach of two identical rigid spheres in a liquid field, J. of Coll. Sc., **20**, 1965, 188-190.

[15] Palermo, T.: Le Phénomène de coalescence, Revue de l'Institut Français du Pétrole, **46**, Mai-Juin 1991, N° 3, 325-360.

[16] Sherman, P.: Emulsion science, Academic Press, London, 1968.

[17] Strand, C.P., Olney, R.B. and Ackerman, G.H.: Fundamental aspects of rotating disc contactor performance, AIChE journal, **8**, 1962, 252-261.

[18] Warshay, M., Bogusz, E., Johnson, M. and Kintner, R.C.: Ultimate velocity of drops in stationary liquid media, Can. J. Chem. Eng., **37**, 1959, 29-36.

Chapter 3

Gravity oil-water plate separators

3.1 Introduction

Knowledge of the path of an oil droplet towards the interface inside a separator enables us to predict the separation efficiency η as a function of the diameter D of the droplet. The path depends on the physical properties of the mixture and on the dimensions of the separator. In this chapter, continuous-phase flow patterns and the paths of droplets between parallel plates are described and modelled. The model is based on the following assumptions, some of which were discussed in chapter 2:

- spherical droplets,
- validity of Stokes' law,
- laminar flow,
- channels of equal dimensions,
- equal flow rate through each channel,
- uniform distribution of flow over the width of each channel,
- small droplet size compared to the plate distance.

The mechanisms that have been ignored in the model are:

- Brownian motion,
- particle-interface coalescence time,
- droplet-droplet interaction,
- droplet break-up,
- other forces than gravity acting on the droplets.

It will be demonstrated that η is not dependent on the flow velocity profile in the direction of gravity and is also independent of the shape of the plates.

As in chapter 2, oil is taken to be the dispersed phase and assumed to be of a lower density than the continuous (water) phase.

3.2 The path of an oil droplet in water

3.2.1 Horizontal skimmer separator (settling tank)

Basically, a horizontal skimmer separator can be considered as a plate separator with only one channel. Figure (3-1) shows schematically the settling section of a horizontal skimmer separator with a rectangular cross-section. The settling section is that part of the separator where the separation process takes place. The oily water flows horizontally, over length L, through the separation section from the front towards the back of the section. Meanwhile the oil droplets rise perpendicularly to the flow of the water towards the surface of the settling section, where they coalesce and form an oil layer which can be removed. The maximum vertical distance a droplet may have to travel to the surface is equal to the height H of the separation section. The terminal rising velocity v_t (figure (3-2)) of the droplets can be derived from Stokes' law and is given by equation (2-6). The average flow velocity v_f of the oil-water mixture is given by:

$$v_f = \frac{Q}{H\,W} \tag{3-2-1}$$

A droplet entering the separation section close to the bottom will reach the surface if:

$$\frac{v_t}{v_f} \geq \frac{H}{L} \tag{3-2-2}$$

We consider a droplet to be separated from the continuous phase when it reaches the surface. Since smaller droplets rise with a lower velocity than larger ones, the size for droplets which are completely separated is limited to a minimum value. All larger droplets will be separated,

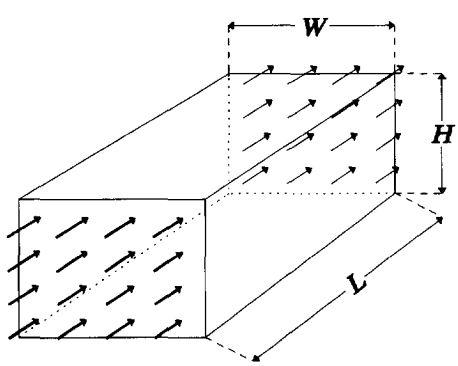

Figure (3-1) Part of a settling tank in which separation occurs, with Length L, Width W and Height H.

while at least part of the droplets smaller than this minimum droplet size will pass the separation section, i.e. those that enter the tank near the bottom. Generally, this minimum droplet size is called the 'critical droplet size' or 'critical droplet diameter'. Combination of equations (2-6), (3-2-1) and (3-2-2) then gives the expression for the critical droplet diameter D_c:

$$D_c = \sqrt{\frac{18\ Q\ \mu}{L\ W\ (\rho_w - \rho_o)\ g}} \qquad \textbf{(3-2-3)}$$

Note that H does not influence D_c. However, it does affect the flow regime inside the separation section, since the Reynolds number is given by:

$$Re = \frac{\rho_w\ v_f\ D_h}{\mu} \qquad \textbf{(3-2-4)}$$

where D_h represents the hydraulic diameter, which is given by:

$$D_h = \frac{2\ H\ W}{H + W} \qquad \textbf{(3-2-5)}$$

Combination of equations (3-2-1), (3-2-4) and (3-2-5) gives:

$$Re = \frac{2\ \rho_w\ Q}{\mu\ (H + W)} \qquad \textbf{(3-2-6)}$$

Laminar flow requires a low value of Re. Thus, a minimum value for H may be necessary in order to keep Re sufficiently low.

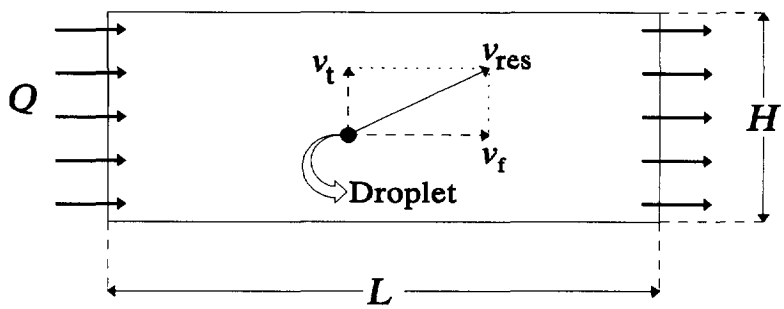

Figure (3-2) Velocity components of a droplet in a horizontal separator, with rise velocity v_t and flow velocity v_f.

3.2.2 Plate separators with flat plates

If a pack of equidistant parallel flat plates is installed inside a horizontal skimmer separator (see figure (3-3)), then the maximum vertical distance to be travelled by a droplet is reduced to the distance between two plates. For the same tank dimensions and the same oily-water flow rate, smaller droplets can now be removed and a lower oil concentration of the effluent can thus be realized. The average flow velocity v_f in a channel between two plates is given by:

$$v_f = \frac{Q}{(H - n\,d)\,W} = \frac{Q}{h\,n\,W} \qquad (3\text{-}2\text{-}7)$$

where n is the number of plates, d the plate thickness and h the channel height. We consider a droplet to be separated from the continuous phase when it reaches the surface of a plate. A droplet entering the separation section close to the bottom of a channel will reach the surface of a plate if:

$$\frac{v_t}{v_f} \geq \frac{H - d\,n}{n\,L} = \frac{h}{L} \qquad (3\text{-}2\text{-}8)$$

Combination of equations (2-6), (3-2-7) and (3-2-8) gives the expression for the critical droplet diameter D_c:

$$D_c = \sqrt{\frac{18\,Q\,\mu}{n\,L\,W\,(\rho_w - \rho_o)\,g}} \qquad (3\text{-}2\text{-}9)$$

Note that H and d do not influence D_c. However, they do affect the flow regime inside the separation section, since the Reynolds number is given by:

$$Re = \frac{\rho_w\,v_f\,D_h}{\mu} \qquad (3\text{-}2\text{-}10)$$

and:

$$D_h = \frac{2\,h\,W}{h+W} \qquad (3\text{-}2\text{-}11)$$

Combination of equations (3-2-7), (3-2-10) and (3-2-11) gives:

$$Re = \frac{2\,\rho_w\,Q}{\mu\,\left((H - nd) + nW\right)} \qquad (3\text{-}2\text{-}12)$$

Laminar flow corresponds to a low Re. Thus, a minimum value for H and a maximum value for d may be necessary in order to keep Re sufficiently low.

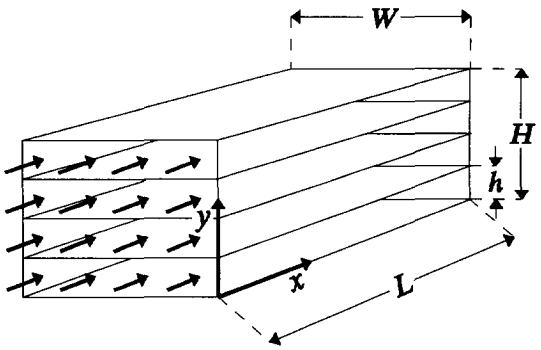

Figure (3-3) Horizontal plate separator with 5 plates (4 channels).

3.2.3 Flow velocity profiles

In the previous sections v_f was assumed to be uniform throughout the separation section. However, due to build-up of a boundary layer at the plate surfaces, a parabolic velocity profile will develop (see figure (3-4)). The thickness of the boundary layer δ is given by [2,3]:

$$\delta \approx 4.64 \sqrt{\frac{\mu\, x}{\rho_w\, v_\infty}} \qquad \textbf{(3-2-13)}$$

where x is the distance from the plate edge where the flow enters the channel, and v_∞ is the flow velocity outside the boundary layers. From figure (3-4) it follows that $v_\infty = v_F(y=\frac{1}{2}h)$ which, however, is not a constant. If $x=0$, then $v_\infty = v_f$, but if x increases then v_∞ increases too, because:

$$\frac{Q}{n\, W} = v_f\, h = \int_0^h v_F(y)\, dy \qquad \textbf{(3-2-14)}$$

and if a parabolic flow profile exists when $\delta = \frac{1}{2}h$, then:

$$v_F = C\,(y\, h - y^2) \qquad (0 \le y \le h) \qquad \textbf{(3-2-15)}$$

From equations (3-2-14) and (3-2-15) follows:

$$v_f\, h = \int_0^h C\,(y\, h - y^2)\, dy \qquad \textbf{(3-2-16)}$$

which gives:

$$C = \frac{6\, v_f}{h^2} \tag{3-2-17}$$

Substitution of C in equation (3-2-15) yields:

$$v_F = \frac{6\, v_f}{h^2}\,(y\, h - y^2) \tag{3-2-18}$$

and this gives for $y=\frac{1}{2}h$:

$$v_F(y=\tfrac{1}{2}h) = \tfrac{3}{2}v_f \tag{3-2-19}$$

Based on these equations, it can be said that the value of v_∞ will increase from $v_\infty=v_f$ for $\delta=0$, to $v_\infty=\frac{3}{2}v_f$ for $\delta=\frac{1}{2}h$.

An approximation for the value of x for $\delta=\frac{1}{2}h$, can be found by taking $v_\infty=\frac{3}{2}v_f$:

$$x_{\delta=\frac{1}{2}h} \approx \frac{(H - n\, d)\, \rho_w\, Q}{57.41\, n^2\, \mu\, W} = \frac{h\, \rho_w\, Q}{57.41\, n\, \mu\, W} \tag{3-2-20}$$

In practice, typical dimensions of plate packs used in oil-water separators are about: L=**1 m**, W=**0.5 m** and h=**0.02 m**. If we take ρ_w=**1000 kg/m^3**, μ=**0.001 P·as** and Re=**1000** then: v_f=**0.026 m/s** and Q/n=**0.00026 m^3/s**. Hence: $x_{\delta=\frac{1}{2}h}$~**0.18 m**, which is large compared with L. In the next section, however, it will be shown that the separation efficiency is not affected by the value of $x_{\delta=\frac{1}{2}h}$.

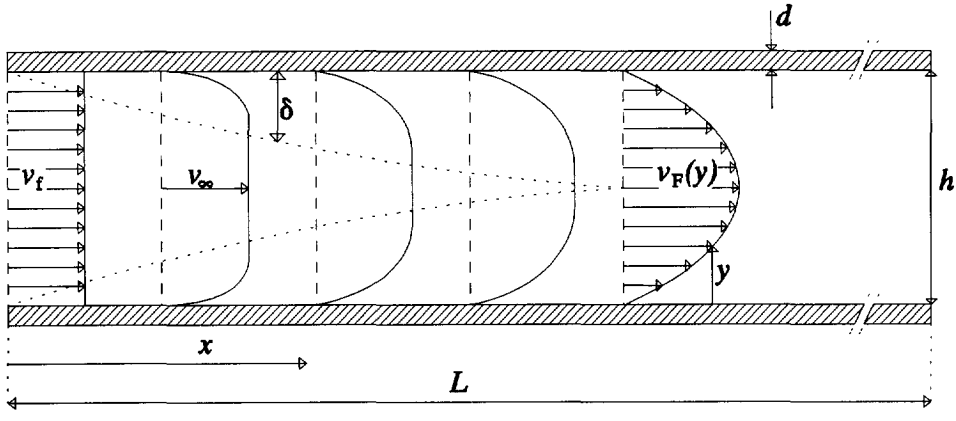

Figure (3-4) Build-up of boundary layers between two plates.

3.2.4 Separation efficiency and particle size

Combination of equations (3-2-7) and (3-2-18) yields:

$$v_F = \frac{6\,Q}{n\,h^3\,W}(y\,h - y^2) \qquad (0 \le y \le h) \qquad \textbf{(3-2-21)}$$

An oil droplet will rise (see figure (3-5)) in a vertical direction from h_1 to h_2 in time:

$$t_2 - t_1 = \frac{h_2 - h_1}{v_t} \qquad \textbf{(3-2-22)}$$

where t_1 is the time when the droplet is at $y=h_1$ and t_2 is the time when the droplet is at position $y=h_2$. If $t_1=0$, then the vertical position of the rising droplet at time t is given by:

$$y = h_1 + v_t\,t \qquad \textbf{(3-2-23)}$$

Its corresponding horizontal velocity, denoted by v_F, is then:

$$v_F = \frac{6\,Q}{n\,h^3 W}\left(h_1 h - h_1^2 + (v_t h - 2v_t h_1)t - v_t^2 t^2\right) \qquad \textbf{(3-2-24)}$$

Thus the horizontal distance l travelled by the droplet from time $t_1=0$ to t_2 is:

$$l = \int_0^{t_2} v_F\,dt = \frac{6\,Q}{n\,h^3 W}\left[(h_1 h - h_1^2)t + (\tfrac{1}{2}v_t h - v_t h_1)t^2 - \tfrac{1}{3}v_t^2 t^3\right]_0^{t_2} \qquad \textbf{(3-2-25)}$$

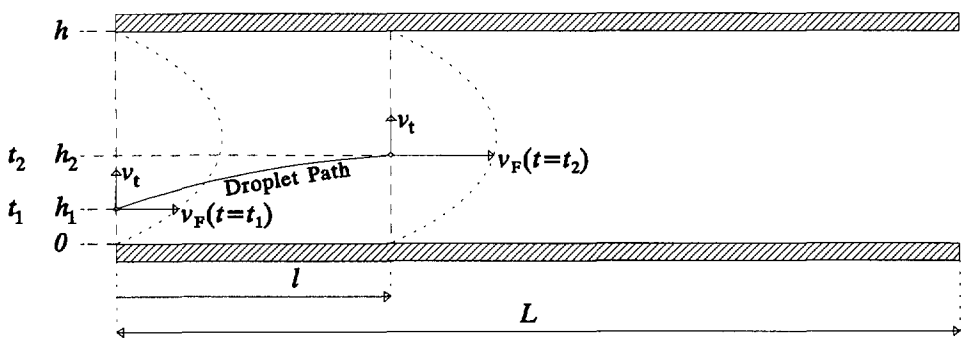

Figure (3-5) Path of an oil droplet entering the plate pack at h_1 and t_1, assuming a parabolic flow velocity profile throughout the plate pack.

A special situation is sketched in figure (3-6). An oil droplet rises from the bottom of a channel ($h_1=0$) to the surface of the overhead plate ($h_2=h$) and has velocities v_t and v_F so that, when the droplet reaches the plate surface, its horizontally travelled distance is equal to the plate length ($l=L$). The diameter of this droplet will be the critical droplet diameter D_c of the plate separator in the case of a uniform parabolic flow profile throughout the channels. Thus, when $h_1=0$, $h_2=h$, $t_1=0$, $t_2=h/v_t$ and $l=L$, equation (3-2-25) yields:

$$L = \frac{Q}{n\, v_t\, W} \qquad \textbf{(3-2-26)}$$

The combination of equations (3-2-26) and (2-6) yields for D_c:

$$D_c = \sqrt{\frac{18\, Q\, \mu}{n\, L\, W\, (\rho_w - \rho_o)\, g}} \qquad \textbf{(3-2-27)}$$

Note that D_c in the case of parabolic flow (equation (3-2-27)) is equal to D_c in the case of plug flow (equation (3-2-9)).

Combination of equations (3-2-14) and (3-2-26) yields:

$$\frac{Q}{n\, W} = v_f\, h = \int_0^h v_F\, dy = v_t\, L \qquad \textbf{(3-2-28)}$$

and substitution of equation (3-2-28) into (3-2-27) yields:

$$D_c = \sqrt{\frac{18\, \mu \int_0^h v_F\, dy}{L(\rho_w - \rho_o)\, g}} \qquad \textbf{(3-2-29)}$$

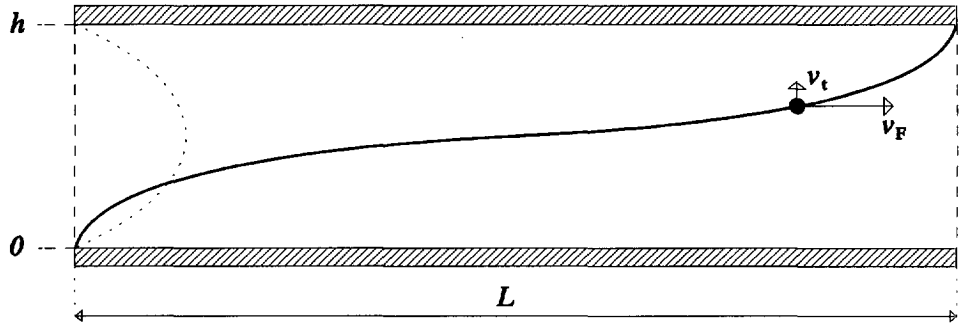

Figure (3-6) Path of an oil droplet with diameter D_c, entering the plate pack at $h_1=0$.

Because of their higher rising velocities, droplets larger than D_c will reach the plate surface for $l<L$. Consequently, the separation efficiency of a separator is 100% for droplets having a diameter D_c or larger.

An expression for the separation efficiency for droplets smaller than D_c is derived as follows. Assume an oil droplet with diameter D entering the plate pack at position h_1 and having velocities v_t and v_F, so that when the droplet reaches the overhead plate, its horizontally travelled distance is equal to the plate length. Thus, when $0 \le h_1 \le h$, $h_2=h$, $t_1=0$, $t_2=(h-h_1)/v_t$ and $l=L$, equation (3-2-25) yields:

$$L = \frac{6\,Q}{n\,h^3 W\,v_t}\left(\frac{1}{6}h^3 - \frac{1}{2}hh_1^2 + \frac{1}{3}h_1^3\right) \qquad \textbf{(3-2-30)}$$

Combination of equations (2-6), (3-2-27) and (3-2-30) then yields:

$$\frac{D}{D_c} = \sqrt{1-3\frac{h_1^2}{h^2}+2\frac{h_1^3}{h^3}} \qquad \textbf{(3-2-31)}$$

Droplets with diameter D entering the plate pack at positions between h_1 and h will reach the plate surface for $l \le L$, while droplets with diameter D entering the plate pack below h_1 will not reach the plate surface.

Consequently, if we define the separation efficiency η as the fraction of the total amount of droplets with diameter D reaching the plate surface, then:

$$\eta = \frac{Q_{h_1-h}}{Q} = \frac{nW\int_{h_1}^{h} v_F dy}{nW\int_0^h v_F dy} = 1-3\frac{h_1^2}{h^2}+2\frac{h_1^3}{h^3}, \qquad \textbf{(3-2-32)}$$

assuming the oil-water mixture entering the plate pack to be homogeneous with respect to droplet size distribution, and assuming a ***parabolic flow profile*** exists throughout the plate pack. Combination of equations (3-2-31) and (3-2-32) in the case of ***parabolic flow*** yields:

$$\eta = \left(\frac{D}{D_c}\right)^2 \qquad (0 \le D \le D_c) \qquad \textbf{(3-2-33)}$$

In the case of ***plug flow*** within the plate pack, the distance l, travelled by a droplet, is given by:

$$l = \int_{t_1}^{t_2} v_f\,dt = \frac{Q(t_2-t_1)}{(H-n\,z)W} \qquad \textbf{(3-2-34)}$$

Thus, when $0 \le h_1 \le h$, $h_2=h$, $t_1=0$, $t_2=(h-h_1)/v_t$ and $l=L$, equation (3-2-34) yields:

$$L = \frac{Q}{n\,W\,v_t}\left(1-\frac{h_1}{h}\right) \qquad \textbf{(3-2-35)}$$

which gives for η in the case of ***plug flow***:

$$\eta = 1-\frac{h_1}{h} = \left(\frac{D}{D_c}\right)^2 \qquad (0\le D\le D_c) \qquad \textbf{(3-2-36)}$$

Note that equation (3-2-36) (separation efficiency as a function of the droplet diameter in the case of plug flow) is identical to equation (3-2-33) (separation efficiency as a function of the droplet diameter in the case of parabolic flow). This finding suggests that the relation between droplet size and separation efficiency is described by equation (3-2-33) for ***any possible*** flow velocity profile $v_x(y)$ which satisfies: $\int_o^h v_x dy = Q/(nW)$. Thus:

Theorem: $\forall v_x(y), \int_o^h v_x(y)\,dy = \frac{Q}{nW} : \eta = \left(\frac{D}{D_c}\right)^2 \quad 0\le D\le D_c$ **(3-2-37)**

The following derivation will prove this theorem.

Assume an oil droplet with diameter D entering the plate pack at position h_1 and having velocities v_t and v_F, so that when the droplet reaches the overhead plate, its horizontally travelled distance is equal to the plate length. Consequently, the time t which it takes the droplet to travel from h_1 to h is given by:

$$t = \frac{h-h_1}{v_t} = \frac{L}{\overline{v_{x,h_1\to h}}} \qquad \textbf{(3-2-38)}$$

The average horizontal velocity of the droplet is per definition:

$$\overline{v_{x,h_1\to h}} = \frac{\int_{h_1}^h v_x dy}{h-h_1} \qquad \textbf{(3-2-39)}$$

Combination of equations (3-2-38) and (3-2-39) yields:

$$v_t = \frac{\int_{h_1}^h v_x dy}{L} \quad \overset{(+eq.(2-6))}{\Rightarrow} \quad D = \sqrt{\frac{18\,\mu\int_{h_1}^h v_x dy}{L(\rho_w-\rho_o)g}} \qquad \textbf{(3-2-40)}$$

The same procedure to determine D_c yields:

$$v_t = \frac{\int_0^h v_x dy}{L} = \frac{Q}{nLW} \quad (+eq.(2\text{-}6)) \Rightarrow \quad D_c = \sqrt{\frac{18Q\mu}{nLW(\rho_w - \rho_o)g}} \tag{3-2-41}$$

This means that, in one system, for every flow velocity profile $v_x(y)$, the critical droplet diameter D_c always has the same value.

Combination of equations (3-2-41) and (3-2-40) gives:

$$\frac{D}{D_c} = \sqrt{\frac{\int_{h_1}^h v_x dy}{\int_0^h v_x dy}} \tag{3-2-42}$$

Droplets with diameter D entering the plate pack at positions between h_1 and h will reach the plate surface at $l<L$, while droplets with diameter D entering the plate pack below h_1 will not reach the plate surface. Thus if we define the separation efficiency η as the fraction of the total amount of droplets with diameter D reaching the plate surface, then:

$$\eta = \frac{Q_{h_1-h}}{Q} = \frac{\int_{h_1}^h v_x dy}{\int_0^h v_x dy} \tag{3-2-43}$$

assuming that the oil-water mixture entering the plate pack is homogeneous with respect to droplet size distribution.

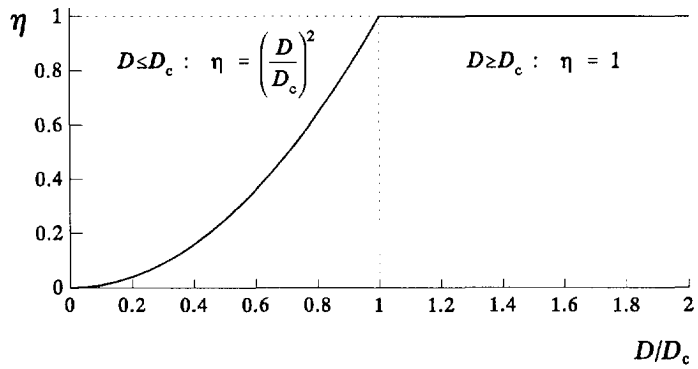

Figure (3-7) Separation efficiency η as a function of D/D_c.

Finally, combination of equations (3-2-42) and (3-2-43) gives:

$$\forall v_x(y), \int_o^h v_x(y)\,dy = \frac{Q}{nW} \quad : \quad \eta = \left(\frac{D}{D_c}\right)^2 \tag{3-2-44}$$

Figure (3-7) shows the resulting graph of the separation efficiency η as a function of D/D_c.

As discussed before, due to the build-up of a boundary layer, the flow velocity profile $v_x(y)$ does not remain constant over the plate length (see figure (3-4)). Appendix **B** gives the derivation of the following theorem (for $D \leq D_c$ and $0 \leq x \leq L$):

$$\forall v_x(x,y), \int_o^h v_x(x,y)\,dy = \frac{Q}{nW} \quad : \quad D_c = \sqrt{\frac{18\,Q\,\mu}{nLW(\rho_w - \rho_o)g}} \quad \wedge \quad \eta = \left(\frac{D}{D_c}\right)^2 \tag{3-2-45}$$

3.3 Plate separators with corrugated plates

The corrugated plate separator (CPS) contains a series of corrugated plates instead of flat ones. A configuration with horizontal flow perpendicular to the corrugations of the plates is shown in figure (3-8). Figure (3-9)**a** shows the cross-section of a channel between two sinusoidally corrugated plates. Note that the shortest distance between the plates varies between the tops and sides of the corrugations. Figures (3-9)**b** and (3-9)**c** show cross-sections of circularly shaped plates and irregularly shaped plates, respectively. The shape of each corrugated plate can be described by a cyclic function. For sinusoidally corrugated plates as shown in figure (3-9)**a**, the equation for Y_1 is given by:

$$Y_1 = A + A\cos\left(2\pi\frac{x}{\lambda}\right) \tag{3-3-1}$$

and the equation for Y_2 is given by:

$$Y_2 = A + A\cos\left(2\pi\frac{x}{\lambda}\right) + d + h(x{=}0) \tag{3-3-2}$$

The equation for the vertical distance h between the plates as a function of x is derived as follows. Because the plate thickness d (see figure (3-10)) is constant, the actual plate thickness d_γ (in a vertical direction) varies with the angle of inclination γ of the plate. Consequently $h(x)$ is given by:

$$h(x) = Y_2 - Y_1 - d_\gamma \tag{3-3-3}$$

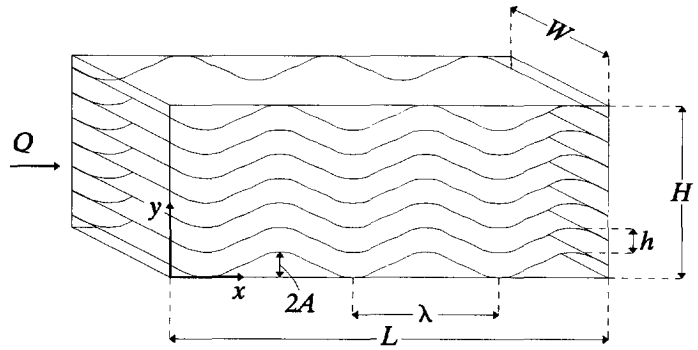

Figure (3-8) Corrugated Plate Separator (CPS).

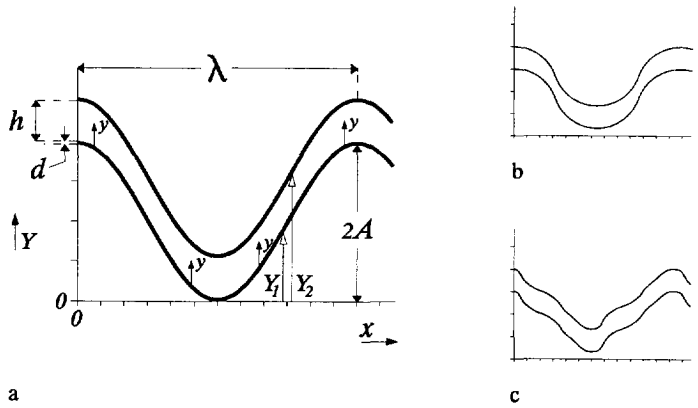

Figure (3-9) Corrugated flow channel, **a.** Sinusoidal, **b.** Segments of a circle, **c.** Undefined function.

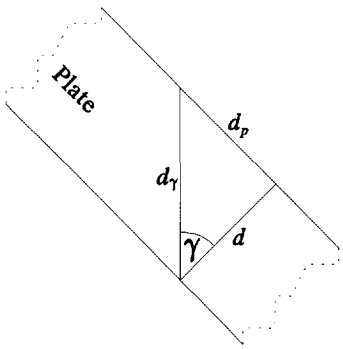

Figure (3-10) Actual plate thickness d_γ as a result of the angle of inclination γ.

From figure (3-10) follows that:

$$\frac{d_p}{d} = \tan\gamma = \frac{dY}{dx} = -A\,\frac{2\pi}{\lambda}\,\sin\left(2\pi\frac{x}{\lambda}\right) \qquad \textbf{(3-3-4)}$$

hence:

$$d_p = -d\,\frac{2\pi A}{\lambda}\,\sin\left(2\pi\frac{x}{\lambda}\right) \qquad \textbf{(3-3-5)}$$

Then the equation for d_γ will be:

$$d_\gamma = \sqrt{d_p^2 + d^2} = d\sqrt{\frac{4\pi^2A^2}{\lambda^2}\sin^2\left(2\pi\frac{x}{\lambda}\right) + 1} \qquad \textbf{(3-3-6)}$$

Finally, an expression for $h(x)$ is found by substitution of the previous equations:

$$h(x) = h(x=0) + d\left(1 - \sqrt{\frac{4\pi^2A^2}{\lambda^2}\sin^2\left(2\pi\frac{x}{\lambda}\right) + 1}\right) \qquad \textbf{(3-3-7)}$$

For small values of d in relation to the value of $h(x)$ and for small values of A, the expression for h can be somewhat simplified. In practice, typical dimensions of corrugated plates used in oil-water separators are: A=**0.05 m**, λ=**0.2 m**, d=**0.001 m** and $h(x=0)$= **0.02 m**. From equation (3-3-7) can be calculated that the lowest value for h is: $h(x=\frac{1}{4}\lambda)$= **0.01966 m**, which is practically equal to $h(x=0)$. Therefore, from now on we assume (see figure (3-11)):

$$\forall 0 \le x \le L:\ h(x) = h(x=0) = h$$

The flow velocity profile $v_x(x,y)$ between the corrugated plates will most probably not be parabolic. However, for each value of x is valid:

$$\int_0^h v_x(x,y)\,dy = \frac{Q}{nW} \qquad (0 \le x \le L) \qquad \textbf{(3-3-8)}$$

If we define v_Y as the component of the vertical velocity caused by the angle of inclination γ, then:

$$v_Y = v_x\tan\gamma = -v_x\frac{2\pi A}{\lambda}\,\sin\left(2\pi\frac{x}{\lambda}\right) \qquad \textbf{(3-3-9)}$$

The remaining component v_y of the vertical velocity is a result of the variation of the flow profile:

$$v_y = v_x\frac{dy}{dx} \quad \Rightarrow \quad \int_0^y v_x(x,y)\,dy = \int_0^{y+dy} v_x(x+dx,y)\,dy \qquad \textbf{(3-3-10)}$$

This suggests the validity of the following **theorem** (for $D \leq D_c$ and $0 \leq x \leq L$):

$$\int_0^h v_x(x,y)\,dy = \frac{Q}{nW} \quad \Rightarrow \quad D_c = \sqrt{\frac{18\,Q\,\mu}{nLW(\rho_w - \rho_o)g}} \quad \wedge \quad \frac{D}{D_c} = \sqrt{\eta} \qquad (0 \leq x \leq L) \qquad \textbf{(3-3-11)}$$

This theorem can be proved by means of the derivation given in appendix B.

These findings lead to the conclusion that the critical droplet diameter D_c of a corrugated-plate separator and its corresponding efficiency η are independent of the values of A and λ. This means that, under the assumptions made in this section, the use of corrugated plates instead of flat ones does not result in a better separation performance. Nevertheless, some manufactures of corrugated-plate separators claim higher separation efficiencies due to the occurrence of flow-velocity deviations resulting in collision of oil droplets. This would cause coalescence of these droplets and therefore lead to an improved separation efficiency. These and other alleged advantages of corrugated plates have not been taken into account in the theory described in this section.

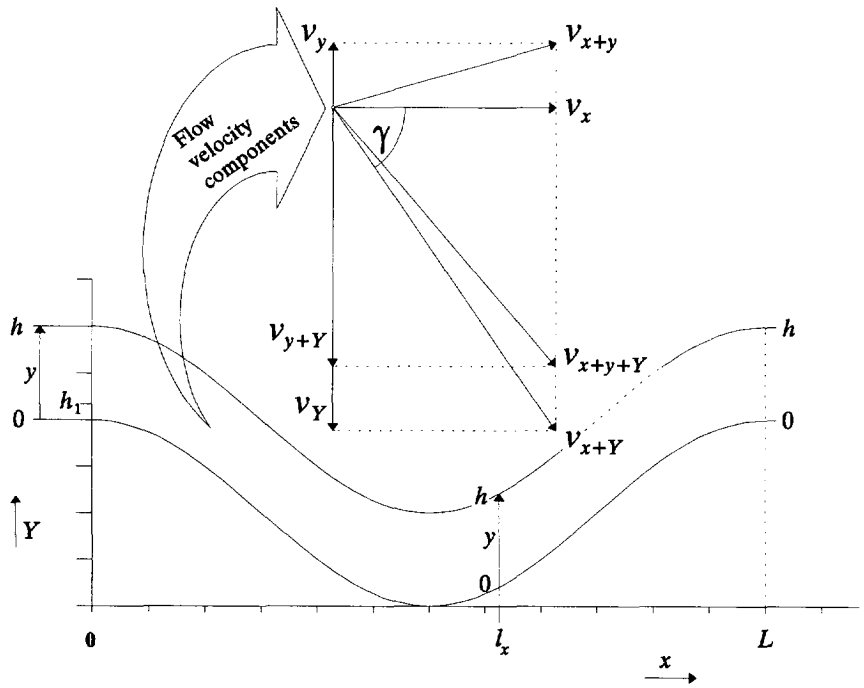

Figure (3-11) Velocity components of flow between corrugated plates.

3.4 Inclination of plate packs

To enhance the removal of oil collected at the underside of the plates, the plate pack is often placed under an angle with the horizontal (figures (3-12) and (3-13)).

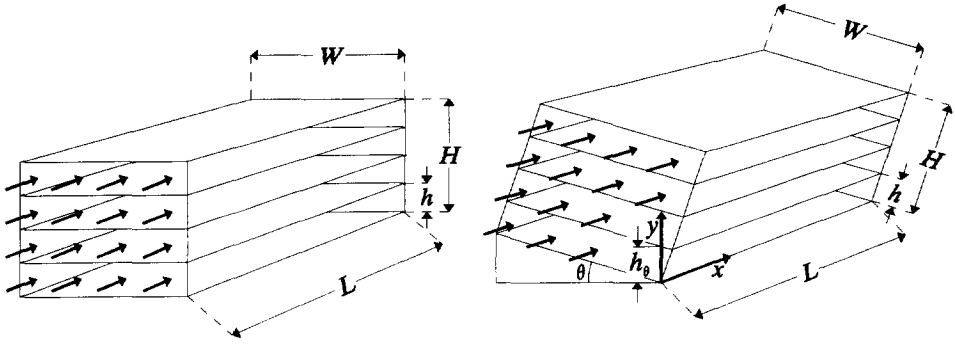

Figure (3-12) Plate separator with flat plates.
Left: Horizontal. **Right:** Tilted.

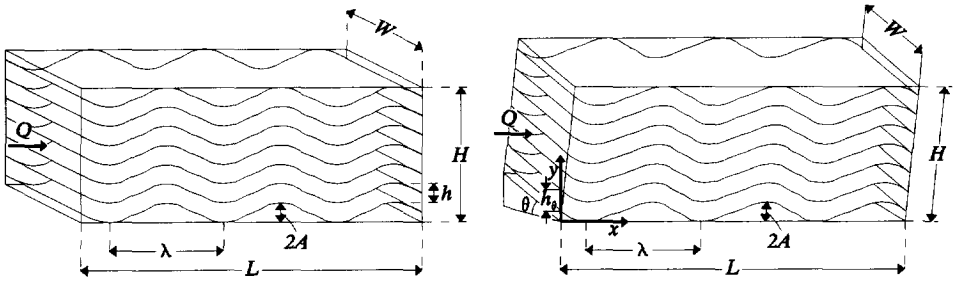

Figure (3-13) Corrugated plate separator (CPS).
Left: Horizontal. **Right:** Tilted.

Generally, the plate pack is inclined at an angle θ between 30 and 60 degrees. The oil film moves upward more or less perpendicularly to the water flow and is, in the case of corrugated plates, concentrated at the top of a corrugation. When the oil reaches the end of a corrugation, it rises to the oil-water interface where it can be removed. An even more important advantage is that solids settling down can be collected in the lower part of the separator, not clogging the channels.

Tilting the plate pack, however, affects the separation efficiency, because the droplets have to travel the vertical distance h_θ, which is given by:

$$h_\theta = \frac{h}{\cos\theta} = \frac{(H - nd)}{n\cos\theta} \tag{3-4-1}$$

Following the same procedure as in section 3.2.4, a new equation for D_c can be derived:

$$D_c = \sqrt{\frac{18\,Q\,\mu}{nLW(\rho_w - \rho_o)g\cos\theta}} \tag{3-4-2}$$

Also the following equation is valid:

$$\int_0^{h_\theta} v_x(x,y)\,dy = \frac{Q}{nW\cos\theta} \tag{3-4-3}$$

With the same procedure as given in appendix B, it can be demonstrated that the general separation efficiency function remains unchanged.

3.5 Oil concentration and particle size

In practice one is usually more interested in the total oil concentration in the effluent of a separator than in its critical droplet diameter.

The total oil concentration in the effluent of a separator depends both on D_c of the system and on the droplet-size distribution of the influx. If we characterize the cumulative oil concentration of the influx by a linear function [1] then:

$$C_{in,cum} = C_D\,D \tag{3-5-1}$$

where C_D is the oil concentration distribution constant. In practice, C_D has a value between about 2 and 8 ppm/μm [1]. The total oil concentration in the effluent then is:

$$C_{out} = C_D D_c\,10^{-6} \int_0^1 \frac{D}{D_c} d\eta = \frac{2}{3} C_D D_c \tag{3-5-2}$$

Note that $C_{out} \propto D_c$. From equation (3-2-27) we know that $D_c \propto (n\ L\ W)^{-1/2}$. Thus, theoretically, for a decrease of the effluent oil concentration of an existing separator by 50%, an increase of the specific area $n\ L\ W$ by 300% is needed.

3.6 Discussion and conclusions

The most important contribution of this chapter is the derivation of a generally applicable separation efficiency function. Besides predicting the oil concentration in the effluent of an oil-water separator more accurate, it provides insight into every sedimentation process which satisfies the conditions given in section 3.2.

Another finding, presented in section 3.3, is that corrugated plates do not improve the separation efficiency. Corrugated plates may promote coalescence of oil droplets due to flow velocity fluctuations. However, coalescence will only occur when the oil droplets are close together, thus when the oil concentration exceeds a certain value. This study, however, concentrates on processes concerning separation of oil-water mixtures with relatively low oil concentrations (<2000 ppm).

References

[1] Arnold, K. and Steward, M.: Surface production operations, Vol. 1, Design of oil-handling systems and facilities, Gulf Publishing Company, Houston, 1986.

[2] Bird, R., Steward, W.E. and Lightfoot, E.N.: Transport Phenomena, John Wiley & Sons, New York, 1960.

[3] Hoogendoorn, C.J. and Meer, T.H. van der, Fysische Transportverschijnselen II, Delftse Uitgevers Maatschappij, Delft, 1991.

Chapter 4

Gravity plate separators: numerical simulations and laboratory experiments

4.1 Introduction

This chapter deals with calculations and experiments on plate separators with flat as well as with corrugated plates. Section 4.2 describes the numerical simulations. The flow profiles of different plate configurations have been determined by means of a numerical model, the computer program Hydro Sepran. Using the results of Hydro Sepran, another computer program has been developed to determine the oil-water separation efficiency by computing the paths of the oil droplets towards the plate. Section 4.3 describes the laboratory experiments. Flow velocity profiles in straight as well as in corrugated channels were measured by means of Laser Doppler Anemometry. The separation efficiency as a function of droplet size was measured by means of a Laser Diffraction Based Particle Sizer. Results are given for different oily-water flow rates. These results have been compared with the general separation efficiency function (derived in chapter 3), and with the results of the numerical simulations.

4.2 Numerical simulations

4.2.1 Flow profiles

In order to investigate the separation performance of plate separators, the first step will be to determine the flow profiles. For straight channels (flat plates) there is plug flow at the beginning of the channel, which gradually develops into parabolic flow (see section 3.2.3). To determine the flow profile in corrugated channels, the computer program Hydro Sepran was used [1]. The Sepran package solves the mass balance and the Navier Stokes equations by means of the finite element method. For the flow between plates, it is assumed that the conditions of laminar, isothermal and incompressible flow pertain.

The output of the Hydro Sepran program consists of streamlines, velocity vectors and shear-stress contour lines. As an example, one of the resulting streamline plots is given in figure (4-1). It shows that the velocity-maximum shifts towards the inner curve of the corrugations. The values of the corresponding velocity vectors are used in a computer program which determines the separation efficiency. This will be treated in the next section.

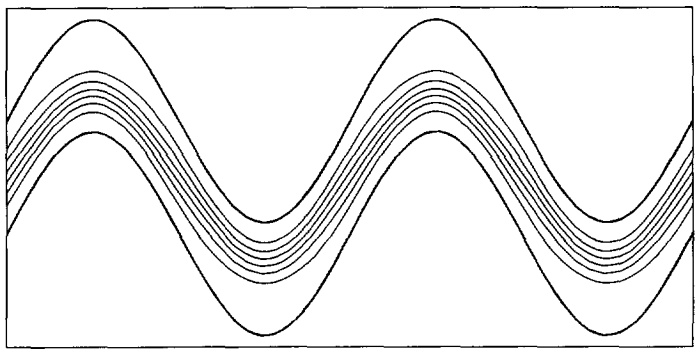

Figure (4-1) Streamlines in a channel of a plate separator with corrugated plates.

4.2.2 Separation efficiency

Figures (4-2) and (4-3) give results of calculated droplet paths in a **corrugated** channel for two different amplitudes of the corrugation. The thin lines represent the streamlines and the thick lines represent the droplet paths. The direction and value of the flow velocity were taken from the data generated by the program Hydro Sepran (section 4.2.1). The droplets' rising velocity was determined by equation (2-6):

$$v_t = \frac{(\rho_w - \rho_o)\, g\, D^2}{18\, \mu} \tag{4-1}$$

The lowest droplet path in all figures represents the path of the critical droplet diameter given by equation (3-2-27):

$$D_c = \sqrt{\frac{18\, Q\, \mu}{n\, L\, W\, (\rho_w - \rho_o)\, g}} \tag{4-2}$$

Each of the four other paths represents the path of a droplet with diameter D given by equation (3-2-44):

$$\eta = \left(\frac{D}{D_c}\right)^2 \qquad (0 \le D \le D_c)$$

for separation efficiencies η= 0.8; 0.6; 0.4 and 0.2. The starting position $y(x=0)$ of these droplets is given by:

$$\frac{\int_{y(x=0)}^{h} v_{x=0}(y)\,dy}{\int_{0}^{h} v_{x=0}(y)\,dy} = \eta = \left(\frac{D}{D_c}\right)^2 \qquad (4\text{-}3)$$

Figures (4-4) to (4-7) give the results of the numerical simulations in a **straight** channel. Basically, figures (4-4) to (4-7) show droplet paths for three different flow profiles **FP**:

FP_1: (plug flow) $$v_x(y) = \frac{Q}{n\,h\,W} \qquad (4\text{-}4)$$

FP_2: (parabolic flow) $$v_x(y) = \frac{6\,Q}{n\,h^3\,W}(yh - y^2) \qquad (4\text{-}5)$$

FP_3: (transition zone) $$v_x(y) = \frac{x_e - x}{x_e - x_s}\,FP_1 + \frac{x - x_s}{x_e - x_s}\,FP_2 \quad (x_s < x < x_e) \qquad (4\text{-}6)$$

where x_s and x_e are, respectively, the beginning and the end of the transition zone.

From the figures (4-2) to (4-7) it can be concluded that all droplets reach the upper plate at $x=L$, confirming the theory described in chapter 3. Consequently, the simulations also predict identical separation efficiencies for either flat or corrugated plates.

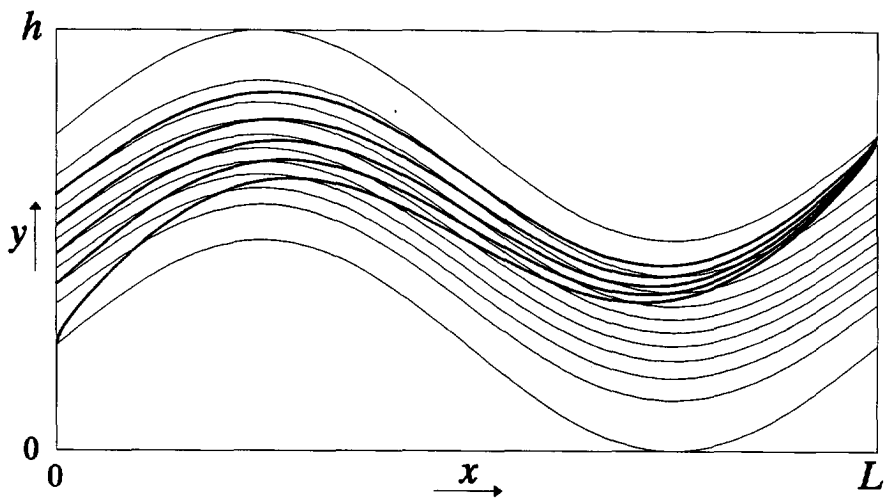

Figure (4-2) Paths of droplets in a corrugated channel with $A=½h$ and $\lambda=L$.
Thin lines: streamlines. Thick lines: droplet paths (η= 1 {lowest path}; 0.8; 0.6; 0.4; 0.2 {uppermost path}).

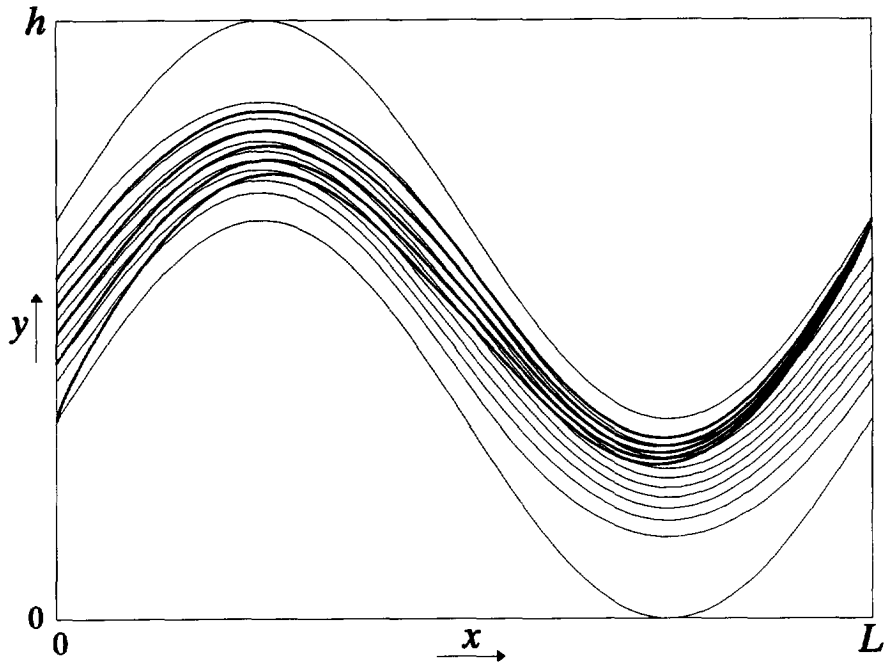

Figure (4-3) Paths of droplets in a corrugated channel with $A=h$, $\lambda=L$ and $\eta=$ 0.2 to 1.

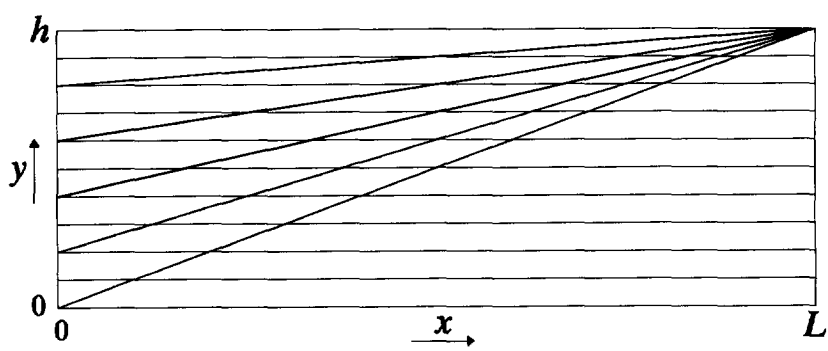

Figure (4-4) Paths of droplets in **plug** flow (FP_1).
Thin lines: streamlines. Thick lines: droplet paths ($\eta=$ 1 {lowest path}; 0.8; 0.6; 0.4; 0.2 {uppermost path}).

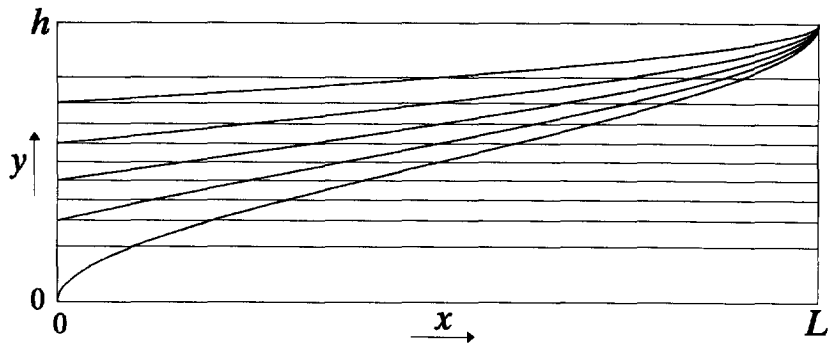

Figure (4-5) Paths of droplets in **parabolic** flow (FP_2) for $\eta = 0.2$ to 1.

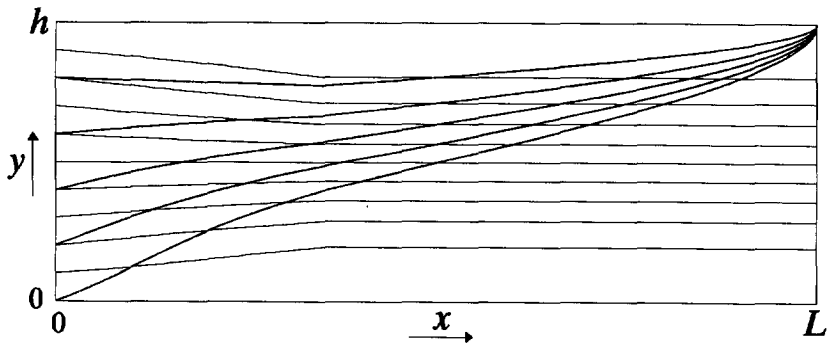

Figure (4-6) Paths of droplets in a transition/parabolic flow for x_s=0, x_c=**0.35***L* and $\eta = 0.2$ to 1.

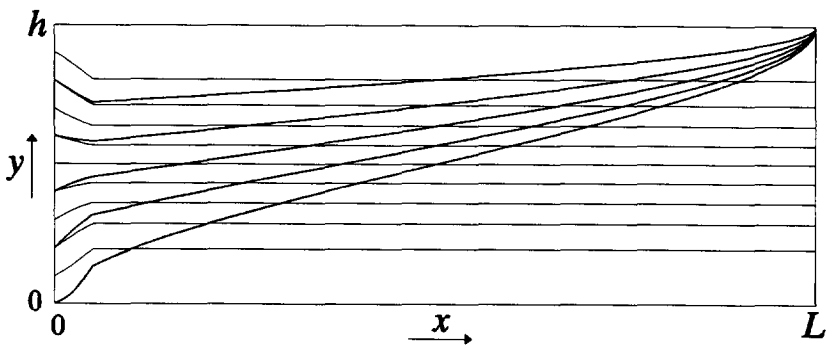

Figure (4-7) Paths of droplets in a transition/parabolic flow for x_s=0, x_c=**0.05***L* and $\eta = 0.2$ to 1.

4.3 Experimental verification

4.3.1 Introduction

Two types of experiments were carried out. The objective of the first type was to determine the flow velocity profiles between two corrugated plates. The objective of the second type of experiment was to determine the separation efficiency as a function of oil droplet size. The experiments were carried out with flat as well as with corrugated plates.

A simplified flow sheet of the experimental set up is shown in figure (4-8). The flow velocities were measured by means of a laser doppler anemometer (LDA). To determine the separation efficiency as a function of oil droplet size, a laser-diffraction based particle sizer (LPS) in combination with an oil-content analyzer based on ultra-violet light absorption were used. For the LPS an in-line measuring cell was developed and constructed. Appendix C describes this measuring cell and the rest of the set-up in detail.

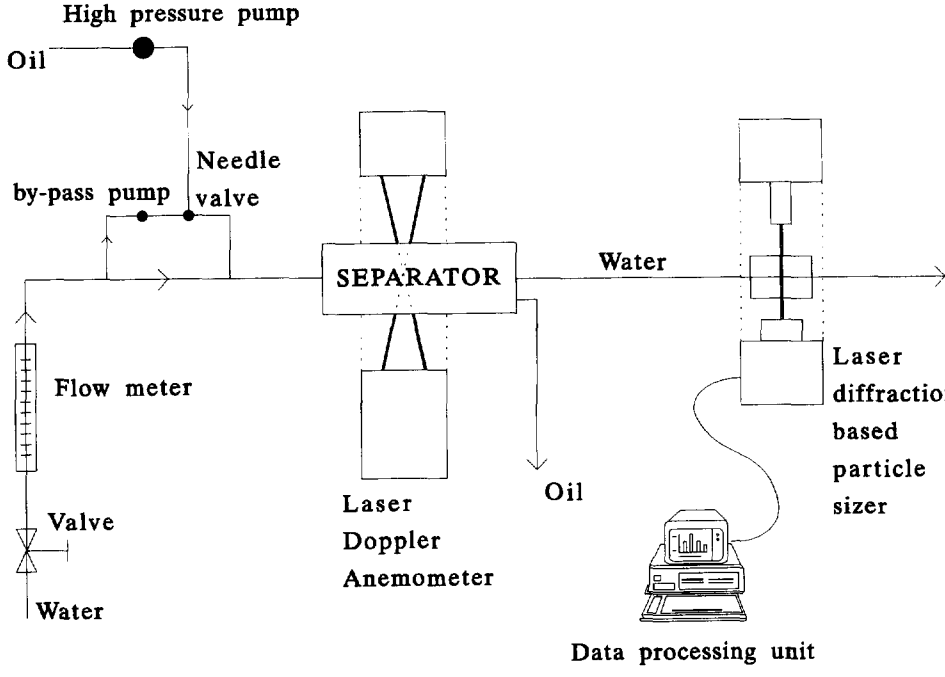

Figure (4-8) Simplified flow sheet of the experimental set-up.

4.3.2 Flow velocity profiles

The experiments were carried out on two experimental plate separators, one with corrugated plates and one with flat plates.

The corrugated plate separator has the following properties [1]:

- Number of channels	n:	1 (top and bottom plates only)
- Plate length	L:	1.50 m
- Plate width	W:	0.50 m
- Channel height	h:	0.02 m
- Amplitude	A:	0.10 m
- Wavelength	λ:	0.35 m

The properties of the flat plate separator are [1]:

- Number of channels	n:	1 (top and bottom plates only)
- Plate length	L:	1.50 m
- Plate width	W:	0.50 m
- Channel height	h:	0.01 m

The flow velocities have been measured in the direction of flow and parallel to the plates, at points on a line perpendicular to the plate surface.

Figures (4-9) and (4-10) show the typical velocity profiles. Measurements were taken at the wave peak and the wave trough. The figures show that the velocity maximum shifts towards the inner curve of the corrugations.

Figure (4-11) presents the velocity profile in the straight channel. It confirms that the flow profile is parabolic.

The LDA measurements were carried out at variable flow rates, to be able to correlate the numerical simulations with the LDA experiments. The velocity profiles show that all wave peaks and all wave troughs, respectively, have the same velocity profile. Plug flow was not detected; the parabolic velocity profile develops very rapidly. It was established that in our system the transition to turbulent flow occurs at Reynolds numbers around 1200.

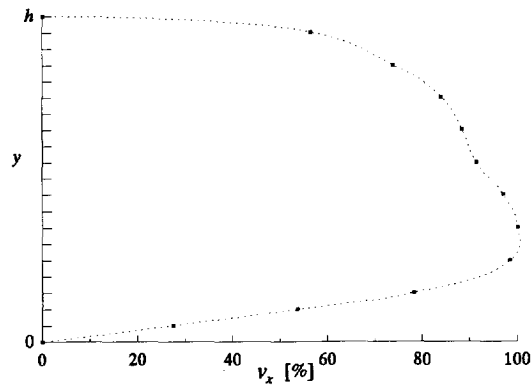

Figure (4-9) Flow profile at a wave peak.

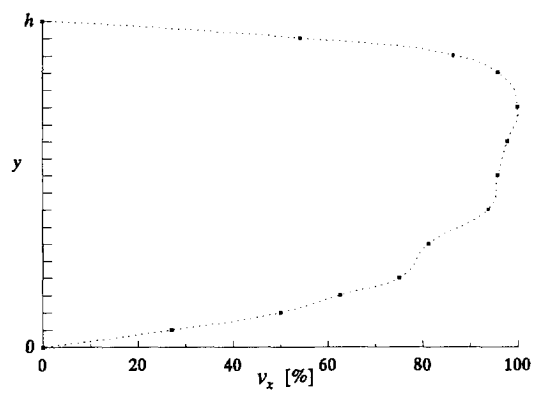

Figure (4-10) Flow profile at a wave trough.

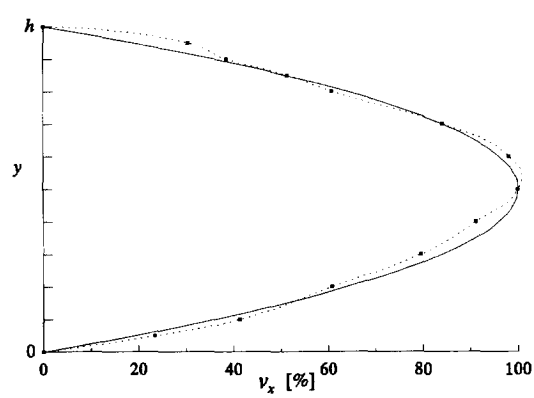

Figure (4-11) Flow profile in a straight channel.
Dotted line: experimental.
Continuous line: theory.

4.3.3 Oil-water separation efficiency experiments

Two experimental plate separators were constructed by Burgess-Manning Europe. One with flat plates and one with corrugated plates. The respective outer dimensions, as well as the plate thickness and number of channels, were the identical. The dimensions of these separators were:

- Channel length	L:	0.2 m
- Channel width	W:	0.135 m (average)
- Channel height	h:	0.0146 m
- Number of channels	n:	11
- Wave length	λ:	0.05 m (corrugated plate separator)
- Amplitude	A:	0.00375 m (corrugated plate separator)
- Tilt angle	θ:	45 degrees

Figure (4-12) shows a sketch of the plate separator. The central part contains a plate pack. There are two central parts. One with flat plates and one with corrugated plates. The stream divider in the inlet section consists of two perforated plates (the dashed and the dotted line in the figure). Their performance has been verified by the injection of dye into clean water flowing steadily through the separator.

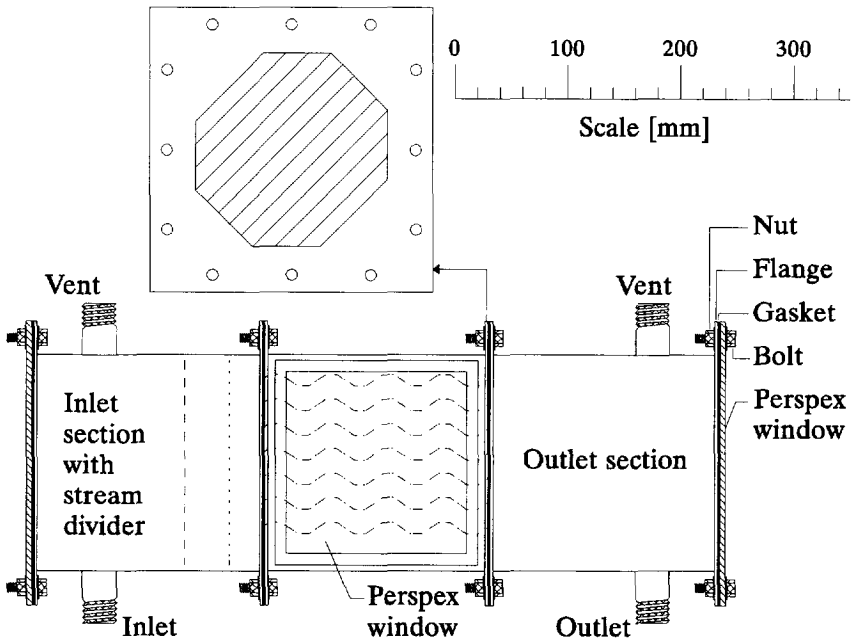

Figure (4-12) Drawing of the Burgess Manning plate separator.

The parameters of the used oil-water mixture were:

- Temperature:	T:	287 K ($\Rightarrow \mu_w$=0.00115 kg/ms)
- Density of water	ρ_w:	1000 kg/m^3
- Density of oil	ρ_o:	899 kg/m^3 (Shell Omala 220)
- Oil-water interfacial tension	σ:	0.010 N/m
- Flow rate (water)	Q:	0.2 to 1 m^3/hr (in steps of 0.1 m^3/hr), (5.55 10^{-5} to 2.78 10^{-4} m^3/s)
- Flow rate (oil)	Q_{oil}:	0.6 10^{-3} m^3/hr (1.67 10^{-7} m^3/s); constant

According to equation (3-4-2) the critical droplet diameter D_c of this system is:

$$D_c = 0.00975\sqrt{Q} \qquad (D_c\text{: [m]} \ \wedge \ Q\text{: [m}^3\text{/s]})$$

or

$$D_c = 162.56\sqrt{Q} \qquad (D_c\text{: [}\mu\text{m]} \ \wedge \ Q\text{: [m}^3\text{/hr]}) \qquad (4\text{-}7)$$

Figures (4-13) to (4-21) show the results of the experiments. In each graph a theoretical line is drawn which is calculated from the general separation efficiency function and the corresponding value of D_c, given by equation (4-7).

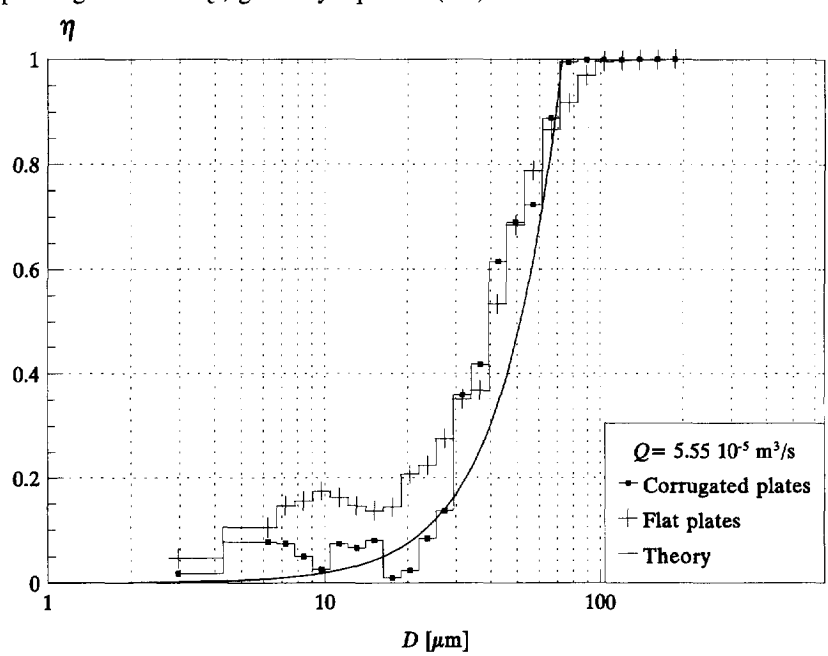

Figure (4-13) Separation efficiency as a function of the droplet size (Q=0.2 m^3/hr, D_c=72.7 μm).

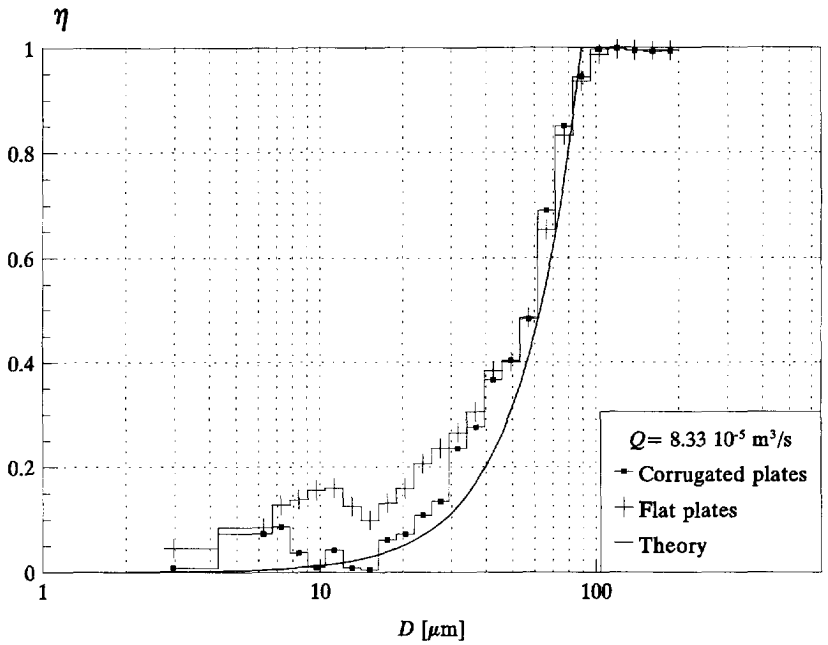

Figure (4-14) Separation efficiency as a function of the droplet size (Q=0.3 m³/hr, D_c=89.0 μm).

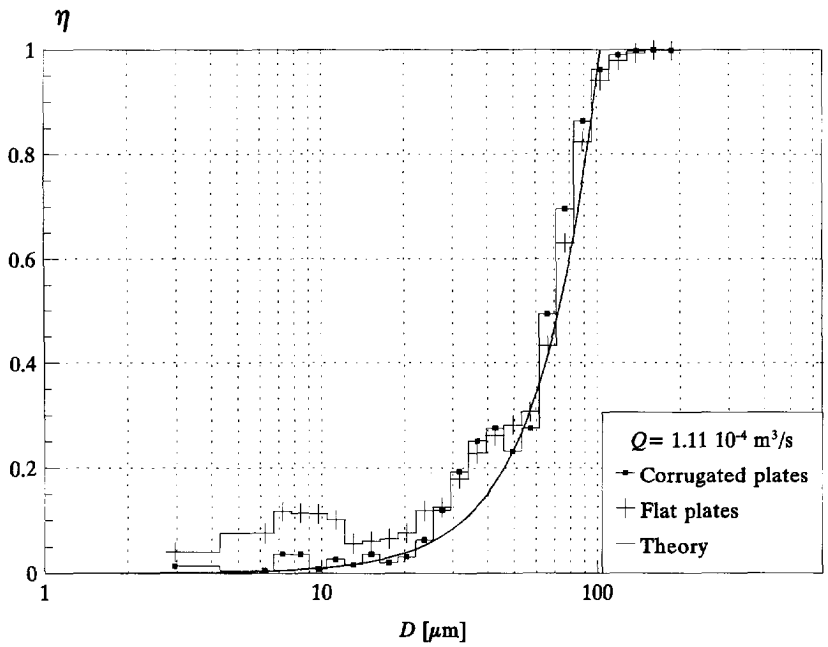

Figure (4-15) Separation efficiency as a function of the droplet size (Q=0.4 m³/hr, D_c=102.8 μm).

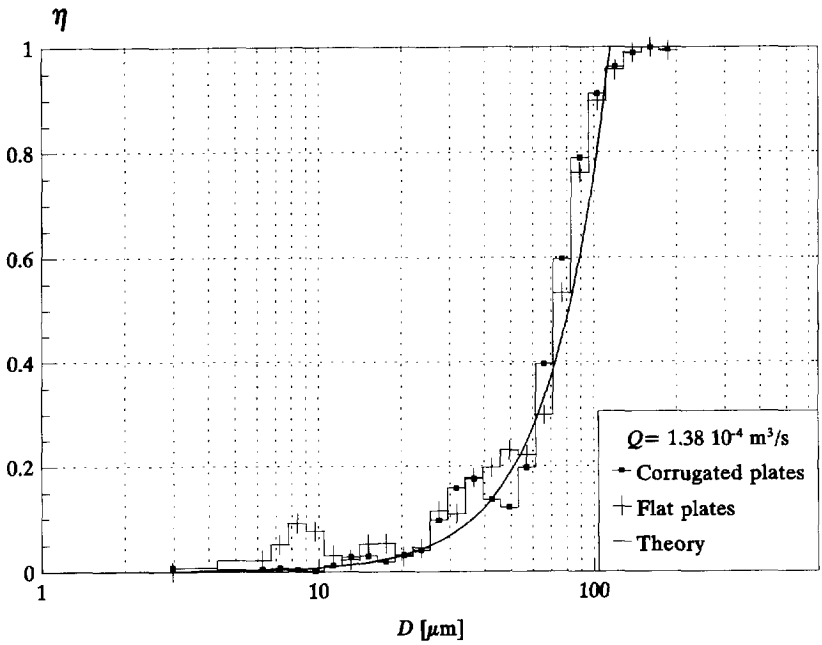

Figure (4-16) Separation efficiency as a function of the droplet size (Q=0.5 m^3/hr, D_c=114.9 μm).

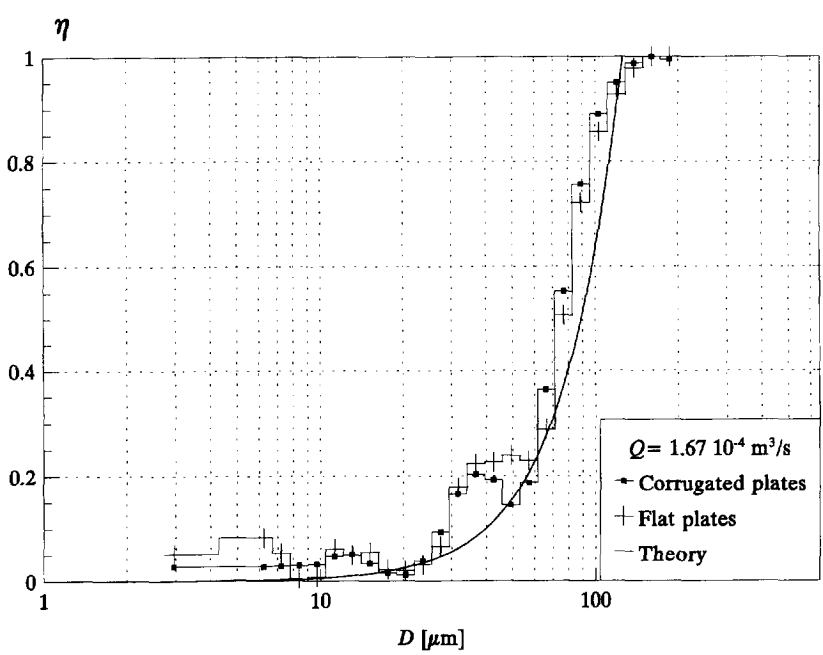

Figure (4-17) Separation efficiency as a function of the droplet size (Q=0.6 m^3/hr, D_c=125.9 μm).

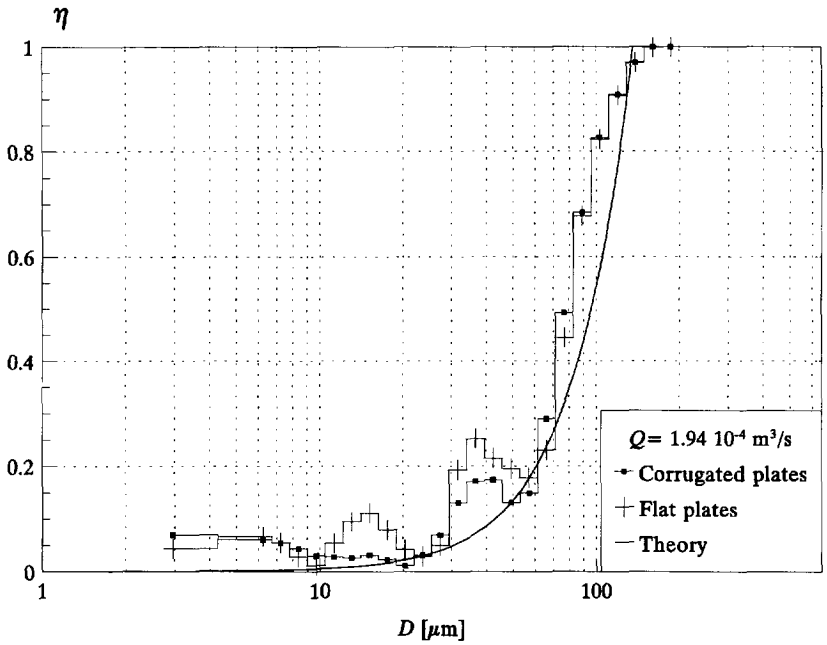

Figure (4-18) Separation efficiency as a function of the droplet size (Q=0.7 m³/hr, D_c=136.0 μm).

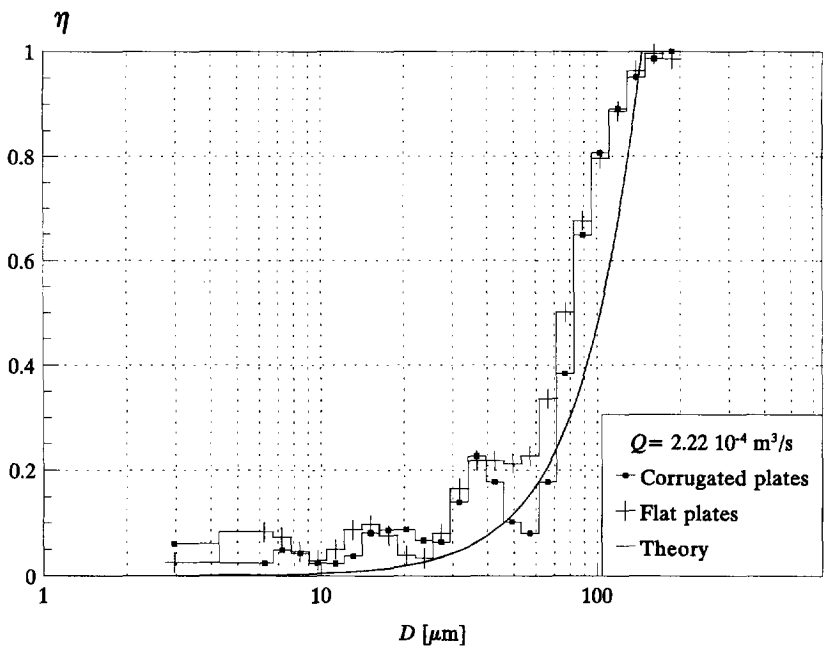

Figure (4-19) Separation efficiency as a function of the droplet size (Q=0.8 m³/hr, D_c=145.4 μm).

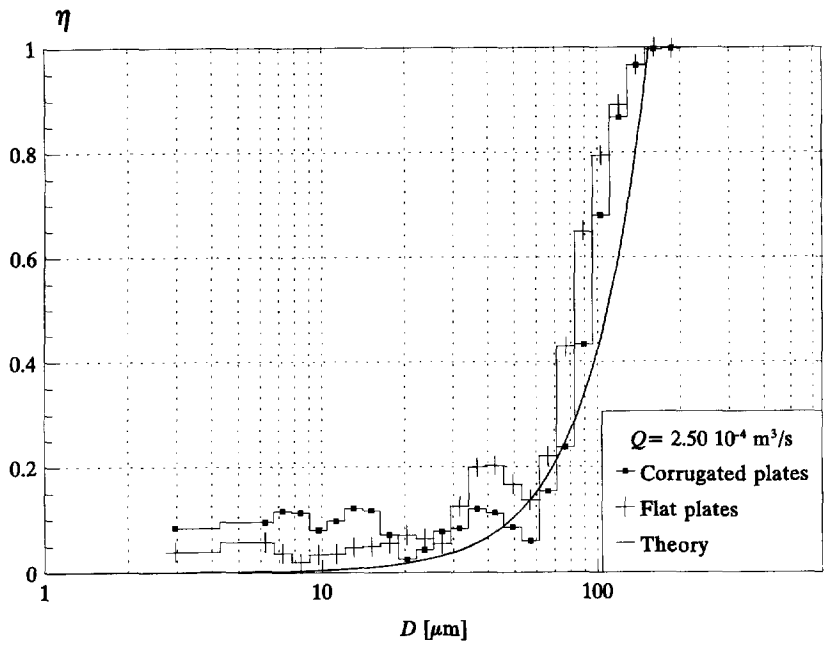

Figure (4-20) Separation efficiency as a function of the droplet size (Q=0.9 m^3/hr, D_c=154.2 μm).

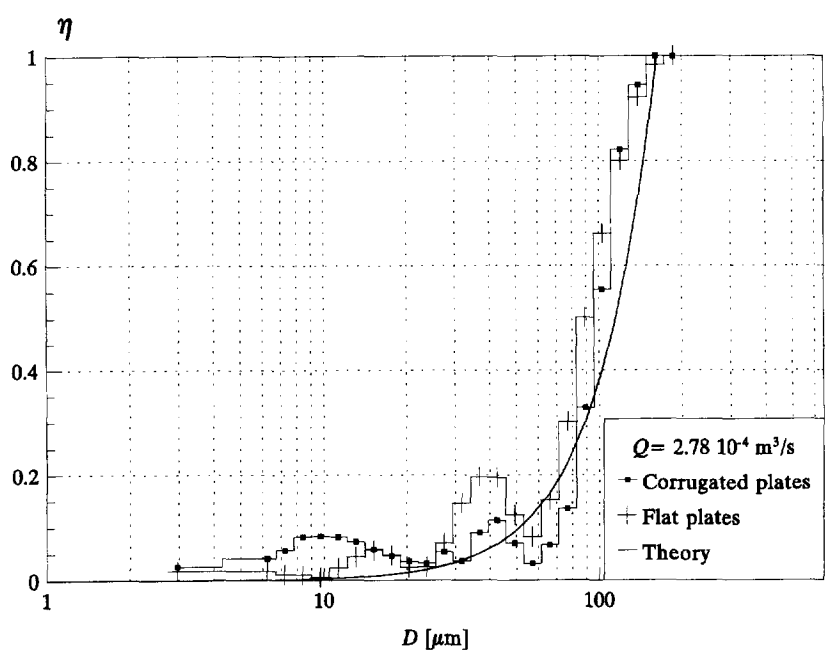

Figure (4-21) Separation efficiency as a function of the droplet size (Q=1.0 m^3/hr, D_c=162.5 μm).

4.4 Conclusions

The results of the numerical simulations are in agreement with the theory described in chapter 3. The graphs of the laboratory experiments show that:

- the measured flow profiles conform reasonably well to the theoretical and numerical profiles,
- the separation performance of flat plates is practically equal to that of corrugated plates. Only at higher flow rates, flat plates achieve marginally better results than corrugated plates,
- the general separation efficiency function corresponds well with the measured values.

Chapter 7 presents a discussion of the results of the experiments and the discrepancies between the theory and these results.

References

[1] Groenendijk, M.: Oil-water separation and flow phenomena in corrugated channels, Graduation report for Delft University of Technology, Faculty of Mining and Petroleum Engineering, April 1989.

Chapter 5

Plate packs for rotating separators

5.1 Introduction

To enhance the separation efficiency, centrifuges are usually provided with internals. These internals have the same function as the plate packs in a gravity plate separator and consist in most cases of a stack of conical discs. Appendix D describes the design of a disc-stacked centrifuge and the results of the laboratory experiments carried out on such a centrifuge.

Investigations on gravity plate separators prompted the idea to develop an analogous plate pack for rotating separators. The plates are installed parallel to the axis of rotation (see figure (5-1)) and can be either flat or curved. There are two basic configurations:

- the Parallel Plate Centrifuge (PPC) with plates of uniform thickness, and
- the Parallel Channel Centrifuge (PCC) with uniform distance between the plates.

A PPC-design with flat plates is sometimes used in decanter centrifuges for separation of solids from a liquid.

After a short introduction on the fundamentals of a centrifuge, the dimensions and other relevant parameters of the PPC and PCC will be discussed. Thereafter, some important hydrodynamic aspects will be described.

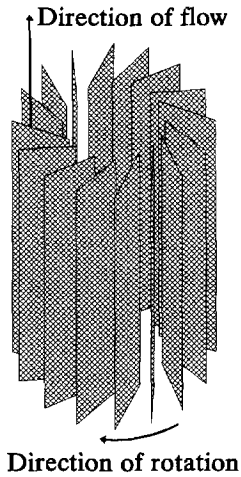

Figure (5-1)
The arrangement of plates in a parallel plate centrifuge.

5.2 Centrifugation

The basic function of all oil-water separators, including centrifuges, is to move the oil droplets which are present in the continuous phase (water) to an interface. The radial settling velocity of the droplets can be derived from Stokes' law: it is proportional to the centrifugal acceleration (see section 2.4, equation (2-9)). We refer to chapter 2 for the theory concerning the behaviour of oil droplets dispersed in water in a centrifugal field. The results of that chapter have been used to determine the theoretical performance of a centrifuge.

The part of the centrifuge where the oil and water are separated is called the **bowl**. Figure (5-2) shows the main parts of the bowl. The bowl body and the bowl hood, constituting the bowl casing, are held together by the large lock ring. In the bowl are located the distributor and the disc stack or plate pack, through which the oily water is passed and wherein separation takes place. Uppermost in the bowl casing lies the top disc, which leads the oil phase to its top where it is discharged. The water phase leaves the bowl through the gravity disc, which is clamped to the bowl hood top by the small lock ring.

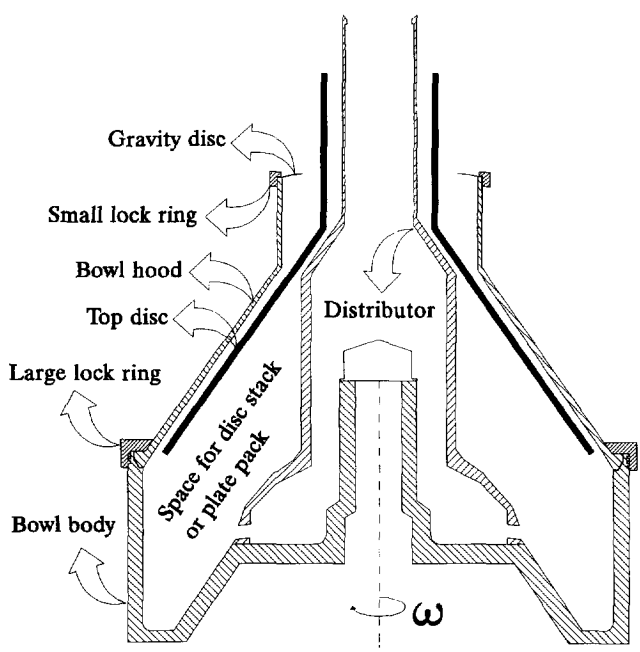

Figure (5-2) The main parts of the centrifuge bowl.

In order to obtain optimum separation results, the oil-water interface has to be located at an adequate position. For the continuous operation it is necessary to keep the separated phases

in a condition of hydrostatic balance. From figure (5-3) can be derived that [2]:

$$\rho_o(R_{int}^2 - R_{oil}^2) = \rho_w(R_{int}^2 - R_{water}^2) \quad \textbf{(5-1)}$$

which is based upon solid body rotation, assuming zero pressure drop over the height of the bowl and neglecting the acceleration of gravity. This equation demonstrates that the position of the interface is only determined by the outlet radii of oil and water and by the densities of the two phases, and not by operating conditions. The position of the interface is established by adjusting R_{water} so that R_{int} complies to the desired value calculated by equation (5-1). Physically, the radius R_{water} can be set by means of an interchangeable ring, the so-called gravity disc, which is screwed on the centrifuge bowl near the water outlet.

Van der Linden [3] found experimentally that equation (5-1) underestimates the interface radius, because it does not take into account the pressure drop of the two phases in passing through the stack of discs and discharge passages. For practical purposes the calculated gravity disc diameter as determined by equation (5-1) serves as a starting point and the optimum interface position is then found by trial and error.

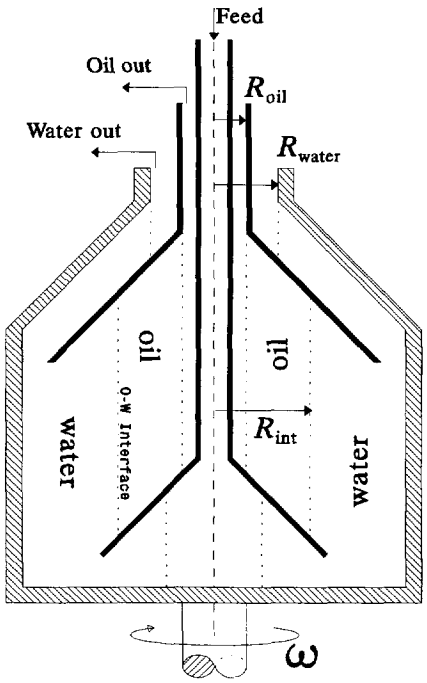

Figure (5-3) Interface position. R_{oil}: radius of the oil outlet port, R_{water}: radius of the water outlet port, R_{int}: radius of the oil-water interface.

5.3 The parallel plate centrifuge and the parallel channel centrifuge

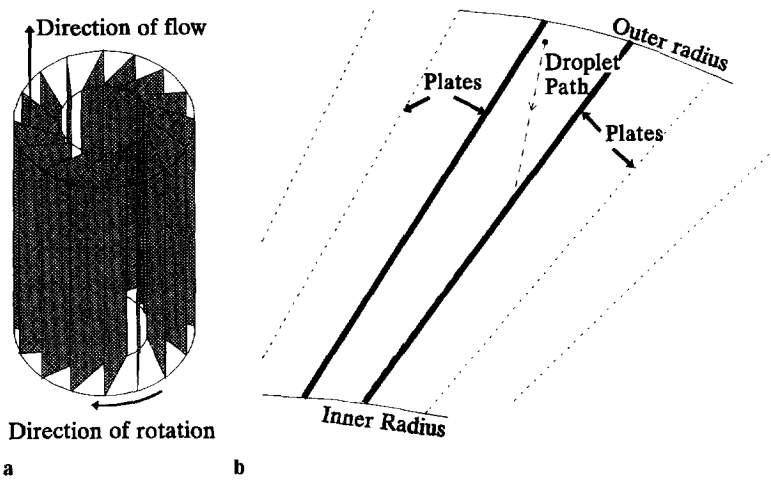

Figure (5-4) Parallel Plate Centrifuge: **a** Basic principle, **b** Radial path of a droplet.

The plate packed centrifuge contains a pack of plates parallel to the axis of rotation (see figure (5-4)a). The idea behind this design is to prevent the occurrence of counter-current flow. This can only be realized when the main water flow is directed parallel to the axis of rotation, while the oil droplets move radially towards the axis in the centrifugal field. To reduce the settling distance of oil droplets, the plates are positioned at an angle relative to the radius. The oily water enters the plate pack at the bottom and flows upwards. Radially moving droplets will make contact with a plate, where they are collected (see figure (5-4)b). The intercepted oil is subsequently forced to flow along the plate surface to the inner radius of the pack of plates, from where it can flow out of the centrifuge via the central channels. At the upper end of the pack there will be separate flows of oil and water.

In a **Parallel Plate Centrifuge** (PPC), plates have a uniform thickness; the plate distance is not constant but increases towards the outer radius. Droplets entering the pack near the outer radius have to travel a longer distance to reach the surface of a plate than droplets entering the pack near the inner radius. Since the continuous-phase flow velocity increases with plate distance -the pressure drop due to wall friction decreases-, the liquid which enters the plate pack near the outer radius will have a relatively low residence time. Together with the longer settling distance, this will negatively affect the separation efficiency near the outer radius. On the other hand, the radial settling velocity, which is proportional to the distance of the droplet to the axis of rotation (equation (2-9)), will be larger at the outer radius. As a result,

the dispersed phase will probably not be evenly separated from the continuous phase. One solution to this problem is to use curved plates instead of flat plates. The variation in plate distance can be reduced, which also reduces the variation of the droplet travelling distance.

Another option is a design in which the plate distance is uniform throughout the pack, rather than the plate thickness. This type of centrifuge is called the **Parallel Channel Centrifuge** (PCC). The channels can be either straight or curved.

Figure (5-5) shows top views of the four plate pack options. In principle, flat plate packs of either uniform plate thickness or plate distance can be considered as curved plate packs with infinite radii curvature. From a practical point of view, however, curved plates or channels require a different construction method than straight plates or channels. Therefore the four types will be treated separately.

In order to carry out calculations on these plate packs, the shape of the curve has to be defined in the form of a mathematical equation. The easiest way is to describe the curve by the arc of a circle. It will be shown in this chapter that this will lead to satisfactory results.

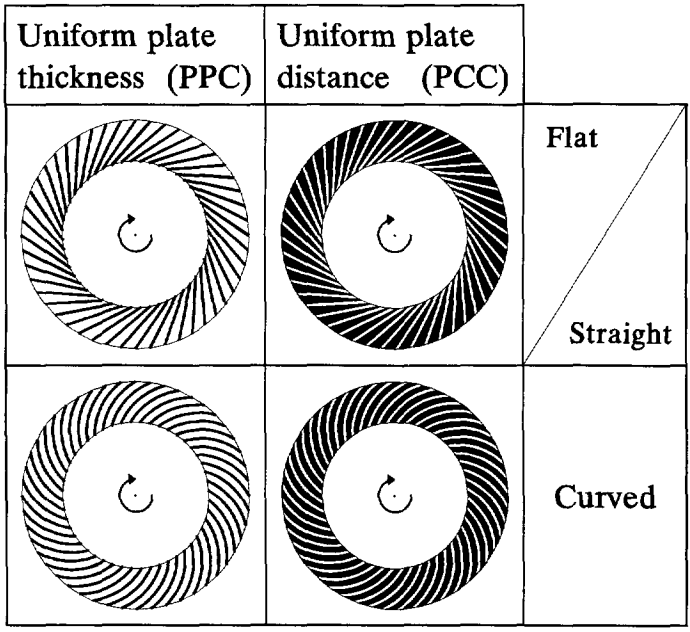

Figure (5-5) Top view of the four different types of Plate Packs.

5.4 Characteristics of plate packed centrifuges

5.4.1 Dimensions of the parallel plate centrifuge and the parallel channel centrifuge

The dimensions of the PPC (figure (5-6)) and of the PCC (figure (5-7)) are characterized by the following parameters:

DIMENSIONS:	PPC	PCC
Length	L	
Outer radius	R_o	
Inner radius	R_i	
Radius of plate curvature	R_p	
Radius of channel curvature		R_c
Channel angle	β	
Plate thickness	d	
Plate distance	h	
Number of plates/channels	n	

In a PPC, the minimum plate distance h_{min} (figure (5-6)**b**) is determined by the combination of R_o, R_i, R_p, β, d and n.

In a PCC, the minimum plate thickness d_{min} (figure (5-7)**b**) is determined by the combination of R_o, R_i, R_c, β, h and n.

If h_{min} (PPC) is too small, clogging of the pack with solid particles may occur. Therefore a certain minimum value should be maintained. In existing commercial disc stacked centrifuges the minimum plate distance is about 0.3 mm. Therefore a minimum value of 0.3 mm was used as a starting point in the simulation runs and the design of the experimental pack of plates.

The stiffness of the plates is determined by d (PPC) and d_{min} (PCC). Therefore a certain minimum value of d or d_{min} should be maintained to avoid excessive bending of the plates.

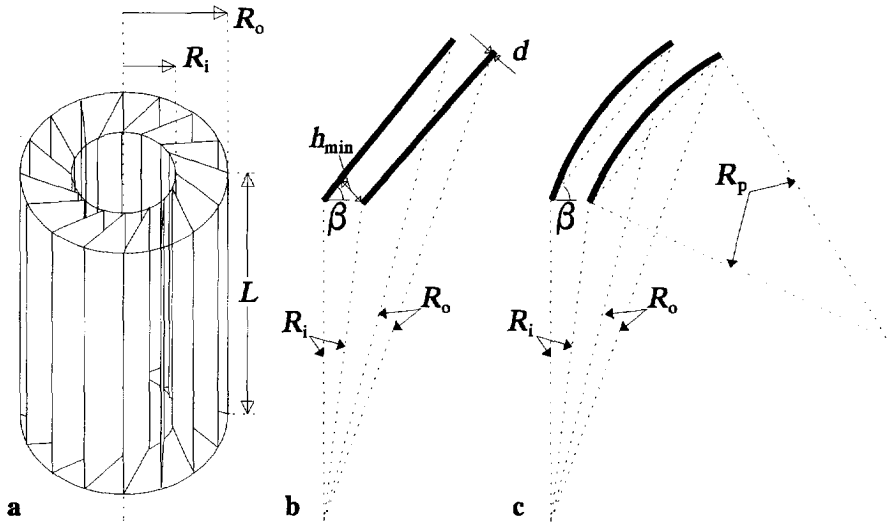

Figure (5-6) Dimensions of the parallel plate centrifuge (**PPC**).

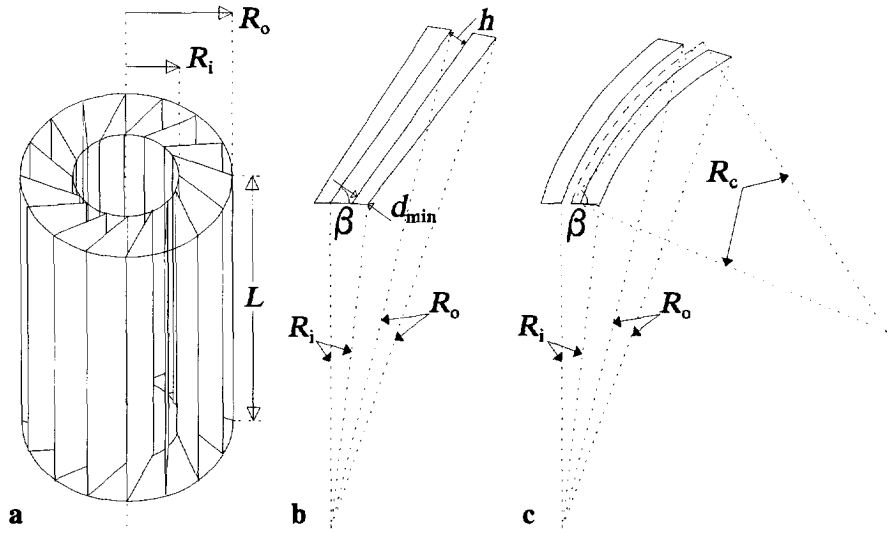

Figure (5-7) Dimensions of the parallel channel centrifuge (**PCC**).

5.4.2 Channel shape of a parallel plate centrifuge (PPC)

The channel shape is one of the most important design criteria of the plate packed centrifuge. It determines the path and the velocity of the oil droplets, and greatly influences the separation efficiency.

If the flow rate is assumed to be the same in all channels, only one channel needs to be considered. Figure (5-8) shows a channel of a PPC. The channel is bounded by two plates, the outer radius, and the inner radius of the pack.

The boundary $\mathbf{B_1}$ related to plate P_1 is defined by:

$$B_1: \quad (x-a_1)^2 + (y-b_1)^2 = R_p^2 \tag{5-2}$$

and the boundary $\mathbf{B_2}$ related to plate P_2 is given by:

$$B_2: \quad (x-a_2)^2 + (y-b_2)^2 = (R_p-d)^2 \tag{5-3}$$

The remaining boundaries related to the outer and inner radii (R_o and R_i) of the pack are by defined, respectively:

$$x^2 + y^2 = R_i^2 \quad \wedge \quad x^2 + y^2 = R_o^2 \tag{5-4}$$

To simplify the calculations, the boundaries $\mathbf{B_3}$ and $\mathbf{B_4}$ are be described by:

$$B_3: \; x = 0 \quad \wedge \quad B_4: \; x = R_2 \tag{5-5}$$

ignoring the channel volumes at the left of $\mathbf{B_3}$ and at the right of $\mathbf{B_4}$. Observing figure (5-8), we see that these volumes seem to take up a considerable amount of the total volume. The validity of neglecting them could be questioned. However, it will be shown that for the optimum PPC configuration the sum of these volumes is less than 1% of the total volume because the plate distance is much smaller than the width of the plate pack. This width is equal to the distance from R_i to R_o along the surface of a plate.

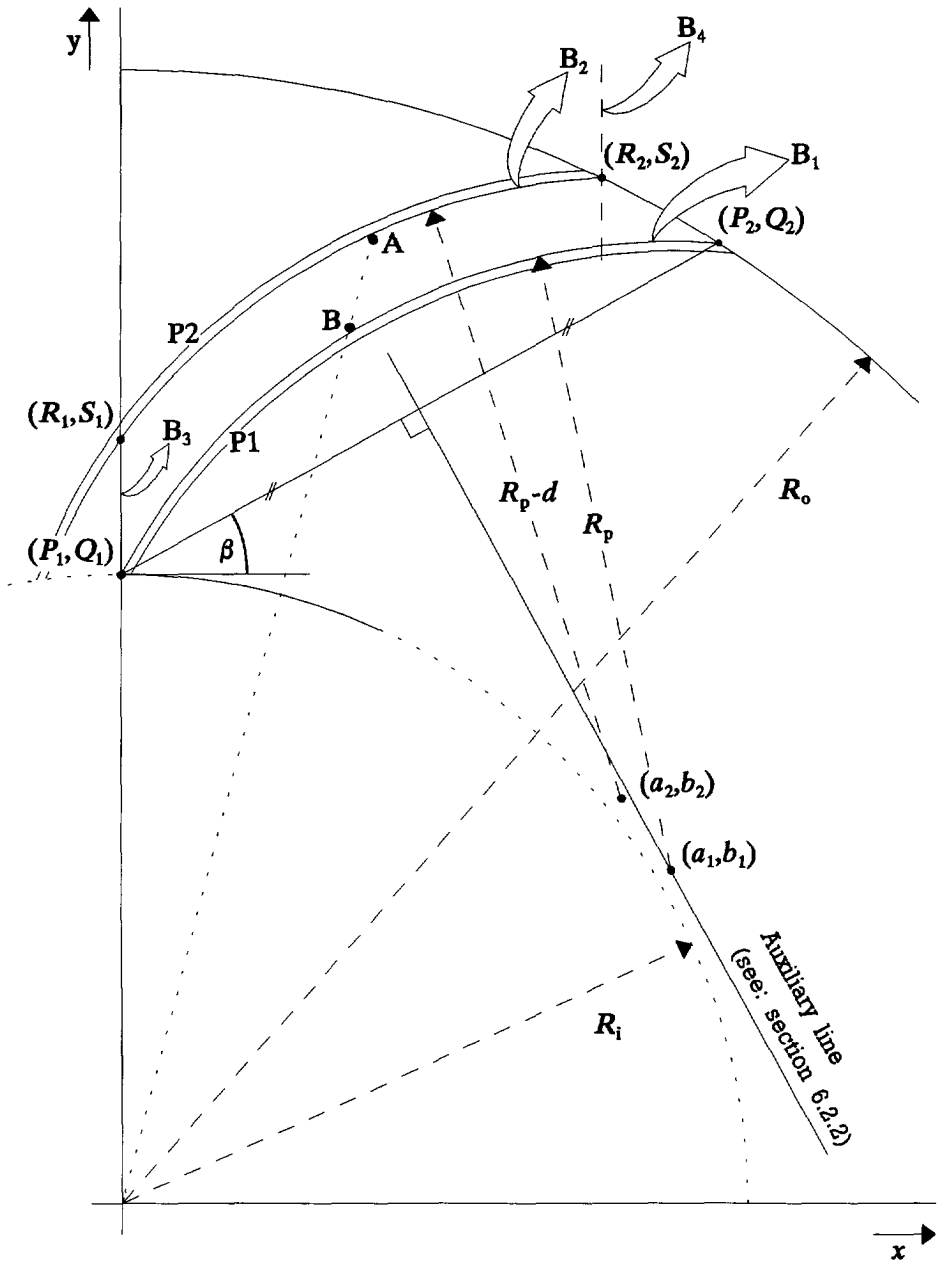

Figure (5-8) Dimensions of a channel in a parallel plate centrifuge (**PPC**).

5.4.3 Channel shape of a parallel channel centrifuge (PCC)

The description of the channel shape of the PCC is for a large part analogous to that of the PPC. Therefore, this section treats only the differences between the two types.

Figure (5-9) shows a channel of a PCC. The channel is bounded by its two radii and by the outer and inner radius of the pack. The first two boundaries are given by:

$$(x-a_1)^2 + (y-b_1)^2 = (R_c - \tfrac{1}{2}h)^2 \qquad (5\text{-}6)$$

and:

$$(x-a_1)^2 + (y-b_1)^2 = (R_c + \tfrac{1}{2}h)^2 \qquad (5\text{-}7)$$

For the same reason as for the PPC, the other two boundaries are given by:

$$x = 0 \quad \wedge \quad x = R_2 \qquad (5\text{-}8)$$

5.5 Hydrodynamic aspects of plate packed centrifuges

For the hydrodynamic behaviour of an oily-water mixture flowing through plate packed centrifuges, the following assumptions are made:

- laminar flow exists between the plates,
- the flow characteristics of oily water are those of a one-phase flow,
- all channels have the same flow rate and oil droplet distribution,
- when calculating the travelling distance of an oil droplet, the diameter of this droplet is neglected.

5.5.1 Path and velocity of an oil droplet

Irrespective of the plate pack configuration -either parallel plates (PPC) or parallel channels (PCC)- the following expressions can be derived with respect to path and velocity of an oil droplet entering the plate pack.

Assume a droplet entering the plate pack at point $A=(x_A,y_A)$. Due to centrifugal forces and

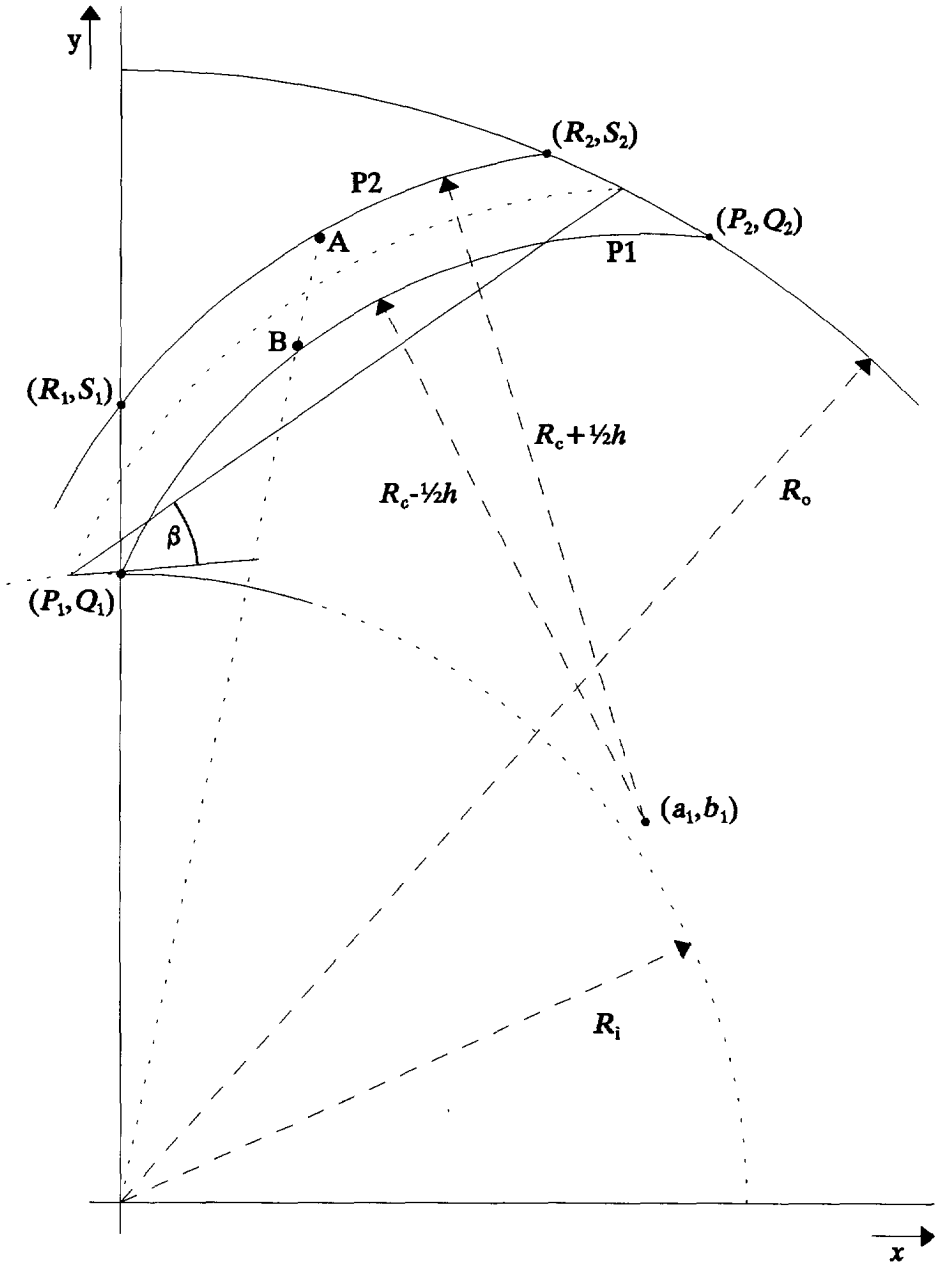

Figure (5-9) Dimensions of a channel in a parallel channel centrifuge (PCC).

neglecting the Coriolis force (see section 5.7), the droplet will travel along a straight line towards point B. This straight line is given by:

$$y = \frac{y_A}{x_A} x \tag{5-9}$$

The velocity of the droplet is not constant, but decreases with its distance from the axis of rotation (equation (2-9)). Thus:

$$v_{tr} = \frac{(\rho_w - \rho_o)\,\omega^2 D^2}{18\,\mu} \sqrt{x^2 + y^2} \tag{5-10}$$

The time to travel from point A to B is:

$$t_{AB} = \ln\left(\frac{\sqrt{x_A^2 + y_A^2}}{\sqrt{x_B^2 + y_B^2}}\right) \frac{18\,\mu}{(\rho_w - \rho_o)\,\omega^2 D^2} \tag{5-11}$$

Assume a droplet entering the plate pack at a position (point A) between the points (R_1,S_1) and (R_2,S_2) and near the boundary related to plate P2 (see figure (5-8)). If this droplet reaches point B at the end of the plate pack, its diameter will be the critical droplet diameter D_c. However, the path length as well as t_{AB} vary with the position of point A. This implies that D_c will probably not have the same value for different values of x. The critical droplet diameter must therefore be given as $D_c(x)$, where $0 < x < R_2$.

5.5.2 Flow velocity and residence time of the continuous phase

In a parallel plate centrifuge with flat plates, the plate distance increases with distance from the axis of rotation. An equation for the flow velocity of a fluid in a circular sector is given by Ward-Smith [5]. For small values of ϕ (see figure (5-10)) the flow velocity can be expressed as:

$$v_F \approx -\frac{1}{\mu}\frac{dp}{dz}\frac{1}{4} r^2 \left(\frac{\cos(2\psi)}{\cos(2\phi)} - 1\right) \tag{5-12}$$

Because:

$$h \propto r \tag{5-13}$$

this results in the following average velocity for a PPC at a location with plate distance h:

$$v_f \approx \frac{1}{h}\int_{-\phi}^{+\phi} v_F \, d\phi \approx \xi h^2 \qquad \text{(PPC)} \qquad \textbf{(5-14)}$$

The average residence time of the fluid at a location with plate distance h is therefore given by:

$$t_{res}(x) \approx \frac{L}{\xi \, h^2(x)} \qquad \text{(PPC)} \qquad \textbf{(5-15)}$$

In case of a parallel channel centrifuge the plate distance h is uniform for $0<x<R_2$. The average flow velocity for a droplet with the critical diameter is the same for any entrance position of that specific droplet. The residence time of all these droplets is given by:

$$t_{res} = n \, L \left(\int_0^{x=R_2} y(B_2)\,dx - \int_0^{x=R_2} y(B_1)\,dx \right) Q^{-1} \qquad \text{(PCC)} \qquad \textbf{(5-16)}$$

which simplifies the calculations concerning the hydrodynamics and performance for PCC's.

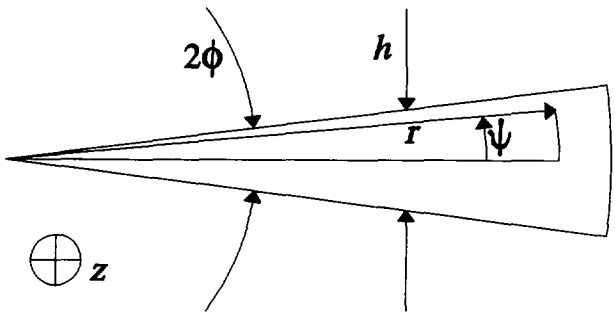

Figure (5-10) Dimensions of a circular sector.

5.6 Direction of rotation

The Coriolis force causes a droplet to deviate from the path defined by equation (5-9), in which the effect of this force is not taken into account. This path is represented by the straight line in figure (5-11). The dotted line represents the path when the Coriolis force is taken into account and the direction of rotation is counter-clockwise. The dashed line represents the path when the Coriolis force is taken into account and the direction of rotation is clockwise. This means that if the Coriolis force plays a significant role, the path length is dependent on the direction of rotation. In this case clockwise rotation results in a shorter path length than counter-clockwise rotation, hence clockwise rotation achieves a higher separation efficiency. The model described in chapter 6 ignores the Coriolis force, which results in somewhat lower theoretical separation efficiencies. In section 2.5 the relative influence of the Coriolis force has been derived (see: equation (2-14)). This equation gives the ratio between the droplet velocity by the Coriolis force (v_{cor}) and the droplet velocity according to Stokes' law (v_{tr}; see equation (2-9)). Figure (5-12) shows this ratio as a function of droplet size. The values of the parameters are those used in the simulations and in the experiments: ρ_o=900 kg/m^3, ω=785 rad/s and μ_w=0.0012 Pa s. We conclude that a significant effect of the Coriolis force is expected for droplets larger than, say, 20 μm. Below this size the effect decreases rapidly.

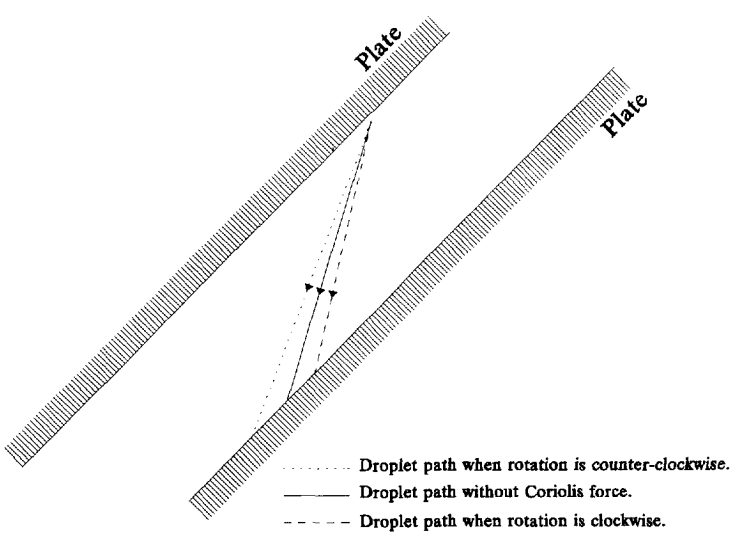

Figure (5-11) Effect of the Coriolis force on the radial movement of an oil droplet in a rotating plate pack.

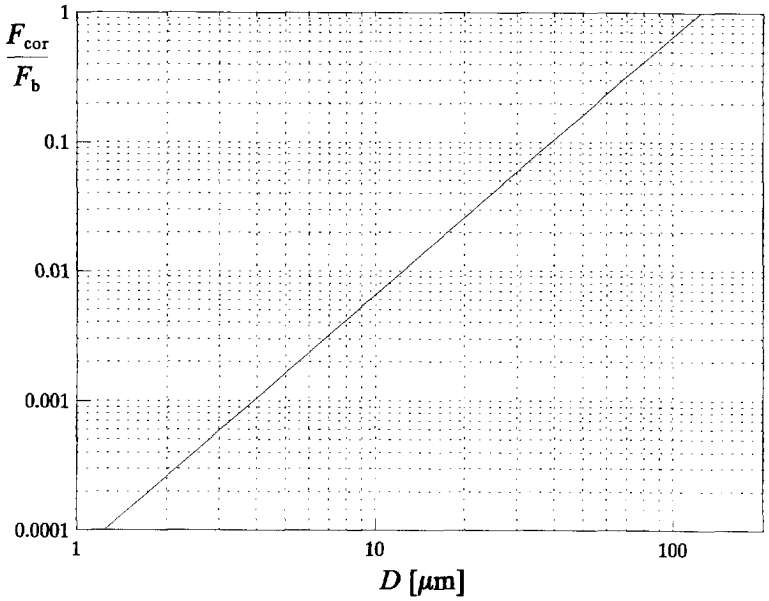

Figure (5-12) Relative influence of the Coriolis force on the buoyant force as a function of the droplet size.

5.7 Separation efficiency

The separation efficiencies as a function of the droplet size and the critical droplet diameter D_c of a PPC or PCC can be determined from the following data:

-the paths of the droplets,
-the radial terminal velocities of the droplets,
-the continuous-phase flow-velocity distribution.

Neither $\eta(D)$ nor D_c can be given by one simple equation, as in the case of gravity plate separators. Van den Berg [1] calculated D_c of a PPC with flat plates. In her calculations she neglected the relation between plate distance and average flow velocity. She found that D_c depends strongly on the entrance position. The critical diameter of droplets entering the pack near the outer radius was found to be about twice as large as those entering the pack near the inner radius. The next chapter discusses the results of a computer simulation program. This program generates the theoretical $\eta(D)$ for any possible PPC or PCC and for any combination of oily water properties. D_c will be dependent on the distance R from the axis of rotation ($R_i \leq R \leq R_o$). For a PPC, C_{out} is given by:

$$C_{out} = \frac{1}{(R_o - R_i)h_{av}} \int_{R_i}^{R_o} \frac{2}{3} C_D D_c(R) \left(\frac{h(R)^3}{h_{av}^2} \right) dR \qquad \text{(PPC)} \qquad \text{(5-17)}$$

where h_{av} is the average plate distance, given by:

$$h_{av} = \frac{1}{R_o - R_i} \int_{R_i}^{R_o} h(R) dR \qquad \text{(5-18)}$$

For a PCC, C_{out} is given by:

$$C_{out} = \frac{1}{R_o - R_i} \int_{R_i}^{R_o} \frac{2}{3} C_D D_c(R) \, dR \qquad \text{(PCC)} \qquad \text{(5-19)}$$

5.8 Bending of the plates

A small plate thickness results in a low critical droplet diameter. To determine the smallest possible plate thickness, the stress in the plates must be calculated. Potter [4] carried out some preliminary calculations. He found that flat plates tend to bend due to the centrifugal forces and become curved with the shape of the arc of a circle. This means that this shape will be a mechanically stable situation. Partly as a consequence of this finding, the plate shape in the computer simulation programs was defined as the arc of a circle.

References

[1] Berg, P.Y. van den: Modification design for a disc stacked centrifuge for the treatment of oily water, Graduation report, The College for Petroleum and Gas Technology, Marine Environmental Sciences, Den Helder, carried out at Delft University of Technology, Faculty of Mining and Petroleum Engineering, April 1990.

[2] Hetsroni, G.: Handbook of Multiphase Systems, Hemisphere Publishing Corporation, Washington, 1982.

[3] Linden, J.P. van der: liquid-liquid separation in disc-stack centrifuges, Thesis, Delft University of Technology, 1987.

[4] Potter, B.J.P.: The Plate Centrifuge, Optimum Design of a Modified Disc Stacked Centrifuge used in Oil-Water Separation, M.Sc. Graduation report, Delft University of Technology, Faculty of Mechanical Engineering, April 1991.

[5] Ward-Smith, A.J.: Internal Fluid Flow, Clarendon Press, Oxford, 1980.

Chapter 6

Simulations and experiments with plate packed centrifuges

6.1 Introduction

This chapter presents the results of numerical simulations and laboratory experiments with centrifuges equipped with a plate pack as described in the previous chapter.

Section 6.2 describes the programs and results of the numerical simulations. Two computer programs have been developed, to determine the separation efficiency. One for a Parallel Plate Centrifuge (PPC) and one for a Parallel Channel Centrifuge (PCC).

Section 6.3 describes results of laboratory experiments. Two different plate packs have been constructed, one with flat plates and one with curved channels. The separation efficiency as a function of droplet size was measured by means of a laser diffraction based particle sizer. Results are given for different oily-water flow rates. These results have been compared with the general separation efficiency function (derived in chapter 3), and with the results of the numerical simulations.

6.2 Numerical simulations

6.2.1 Simulation programs for the PPC and the PCC

The simulation programs were developed with the aim to determine the optimum plate pack configuration. The optimum plate pack configuration is defined as the configuration for which a minimum outlet oil concentration C_{out} is obtained. Significant parameters to determine C_{out} are the critical droplet diameter D_c and the separation efficiency as function of droplet size $\eta(D)$ of the droplets smaller than D_c. To ensure a laminar flow regime of the continuous phase, determination of its Reynolds number Re is essential. D_c, $\eta(D)$ and Re are set by the following system parameters:

1. the dimensions of the plate pack (see figures (5-4) and (5-5)),
2. the angular velocity of the centrifuge,
3. the flow rate and the physical properties of the oily water.

The minimum plate distance h_{min} (figure (5-4)) and the minimum plate thickness d_{min} (figure

(5-5)) are determined by the dimensions of the plate pack; h_{min} and d_{min} are important parameters from which the probability of clogging (PPC) or mechanical stability of the plates (PCC) can be determined. In practice one should have h_{min} (PPC) or d_{min} (PCC) as one of the input parameters. From section 5.4.1 it is clear that $h_{min} \wedge d_{min} = f(\beta)$ and that $d\beta/dh_{min} \wedge d\beta/dd_{min}$ is positive for $0 < \beta < \frac{1}{2}\pi$. Hence, for a given set of separator dimensions, a relatively simple iteration determines β from either h_{min} or d_{min}. The simulation programs have been structured in such a way that either β or h_{min} or d_{min} can be selected as input parameter, while the related parameter will be calculated.

Summarizing, the three groups of input parameters are:

INPUT	PPC	PCC
1. Plate pack	L, R_o, R_i, n	
	R_p, d, β or h_{min}	R_c, h, β or d_{min}
2. Centrifuge	ω	
3. Oily water	Q, ρ_w, ρ_o, μ_w, C_D	

Table 6.1

and the output parameters consist of:

OUTPUT	PPC	PCC
	Re, D_c, $\eta(D)$	
	h_{min} or β, h_{max}	d_{min} or β, d_{max}

Table 6.2

The output of the actual simulation program includes a number of design parameters which are useful for the designer/constructor, but which will not be discussed in this thesis.

6.2.2 The model

The simulation programs are based on theory which has been described in chapters 2, 3 and 5. We will discuss the general structure of the programs first, whereafter each step will be addressed in more detail, including all important equations.

Because all channels are assumed to perform identically, only one channel needs to be considered. Figure (6-1) shows a cross-section of a channel of a PPC, perpendicular to the direction of flow. The figure presents a plate pack with flat plates, which is essentially the same as a plate pack with curved plates with a radius of curvature R_p very much larger than

the outer radius R_o. Consequently, figure (6-1) presents a channel of a PPC essentially the same as the one presented in figure (5-6), but for $R_p \gg R_o$.

The area enclosed by $\mathbf{B_1}$, $\mathbf{B_2}$, $\mathbf{B_3}$ and $\mathbf{B_4}$ is first calculated and then divided into **k** sections of equal area (in this case **k**=5; sections $\mathbf{S_1}$ to $\mathbf{S_5}$). The actual simulation program divides the channel into 20 sections (**k**=20), which provides an acceptable accuracy. In each section the path of a droplet which crosses the centre of the section is determined (maximum length and direction). The centre of each section is given by the intersection of its diagonals (see figure (6-1): dotted lines in section $\mathbf{S_4}$). In each section the average distance between the plates h is determined. The average flow velocity in each section can be calculated. Taking into account the length of the plate pack L, the average residence time in each section can be determined as well. Then the average critical droplet diameter D_c in each section can be determined, as well as the total effluent oil concentration. These results are only valid if the channel Reynolds number Re does not exceed a certain limit (generally: 1200 to 2000). Because Re is maximal where the flow velocity and the plate distance are largest, the section number where these parameters are largest must be found. The section where $v_{f,max}$ is largest coincides with the section where h_{max} is largest (see equation (5-14)).

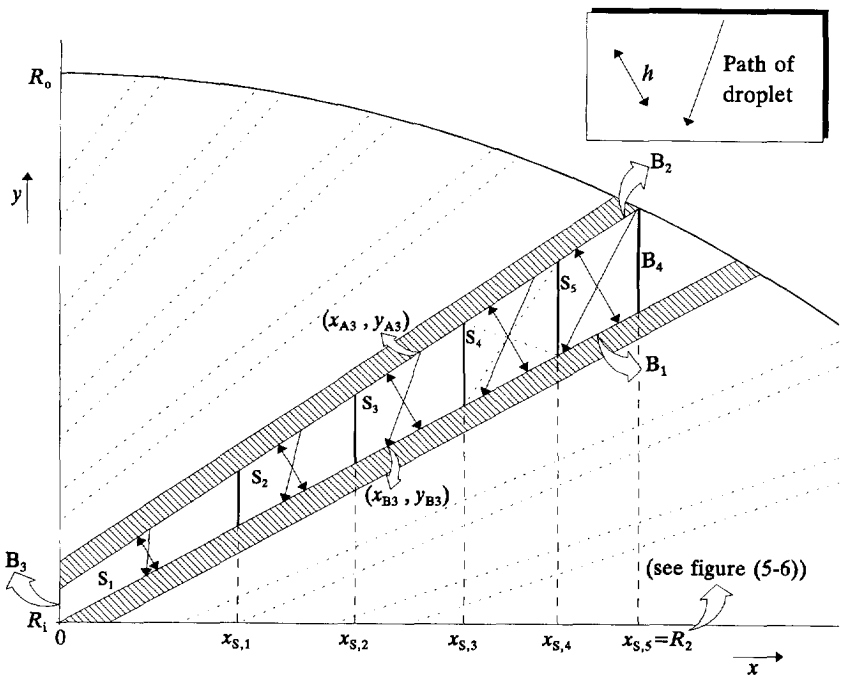

Figure (6-1) Channel of a PPC, divided into 5 sections ($\mathbf{S_1}$ to $\mathbf{S_5}$) of equal area. In each section the path of a droplet is drawn, which crosses the centre of the section.

Figure (6-2) shows the flow chart of the PPC simulation program. The input block sets all parameters given in table 6.1. If β is an input parameter, the iteration-loop is not executed.

With given values for R_o, R_i, R_p, β, d, n and $(P_1,Q_1)=(0,R_i)$ **(see figure (5-6))**, the point of intersection (P_2,Q_2) between the plate P1 and the outer radius can be derived. After some calculation this yields:

$$(P_2,Q_2)=\left(\left(\frac{-\tan(\beta)R_i}{\tan^2(\beta)+1}+\frac{1}{\tan^2(\beta)+1}\sqrt{R_o^2\tan(\beta)+R_o^2-R_i^2}\right),\left(\sqrt{R_o^2-P_2^2}\right)\right) \qquad (6\text{-}1)$$

Point (a_1,b_1) is calculated with the help of the auxiliary line (figure (5-6)), which is the line perpendicular to and intersecting the line (P_1,Q_1)-(P_2,Q_2) half-way. The equation of the auxiliary line is given by:

$$y = p\,x + q = \left(\frac{-x}{\tan\beta}\right) + \left(\frac{R_i+Q_2}{2} + \frac{P_2}{2\tan\beta}\right) \qquad (6\text{-}2)$$

Point (a_1,b_1) is located on this line and at a distance R_p from points (P_1,Q_1) and (P_2,Q_2). After rearrangement and substitution, the following expression for a_1 is obtained:

$$3\left(1+p^2\right)a_1^2 + \left(2pq+2pR_i\right)a_1 + \left(q^2-2qR_i+R_i^2-R_p^2\right) = 0 \qquad (6\text{-}3)$$

which gives two values for a_1. The correct one depends on the value of β: if $0<\beta<90°$, then the larger value of a_1 must be taken, and if $-90° <\beta<0$, the smaller value. If $\beta=0$, then $a_1=\frac{1}{2}P_2$.

Subsequently, b_1 can be derived (except for $\beta=0$) from:

$$b_1 = p\,a_1 + q \qquad (6\text{-}4)$$

and for $\beta=0$:

$$b_1 = R_i - \sqrt{R_p^2 - a_1^2} \qquad (6\text{-}5)$$

Point (a_2,b_2), the centre of curvature of plate P2, is given by:

$$(a_2,b_2) = \left(\left(\sqrt{a_1^2+b_1^2}*\cos\left(\arctan\left(\frac{b_1}{a_1}\right)+\frac{2\pi}{n}\right)\right),\left(\sqrt{a_1^2+b_1^2}*\sin\left(\arctan\left(\frac{b_1}{a_1}\right)+\frac{2\pi}{n}\right)\right)\right) \qquad (6\text{-}6)$$

Hence, the equations for the boundaries $\mathbf{B_1}$ and $\mathbf{B_2}$ are given by:

$$y = b_1 + \sqrt{R_p^2 - (x-a_1)^2} \qquad \text{for } \mathbf{B_1} \qquad (6\text{-}7)$$

and:

$$y = b_2 + \sqrt{(R_p - d)^2 - (x - a_2)^2} \quad \text{for } B_2 \tag{6-8}$$

Now the points (R_1,S_1) and (R_2,S_2) can be determined. To calculate $x_{S,1}$ to $x_{S,k}$ the following equation has been used:

$$\forall m \in \mathbb{N}, 0<m\leq k: \quad \int_{x_{S,m-1}}^{x_{S,m}} B_2 dx - \int_{x_{S,m-1}}^{x_{S,m}} B_1 dx = \frac{\int_0^{x_{S,S_{tot}}} B_2 dx - \int_0^{x_{S,S_{tot}}} B_1 dx}{k} \tag{6-9}$$

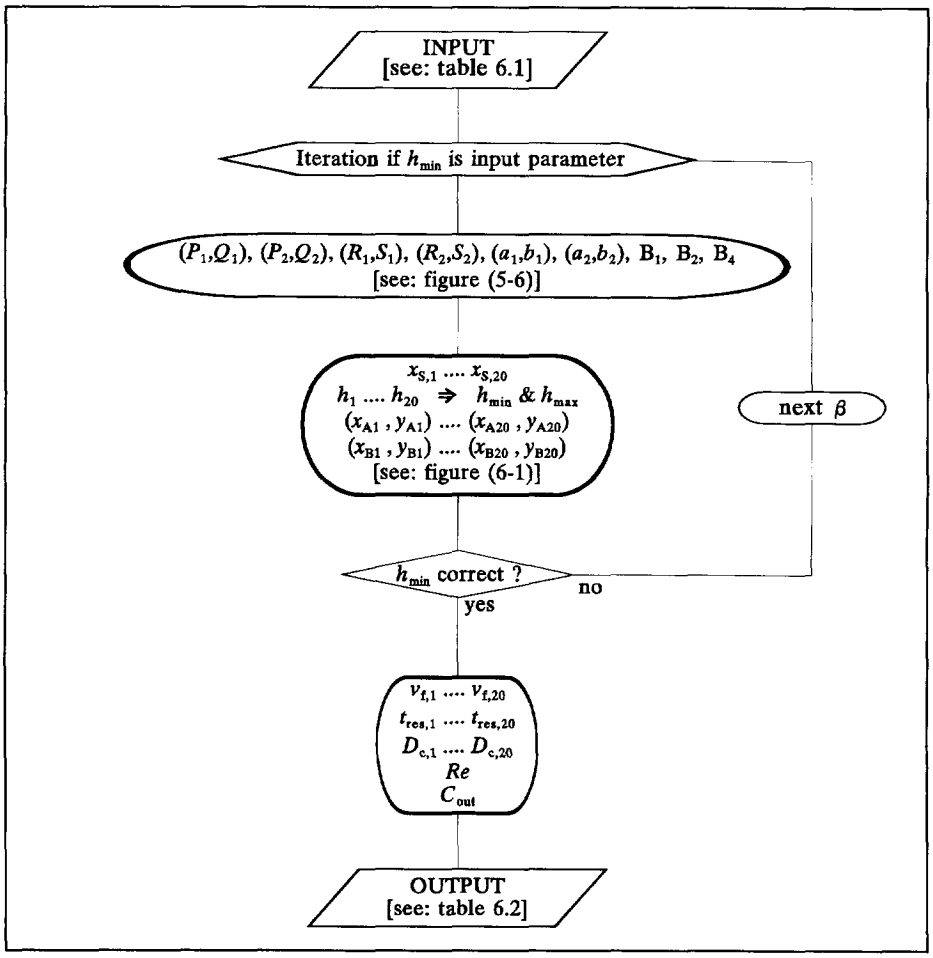

Figure (6-2) Flow chart of the simulation program (PPC), where each channel is divided into 20 sections (k=20).

where:

$$\int_{x_1}^{x_2} \mathbf{B}_1 \, dx = \left[b_1 x + \frac{R_p^2}{2} \arcsin\left(\frac{x-a_1}{R_p}\right) + \frac{x-a_1}{2}\sqrt{R_p^2-(x-a_1)^2} \right]_{x_1}^{x_2} \qquad \textbf{(6-10)}$$

and:

$$\int_{x_1}^{x_2} \mathbf{B}_2 \, dx = \left[b_2 x + \frac{(R_p-d)^2}{2} \arcsin\left(\frac{x-a_2}{R_p-d}\right) + \frac{x-a_2}{2}\sqrt{(R_p-d)^2-(x-a_2)^2} \right]_{x_1}^{x_2} \qquad \textbf{(6-11)}$$

Now it is possible to determine the centre, and subsequently the droplet path length and the average plate distance, of each section. The average plate distance h_1 to h_k is determined by the distance between the two points obtained from intersecting $\mathbf{B}_1$ and $\mathbf{B}_2$,respectively, and the line through the centre of the section and the point half-way (a_1,b_1) and (a_2,b_2).

The average flow velocity in each section $v_{f,1}$ to $v_{f,k}$ can be derived from the material balance equations:

$$Q = n \, \frac{\int_0^{x_{s,k}} \mathbf{B}_2 \, dx - \int_0^{x_{s,k}} \mathbf{B}_1 \, dx}{\mathbf{k}} \, (v_{f,1} + v_{f,2} + \ldots\ldots + v_{f,k}) \qquad \textbf{(6-12)}$$

where (see: equation (5-14)):

$$\forall m \in \mathbb{N},\ 0<m\leq \mathbf{k}: \qquad v_{f,m} = \xi \, h_m^2 \qquad \textbf{(6-13)}$$

Hence:

$$\xi = \frac{Q \, \mathbf{k}}{n \left(\int_0^{x_{s,k}} \mathbf{B}_2 \, dx - \int_0^{x_{s,k}} \mathbf{B}_1 \, dx \right) \left(h_1^2 + h_2^2 + \ldots\ldots + h_k^2 \right)} \qquad \textbf{(6-14)}$$

The average residence time of the continuous phase in each section is then given by:

$$\forall m \in \mathbb{N},\ 0<m\leq \mathbf{k}: \qquad t_{res,m} = \frac{L}{v_{f,m}} \qquad \textbf{(6-15)}$$

The critical droplet diameter of each section can now be calculated. For these droplets, the time t_{AB} to travel from point **A** to **B** (see: figures (5-6) and (6-1), and equation (5-11)) should be equal to the corresponding residence time $t_{res,m}$. Combination of equations (5-11) and (6-15) yields for the section critical droplet diameter:

$$D_{c,m} = \sqrt{\ln\left(\frac{\sqrt{x_{Am}^2+y_{Am}^2}}{\sqrt{x_{Bm}^2+y_{Bm}^2}}\right)\frac{18\ \mu\ v_{f,m}}{(\rho_w-\rho_o)\,\omega^2 L}} \qquad (6\text{-}16)$$

and the largest channel Reynolds number is calculated from equation (3-2-4), where:

$$D_h = \frac{2h_{max}W}{h_{max}+W} \quad \wedge \quad h_{max} \ll W \quad \Rightarrow \quad D_h \approx 2h_{max} \qquad (6\text{-}17)$$

W represents the width of a channel, which is approximately the length of the path from R_i to R_o along the surface of a plate. Re is thus given by:

$$Re = \frac{2\ \rho_w\ v_{f,max}\ h_{max}}{\mu_w} \qquad (6\text{-}18)$$

From section 3.5 we know the relation between D_c and C_{out}. Thus:

$$C_{out} = \frac{2}{3}C_D\left(\frac{v_{f,1}D_{c,1} + v_{f,2}D_{c,2} + \ldots\ldots + v_{f,k}D_{c,k}}{v_{f,1} + v_{f,2} + \ldots\ldots + v_{f,k}}\right) \qquad (6\text{-}19)$$

It is convenient to describe R_i, R_p, d, h_{min} and h_{max} as fractions of R_o. Consequently:

PPC	PCC
$R_i^* = \frac{R_i}{R_o}$	
$R_p^* = \frac{R_p}{R_o}$	$R_c^* = \frac{R_c}{R_o}$
$d^* = \frac{d}{R_o}$	$h^* = \frac{h}{R_o}$
$h_{min}^* = \frac{h_{min}}{R_o}$	$d_{min}^* = \frac{d_{min}}{R_o}$
$h_{max}^* = \frac{h_{max}}{R_o}$	$d_{max}^* = \frac{d_{max}}{R_o}$

Table 6.3

We then **define**:
Re^*, D_c^* and C_{out}^* are the values of Re, D_c and C_{out} in the case of: $L^{ref}=R_o^{ref}=1$ m, $\omega^{ref}=1$ rad/s, $Q^{ref}=1$ m^3/s, $\rho_w^{ref}=(\rho_w-\rho_o)^{ref}=1$ kg/m^3, $\mu_w^{ref}=1$ Pa s and $C_D^{ref}=1$ ppm/m.

Because D_h is proportional to R_o, and v_f is inversely proportional to R_o^2, the equation for Re as a function of ρ_w, Q, R_o and μ_w yields:

$$Re = Re^* \frac{\rho_w \; Q \; R_o^{ref} \; \mu_w^{ref}}{\rho_w^{ref} \; Q^{ref} \; R_o \; \mu_w} \tag{6-20}$$

D_c can be derived from equation (3-2-3):

$$D_c = D_c^* \frac{\omega^{ref} R_o^{ref}}{\omega \; R_o} \sqrt{\frac{Q \; \mu_w \; L^{ref} \; (\rho_w - \rho_o)^{ref}}{Q^{ref} \; \mu_w^{ref} \; L \; (\rho_w - \rho_o)}} \tag{6-21}$$

C_{out} is then given by:

$$C_{out} = C_{out}^* \frac{C_D \; \omega^{ref} R_o^{ref}}{C_D^{ref} \; \omega \; R_o} \sqrt{\frac{Q \; \mu_w \; L^{ref} \; (\rho_w - \rho_o)^{ref}}{Q^{ref} \; \mu_w^{ref} \; L \; (\rho_w - \rho_o)}} \tag{6-22}$$

Based on the theory described in this section, we can conclude:

> **If** there is one minimum C_{out}^* for one plate pack configuration (β, h_{min}^*/d_{min}^*, R_i^*, R_p^*, d^*/h^* and n), this optimum configuration is valid for every value of R_o and L. This means that the shape of the cross-section of the plate pack perpendicular to the axis of rotation will always be the same, whatever the size of the centrifuge. Moreover, R_o and L can be chosen independently from each other.

6.2.3 Results of the PPC and PCC simulations

Before searching for the optimum plate pack parameters, it is necessary to determine the influence of each individual parameter. Tables 6.4 and 6.5 give the values of the input parameters as taken for this part of the procedure. For each simulation, one parameter was varied between two values, while the other ones were kept constant at the values indicated in the tables.

A typical result of a PPC with flat plates is given in figure (6-3). For this simulation n was varied between 0 and 1100, while β, h_{max}^*, $D_{c,1}^*$ to $D_{c,20}^*$, C_{out}^* and Re^* were calculated. In this case h_{min}^* was been kept constant at 0.003. Real output values have been obtained for about $100 < n < 850$. The shaded area represents the values of $D_{c,1}^*$ to $D_{c,20}^*$, where the lower boundary of the area represents the smallest value of the series $D_{c,1}^*$-$D_{c,20}^*$, and the upper boundary corresponds to the largest. C_{out}^* was calculated from $D_{c,1}^*$ to $D_{c,20}^*$ with equation (6-19). It can be noticed that a minimum C_{out}^* exists, in this case for about 600 plates. For a given configuration there is an optimum number of plates.

par.	fixed	interval
R_i^*	0.7	0.5 - 1
R_p^*	0.85	0.4 - 1.5
d^*	0.002	0 - 0.005
h_{min}^* (β var.)	0.003	-
β (h_{min}^* var.)	20	−30 - +50
n	500	0 - 1100

Table 6.4 Parameter values of the **PPC** chosen for the simulations.

par.	fixed	interval
R_i^*	0.7	0.5 - 1
R_c^*	0.85	0.4 - 1.5
h^*	0.002	0 - 0.005
d_{min}^* (β var.)	0.003	-
β (d_{min}^* var.)	20	−30 - +50
n	500	0 - 1100

Table 6.5 Parameter values of the **PCC** chosen for the simulations.

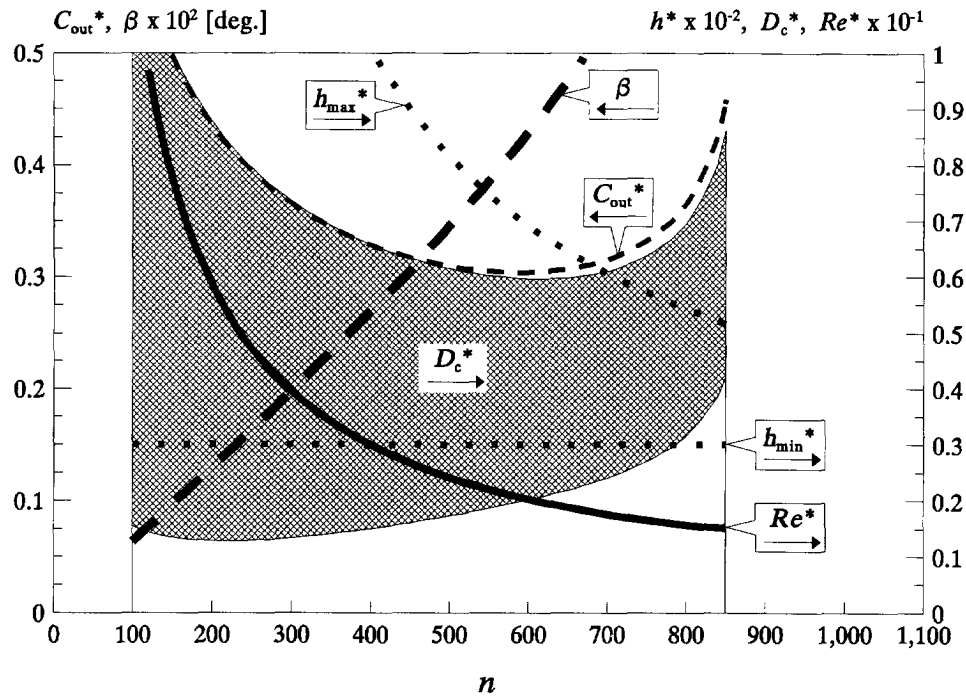

Figure (6-3) Typical result of a simulation. This graph applies to a PPC with flat plates and h_{min}^*=0.003.

Appendix E shows the results of the complete set of simulations. It appears that dC_{out}^*/dd^*, dC_{out}^*/dh_{min}^* (PPC) and dC_{out}^*/dh^*, dC_{out}^*/dd_{min}^* (PCC) are always positive. For practical purposes the values of these parameters should be as low as possible for maximum separation efficiency. The other parameters (R_i^*, R_p^*/R_c^*, β and n) each have one value where C_{out}^* is minimal. A subroutine has been developed which generates the optimum configuration.

Four optima were found:

Flat plates:	$R_i^* \approx 0.76$	$\beta \approx 40$ degrees.	
Straight channels:	$R_i^* \approx 0.70$	$\beta \approx 35$ degrees.	
Curved plates/channels:	$R_i^* \approx 0.60$	$\beta \approx 0$	$R_p^* \approx 0.72$.

Plate packs with the optimum values for R_i^*, R_p^* and β are named **Optimum PPC** or **Optimum PCC**.

The optimum values for R_i^*, R_p^* and β (PPC) and for R_i^*, R_c^* and β (PCC) were found to be valid for **all** values of d^* and h_{min}^* (PPC), respectively, h^* and d_{min}^* (PCC). The number of plates n is set by the combination of d^* and h_{min}^* (PPC), and of h^* and d_{min}^* (PCC). Figure (6-4) illustrates how n relates to d^* and h_{min}^* for an Optimum PPC with flat plates. The thin dotted lines in the graph represent an example for $d^*=0.001$ and $h_{min}^*=0.002$. The graph indicates that 1040 plates should be used to obtain optimum separation performance.

Optimum separation performance is illustrated in figure (6-5), which also here applies to an Optimum PPC with flat plates. It gives n, D_c^*, C_{out}^* and Re^* as a function of d^* when $h_{min}^*=0.002$. For example, when $d^*=0.001$, the number of plates to be used is again 1040. The graph indicates that $Re^* \approx 0.012$, $D_c^* \approx 0.44$ m and $C_{out}^* \approx 0.23$ ppm. How the actual values Re, D_c and C_{out} can be obtained by using equations (6-20), (6-21) and (6-22) is explained below.

Simulation results for all four plate packs are given graphically in figures (6-6) to (6-9). These figures give n, D_c^*, C_{out}^* and Re^* as a function of d^* for four values of h_{min}^* (0.002, 0.003, 0.004 and 0.005). It gives insight into the relationship between plate thickness, plate distance, number of plates and separation performance. It can also be used to make a rough design of a plate pack. Although the simulation program will be faster and more accurate, a **practical guideline** is formulated as follows:

1. Determine the values of the system parameters ρ_w, ρ_o and μ_w and the value of the desired flow rate Q. If possible, determine the value of C_D.
2. Estimate the values of d and h_{min} (PPC), respectively, h and d_{min} (PCC). Generally, d and h_{min} will vary between 0.0003 and 0.001 m.
3. Choose a value for R_o and calculate d^* and h_{min}^* by means of table 6.3. Generally, R_o varies between 0.1 and 0.4 m.
4. Determine n, D_c^*, C_{out}^* and Re^* by use of the appropriate figure ((6-6)/(6-9)).
5. Calculate Re by means of equation (6-20). If Re is too high, choose a larger value for R_o and/or smaller values for d and h_{min} and proceed from step 4.
6. Determine ω_{max}.
7. Take a value for L, so that D_c and/or C_{out} do not exceed the desired limits.

Note that the combination R_o-d-β-ω determines the amount of bending of the plates, which must be calculated before a final design can be made and should be a part of step 6. These mechanical aspects are beyond the scope of this thesis.

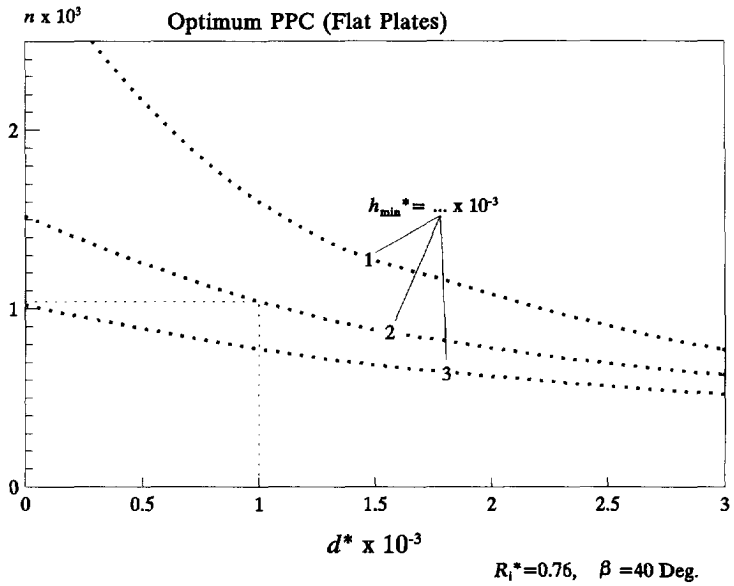

Figure (6-4) Optimum PPC with flat plates; relation between plate thickness, minimum plate distance and number of plates.

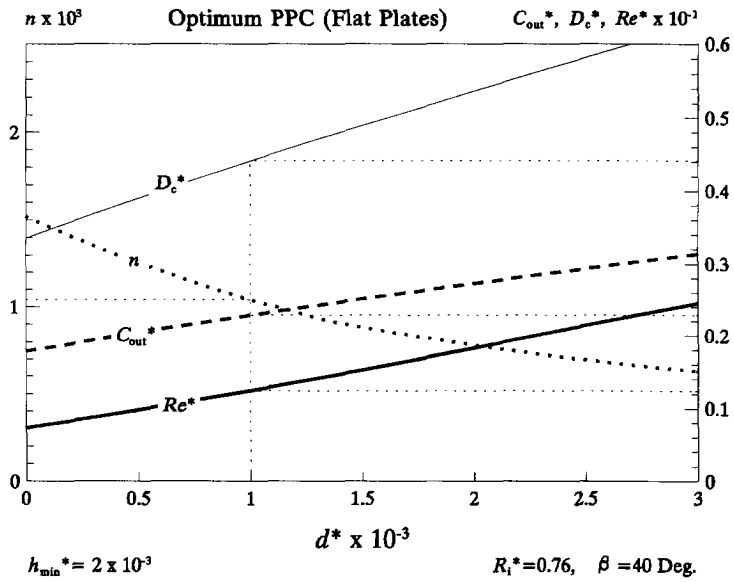

Figure (6-5) Optimum PPC with flat plates; relation between plate thickness, number of plates and separation performance for a specific minimum plate distance of 2 x 10^{-3}.

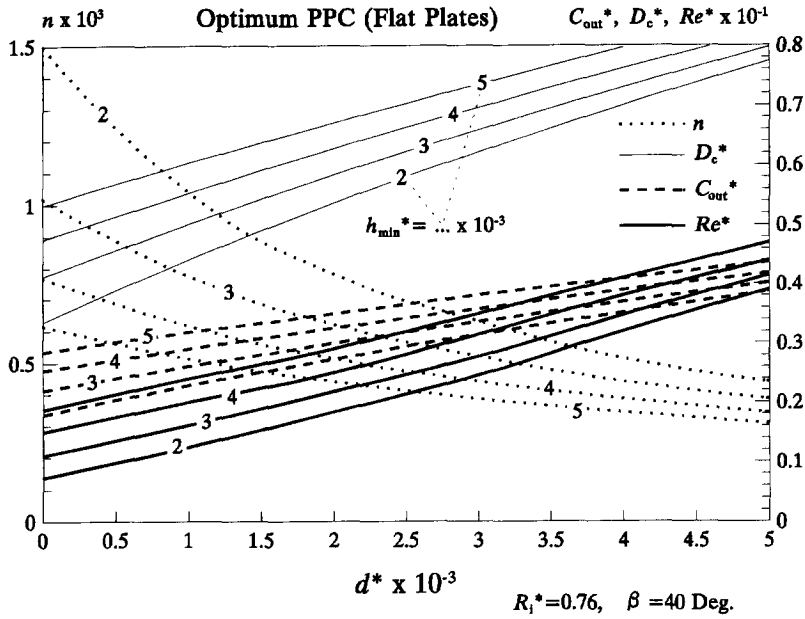

Figure (6-6) Optimum PPC with flat plates.

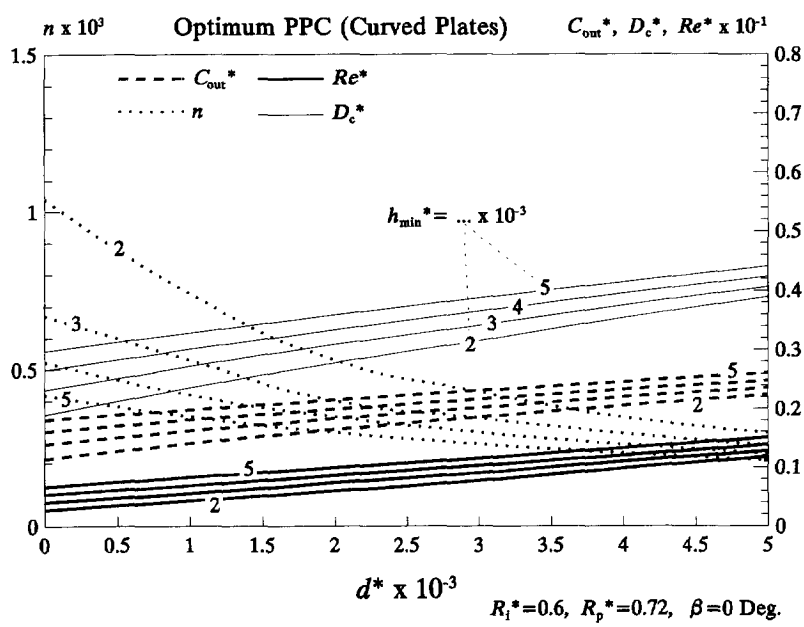

Figure (6-7) Optimum PPC with curved plates.

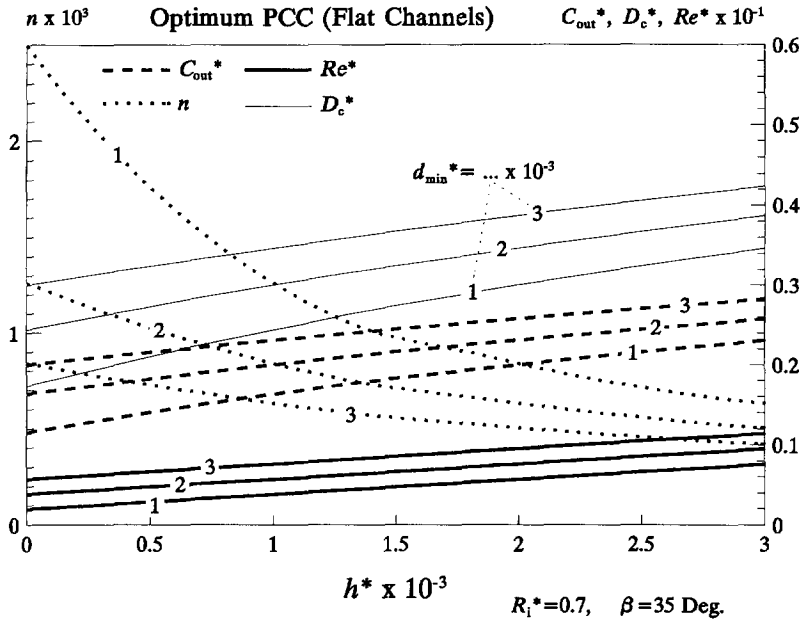

Figure (6-8) Optimum PCC with flat channels.

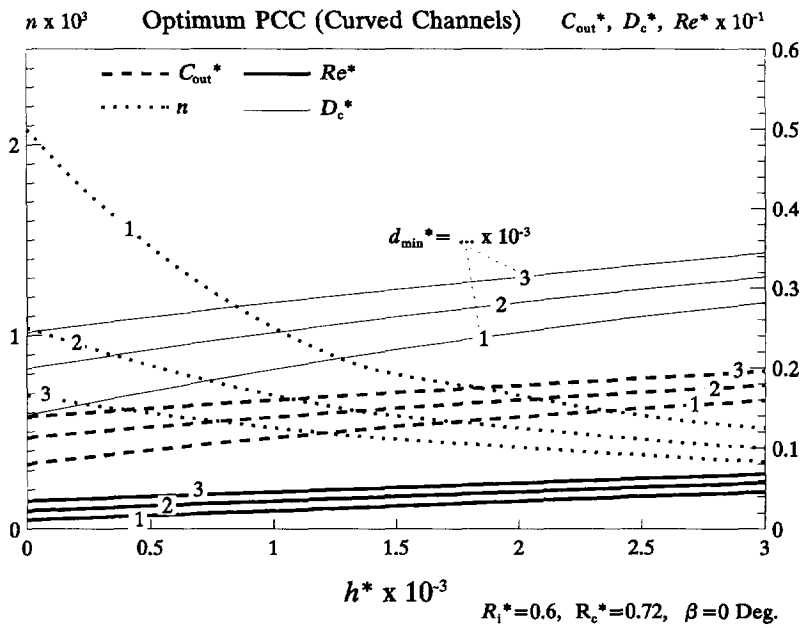

Figure (6-9) Optimum PCC with curved channels.

6.3 Experimental verification

Plate packs with flat and curved plates have been investigated with respect to separation efficiency versus oil droplet size. A simplified flow sheet of the experimental set-up is shown in figure (6-10). The same set-up was used as for the experiments on the gravity separator, which is described in paragraph 4.3.1. The experiments have been performed with tap water at approximately 12° C in which Shell Omala 220 oil was dispersed. Droplet sizes varied between about 0.5 to 200 μm. The central part of this set-up consisted of an Alfa Laval MAB 104 centrifuge. The bowl body of the centrifuge has an inner diameter of 214 mm and a height of 81.5 mm. The experimental plate packs were designed to fit inside the original centrifuge without the need for modifying the bowl body, the bowl hood or the inlet and outlet conduits.

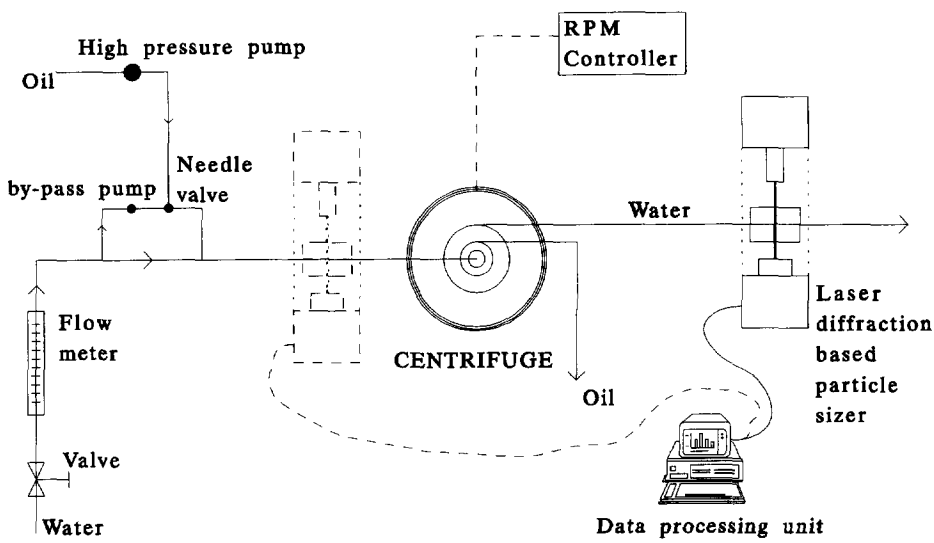

Figure (6-10) Simplified flow sheet of the experimental set-up.

Figure (6-11) gives a cross-section of the experimental centrifuge, showing the flow paths in the different parts. The mixture enters the centrifuge through the feed pipe, which is stationary. The rest of the parts shown in the figure rotate with velocity ω. Oily water flowing down is intercepted by baffles, which are located in the central part. The baffles are radially oriented and cause the incoming oily water to accelerate. The central part of the centrifuge with the baffles and pipes or holes is often called the *distributor*. Then the mixture will pass through 6 pipes and channels towards the plate pack. The pipes have an inner diameter of 6 to 8 mm and the channels are rectangularly shaped with a height of 5 mm and a width of 20 mm. After flowing through the plate pack, the separated streams reach the top

disc. The oil flows upwards underneath the top disc, while the water flows between the top disc and the bowl hood. Both streams leave the centrifuge and are collected by means of a baffle construction (not given in the figure).

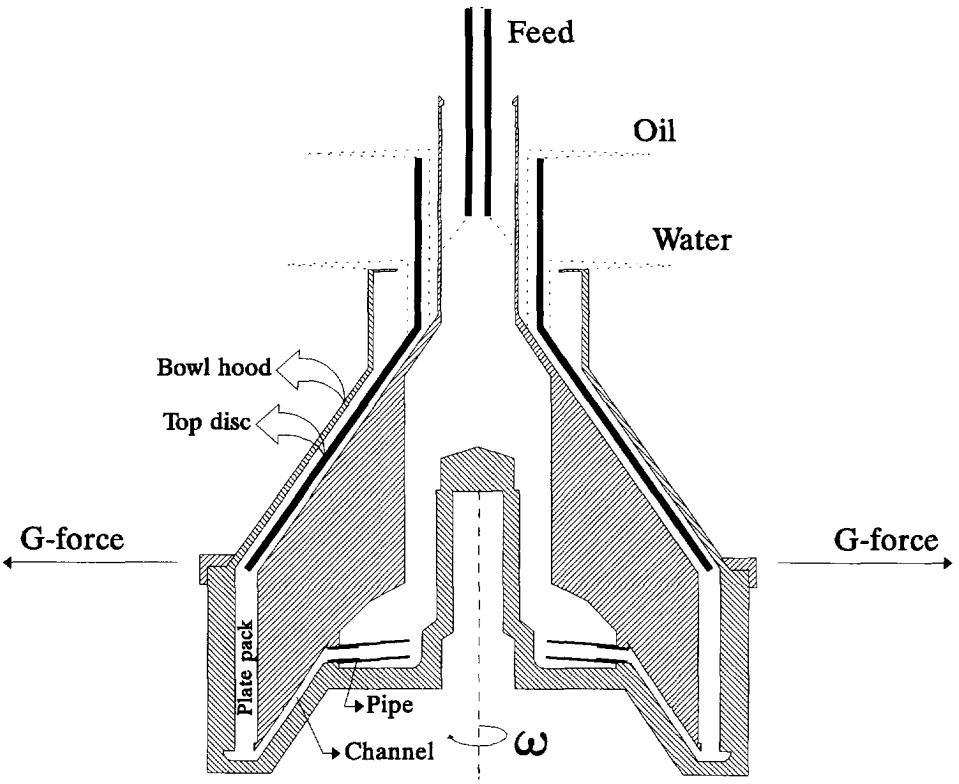

Figure (6-11) Cross-section of the experimental centrifuge, showing the flow paths through the different parts.

Figure (6-12) shows a simplified cross-section of the experimental PPC. The stainless-steel plates are fitted into grooves in the plate support sleeve. The bush prevents the plates from falling out of the grooves. The bush contains also the 6 rectangular channels. The inner support aligns the bush with the top disc and the distributor (the latter not shown in the figure). A drawing of the experimental PCC is not given because it is very similar to the PPC, only the construction of the plate pack is somewhat different. In the PCC the plates and the bush are made out of a single piece of stainless steel. In this case the plate support sleeve is a simple cylindrical bush which is closely fitted over the plates to prevent these from bending when the centrifuge is rotating. The lock ring secures the bowl hood to the bowl body.

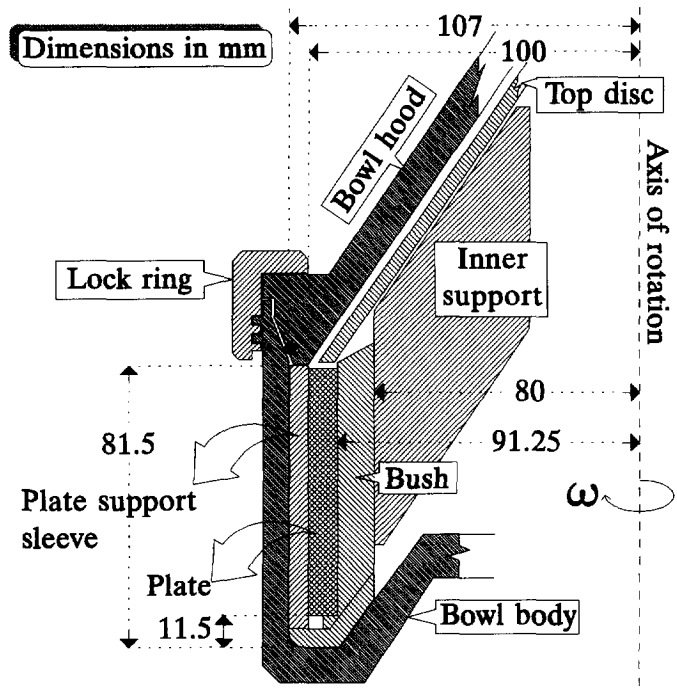

Figure (6-12) Part of a cross-section of the experimental PPC, showing how the plate pack fits within the bowl of the centrifuge.

	PPC	PCC	
R_o	.1	.1	[m]
R_i	.09125	.09	[m]
R_c	-	.086	[m]
β	41.3	18.5	[Deg.]
d	.35	-	[mm]
h	-	.35	[mm]
n	360	36	[-]
L	.07	.07	[m]

Table 6.6 Dimensions of the two experimental plate packs.

The maximum rotation of speed of the bowl is 785 rad/s (7500 rpm). Oily-water flow was varied from 0.1 to 1.5 m^3/hr. The oil flow rate was kept constant during all tests at 0.18 l/hr, which resulted in oil concentrations of 120 ppm (1.5 m^3/hr) to 1800 ppm (0.1 m^3/hr). The

laser particle sizer could be moved to measure either the influx or the water effluent of the centrifuge. A typical result of a set of measurements is shown in figure (6-13).

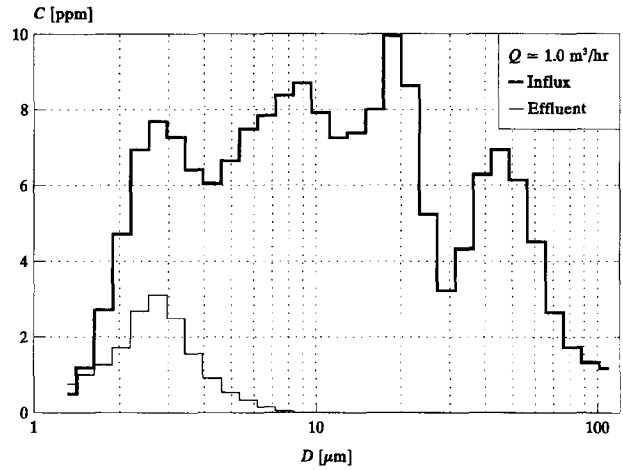

Figure (6-13) Typical result of an experiment.

Two plate packs have been constructed and tested. Their dimensions are given in table 6.6. To prevent distribution problems due to the limited (6) number of distribution channels, 300 channels of the PPC were sealed during the tests. Figures (6-14), (6-15) and (6-16) show results of the experiments with the PPC.

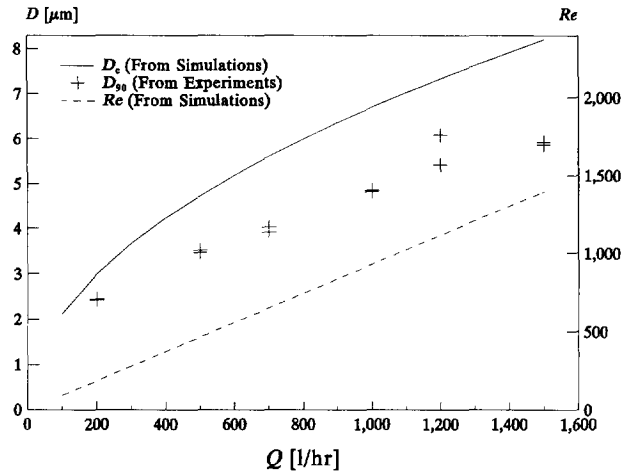

Figure (6-14) Results of experiments on the PPC; D_c, D_{90}, Re versus Q.

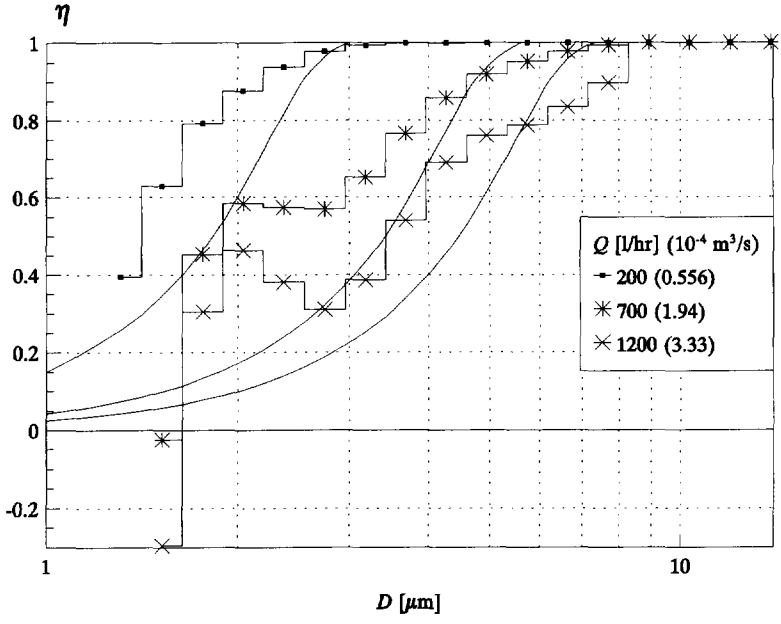

Figure (6-15) Results of experiments on the PPC (η vs. D).
Curves: Simulations. Markers: Experiments.

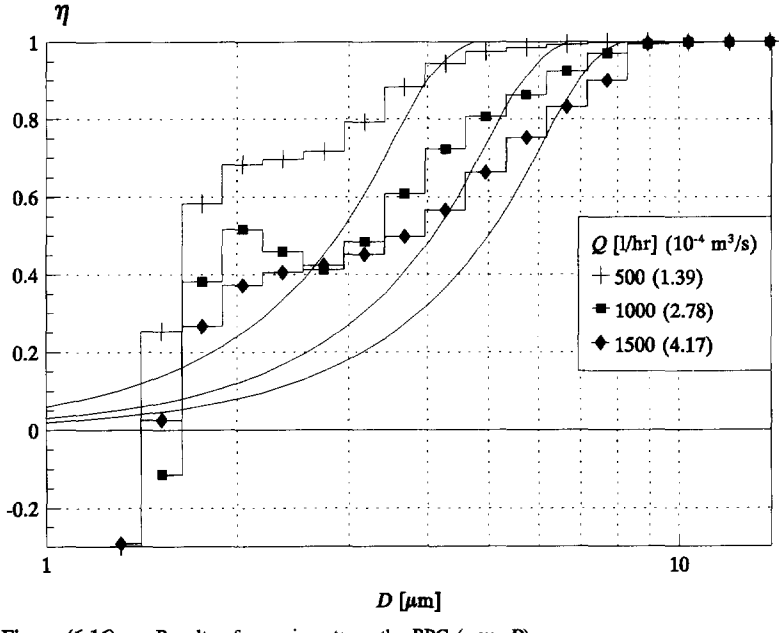

Figure (6-16) Results of experiments on the PPC (η vs. D).
Curves: Simulations. Markers: Experiments.

The following figures ((6-17) to (6-22)) shows results of the experiments on the PCC.

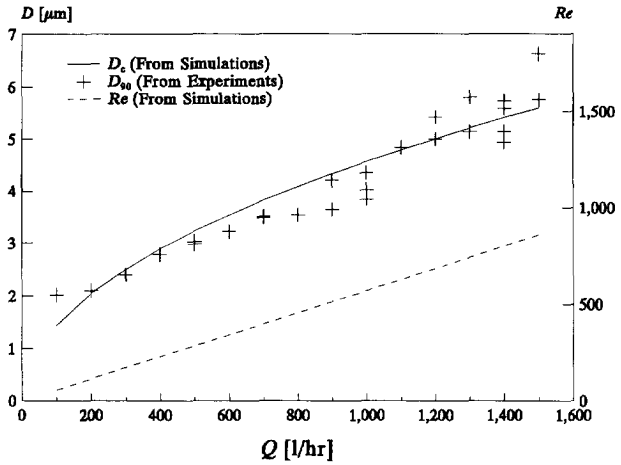

Figure (6-17) Results of experiments on the PCC; D_c, D_{90}, Re versus Q.

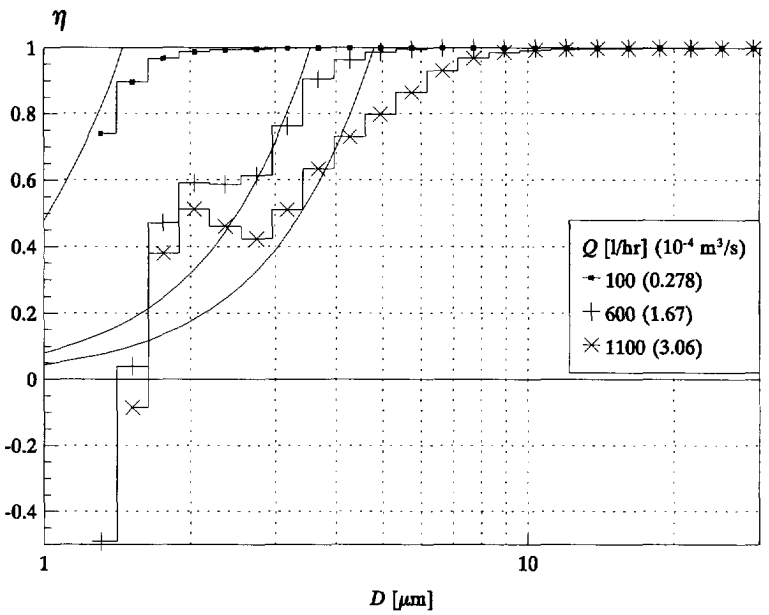

Figure (6-18) Results of experiments on the PCC (η vs. D).
Curves: Simulations. Markers: Experiments.

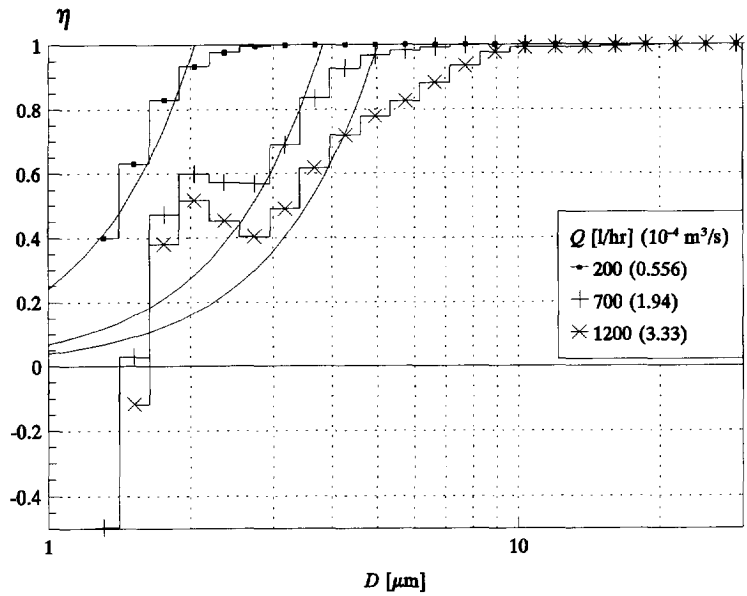

Figure (6-19) Results of experiments on the PCC (η vs. D).
Curves: Simulations. Markers: Experiments.

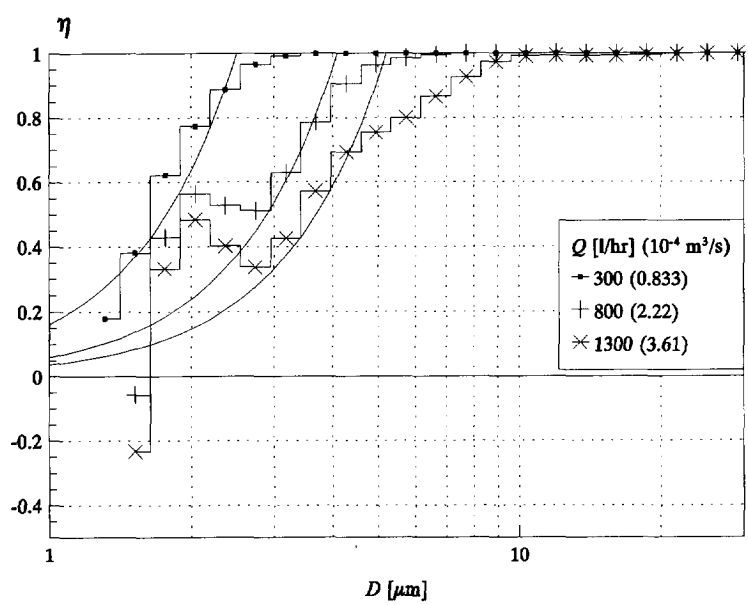

Figure (6-20) Results of experiments on the PCC (η vs. D).
Curves: Simulations. Markers: Experiments.

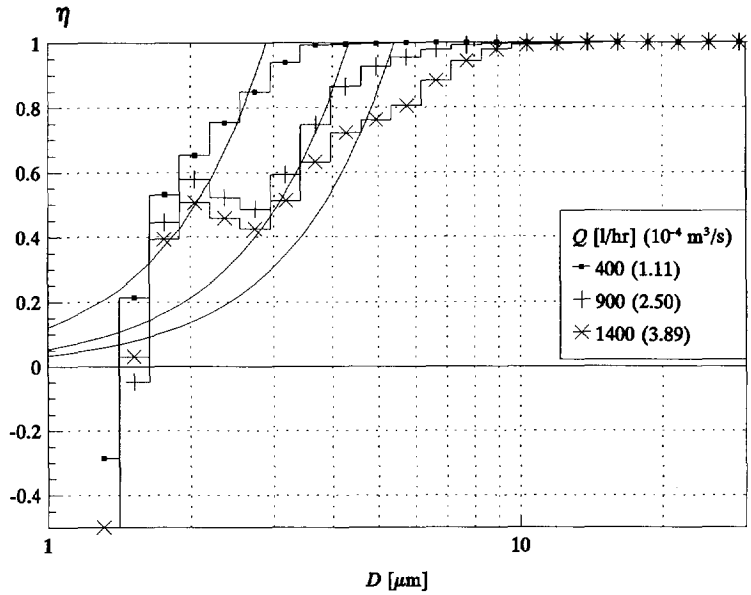

Figure (6-21) Results of experiments on the PCC (η vs. D).
Curves: Simulations. Markers: Experiments.

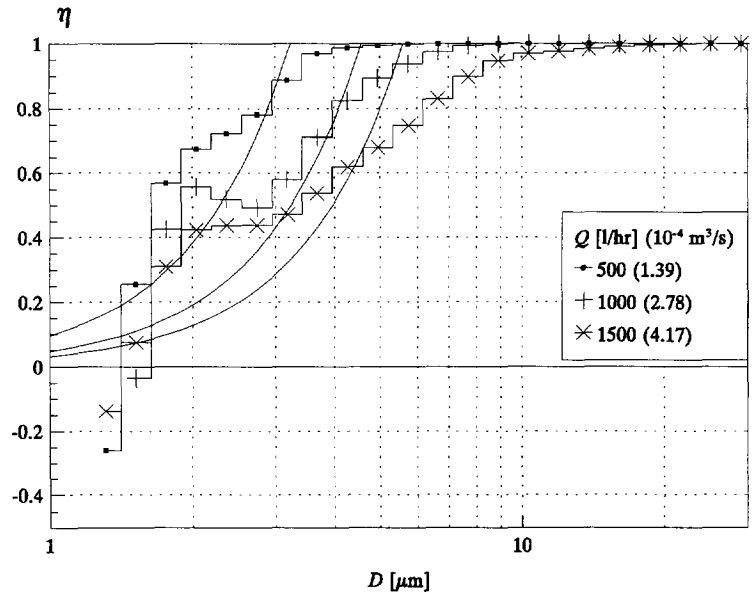

Figure (6-22) Results of experiments on the PCC (η vs. D).
Curves: Simulations. Markers: Experiments.

6.4 Conclusions

The most important conclusions are given below. Chapter 7 presents a more comprehensive discussion of the results of the experiments and the discrepancies between the theory and these results.

- The model of the PPC and PCC gives a satisfactory prediction of the critical droplet diameter as well as of the separation efficiency as function of the oil droplet diameter.
- The general separation efficiency function can be used for centrifuges.
- The simulation program -based on the model- shows one optimum configuration for each of the four plate pack types.
- For both the PPC and the PCC, the optimum configurations for curved plates/ channels perform roughly twice as well as the optimum configurations for flat plates/straight channels.
- The simulation program is a valuable tool for design purposes.
- The PPC/PCC-separation efficiency increases approximately proportionally with a decreasing flow rate.
- Theoretically, the separation efficiency becomes two times better if the length increases fourfold. There are no hydrodynamic restrictions to the length of the PPC/PCC; the length is only restricted by mechanical considerations.

Chapter 7

Discussion and conclusions

GPS = gravity plate separator
CPS = centrifugal plate separator
PPC = parallel plate centrifuge
PCC = parallel channel centrifuge

7.1 Evaluation of the experiments

In this thesis gravity plate separators (GPS) and centrifugal plate separators (CPS) have been investigated. For both types the critical droplet diameter D_c and the separation efficiency as a function of the oil-droplet diameter $\eta(D)$ have been determined by simulation and by experiments (chapters 4 and 6, respectively). For the GPS $\eta(D)$ has also been derived analytically (chapter 3). It was demonstrated that D_c and $\eta(D)$ are independent of the flow velocity profile $v_x(x,y)$. These findings have been used to determine the theoretical separation efficiency, $\eta(D)$, for the experimental CPS. The results of the experiments with the GPS and the CPS (chapters 4 and 6, respectively) show some discrepancies with the predicted values. The possible reasons have been divided into 5 categories:

1. Inadequate estimation of the relevance of the mechanisms (discussed in chapter 2), on which the derivations of D_c and $\eta(D)$ have been based.
2. Variations in the dimensions of the pack of plates due to tolerances and/or inadequacies during construction and/or installation.
3. Uneven flow distribution.
4. Separation outside the pack of plates.
5. Measurement inaccuracies.

7.1.1 Estimation of the dominant mechanisms

The possible influence of mechanisms for either a GPS or a CPS has been described in chapter 2. We will evaluate the influence of each mechanism in the same order as adopted in chapter 2.

Shape regimes for droplets in free motion
Initially, oil droplets sized within the critical range (GPS: $D < 200$ μm; CPS: $D < 10$ μm) have been taken to be spherical. The rising velocity of a droplet by gravity or by centrifugal forces has been derived from Stokes' law, which is based on spherical particles. If deformation of droplets occurs, larger droplets will be more deformed than smaller ones.

Deformed droplets rise with lower velocities than predicted [3]. This will lead to a lower separation efficiency than predicted for droplets sized around D_c. Thus, also droplets slightly larger than D_c will not be separated completely in that case.

In spite of the fact that this phenomenon has been observed, it is not considered to be likely that droplet deformation is the reason for the deviation (and of the magnitude of it, as observed with the CPS). This is because in the GPS the droplets' Reynolds numbers of droplets sized about D_c (200 μm) are approximately 0.4, and those in a CPS ($D_c \approx 10$ μm) are about 0.3.

Gravitational and centrifugal forces

The rising velocity of a droplet due to gravity has been neglected in the calculations on the CPS. Because the directions of the flow and the rising velocity coincide (in our case the axis of rotation was vertical and the oily water flows from the bottom to the top of the pack), the resulting vertical droplet velocity should be increased with its own rise velocity. The effects, however, can be neglected: according to equation (2-6) $v_t \approx 4.5\ 10^{-6}$ m/s and according to equation (2-9) $v_{tr} = 2.8\ 10^{-2}$ m/s, whilst the average flow velocity is $v_f \approx 0.1$ to 1 m/s, depending on the flow rate. Hence, v_t can be neglected.

Coriolis forces

Another mechanism, the Coriolis force, leads to decrease of D_c with less than 1%. This has been discussed in section 5.6.

Shear forces

The relative influence of the lift force F_L can be derived as follows. The shear rate G_S is highest when $y=0$ or $y=h$ in equation (3-2-21). Thus, droplets which nearly make contact with a plate are subjected to the highest shear forces. Presume the shear rate G_s is given by:

$$G_S = \frac{v_F(y=h-D) - v_F(y=h)}{D} = \frac{6\,Q}{h^3\,n\,W}\,(h - D) \qquad (7\text{-}1)$$

Combination of equation (7-1) with equations (2-22) or (2-23) gives:

$$\frac{F_L}{F_b} \approx \frac{1.032\,Q^{\frac{1}{2}}\,(h-D)^{\frac{1}{2}}\,\rho_w^{\frac{1}{2}}\,D\,\sin\gamma\,\cos\theta}{h^{1\frac{1}{2}}\,n^{\frac{1}{2}}\,W^{\frac{1}{2}}\,\mu^{\frac{1}{2}}} \qquad \text{(GPS)} \qquad (7\text{-}2)$$

or:

$$\frac{F_L}{F_b} \approx \frac{1.032\,Q^{\frac{1}{2}}\,(h-D)^{\frac{1}{2}}\,\rho_w^{\frac{1}{2}}\,D\,g\,\sin\gamma\,\cos\theta}{h^{1\frac{1}{2}}\,n^{\frac{1}{2}}\,W^{\frac{1}{2}}\,\mu^{\frac{1}{2}}\,\omega^2\,r} \qquad \text{(CPS)} \qquad (7\text{-}3)$$

Consequently, F_L/F_b increases proportionally with increasing D. The highest value for the experimental GPS is (Q = 1 m^3/hr and D = 200 μm): F_L/F_b= 0.094 sinγ. Thus the lift could be neglected for γ=0. For the experimental PPC (Q = 1.5 m^3/hr and D = 10):

$F_L/F_b = 4.6\ 10^{-6} \sin\gamma$ and for the experimental PCC (Q = 1.5 m³/hr and D = 10): $F_L/F_b = 9.9\ 10^{-5} \sin\gamma$. Thus, notwithstanding the fact that the water flow in the experimental centrifuges was directed upwards, hence γ= 90 degrees, the results do not have to be corrected for F_L.

The values of the parameters which were taken for the calculations are:
PPC: n=60, h=0.0008 m, W=0.0126 m, r=0.0955 m, θ=25 degrees, μ_w=0.0012 Pa s.
PCC: n=36, h=0.00035 m, W=0.0236 m, r=0.095 m, θ=44 degrees, μ_w=0.0012 Pa s.

Brownian motion
The influence of Brownian motion could only be important for relatively small droplets (GPS: $D < 10$ μm; CPS: $D < 1$ μm) and certainly not for the larger ones. If Brownian motion does have any effect, it is not certain whether it increases or decreases η, but it can most likely be neglected.

Particle-interface coalescence times
The particle-interface coalescence time t_c has not been taken into account in the theory and simulations. An oil droplet which reaches the plate close to its end and does not coalesce instantly, could be swept along with the flow towards the end of the plate. The droplet may slide and/or roll over the plate. Suppose that the droplet moves with velocity v_S which the water would have at that point in the absence of the droplet (figure (7-1)). Then, for a parabolic flow profile, this velocity can be estimated with equation (3-2-21):

$$v_S = \frac{3\ Q\ D}{h^3\ n\ W}\left(h - \tfrac{1}{2}D\right) \qquad \textbf{(7-4)}$$

If the droplet does not coalesce before it reaches the end of the plate, it will flow out of the separation channel with the effluent. If this phenomenon is effective, it will result in lower separation efficiencies, even for droplets (slightly) larger than D_c. In the GPS effects due to coalescence times can be neglected, while in the CPS coalescence times may play a role, but this cannot be proved. These conclusions are illustrated for each separator:

GPS: Take, for example, the GPS with flat plates as discussed in section 4.3. Consider an oil droplet 5% larger than D_c (for Q = 1 m³/hr: D = 171 μm) which enters the plate pack at h = 0. From equations (3-2-25) and (3-4-1) and the parameters given in section 4.3.3, the distance l can be calculated for which the droplet reaches the plate (this gives: l = 0.18 m). Assume the droplet will not coalesce but will be swept along with the flow towards the end of the plate. Then: $v_S \approx 4.48\ 10^{-4}$ m/s. The time for the droplet to reach the end of the plate will then be: $t = (L-l)/v_S \approx 44$ s. If that droplet has not coalesced within that period of time, it will presumably not be separated. From visual observations during the experiments, however, it was noted that the droplets (as far as they can be observed with the naked eye) coalesce at the plate surface within a second. Hence, for gravity plate separation, a decrease of the separation efficiency due to relatively long droplet-interface coalescence times did not occur.

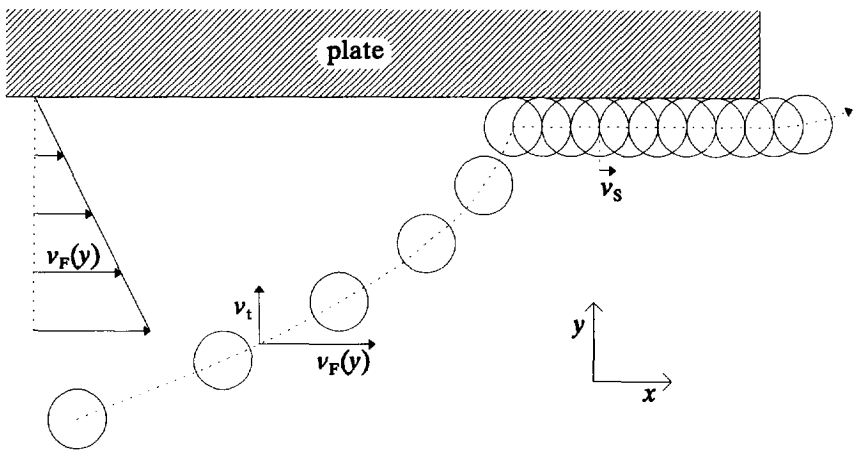

Figure (7-1) Oil droplet, approaching and subsequently making contact with a plate.

CPS: A similar illustration can be given for the experimental centrifuge. In the PCC for Q = 1.5 m³/hr the residence time is about 0.05 s and $D_c \approx 5.5$ μm. Using the parameters as given in table 6.2 gives: $l = 0.063$ m; $v_S \approx 0.069$ m/s (taking W = 0.02363 m, which is the calculated length of the channel curve). The time for the droplet to reach the end of the plate is: $t = (L-l)/v_S \approx 0.1$ s.

Unfortunately, less insight was gained into coalescence times in centrifugal force fields. No literature has been found and we were not able to carry out observations inside the centrifuge during rotation. Examining figures (6-18) to (6-22), the calculated D_c is always found to be smaller than the largest measured droplet diameter $D_{c,M}$. For example, for Q = 0.6 m³/hr (figure (6-18)): $D_c \approx 3.53$ μm and $D_{c,M} \approx$ 5.5 μm. If, for this particular situation, the disagreement between D_c and $D_{c,M}$ is only caused by the existence of a coalescence time t_c, then it is possible to determine t_c. From equations (2-6), (3-2-25) and (3-2-26) the distance l to be travelled by a droplet entering the plate pack at $h = 0$ (thus: $h_1 = 0$) and reaching the plate surface, can be determined. After some calculation this gives:

$$l_{h_1=0} = L\left(\frac{D_c}{D}\right)^2 \qquad \textbf{(7-5)}$$

For the above-stated situation this yields for $l(D_{c,M}) = 28.8$ mm. From equation (7-4) v_S can be determined; the resulting coalescence time will then be:

$$t_c = \frac{L - l}{v_S} \qquad \textbf{(7-6)}$$

which gives: $t_c \approx 1.57$ s. The same operation can be carried out for each of the other

14 experimental flow rates. In fact, this proposed t_c is not only a function of D but also of Q and may be given as $t_c(D,Q)$. Calculation of t_c as a function of D for one value of Q could be carried out as follows. Combination of equations (2-6), (3-2-25) and (3-2-26) gives the distance l to be travelled by a droplet entering the plate pack at h_1 (where: $0 \leq h_1 \leq h$) and reaching the plate surface:

$$l_{0 \leq h_1 \leq h} = L \left(\frac{D_c}{D} \right)^2 \left(1 - 3\frac{h_1^2}{h^2} + 2\frac{h_1^3}{h^3} \right) \qquad (7\text{-}7)$$

Combination of equations (7-7) and (3-2-32) gives:

$$l_{0 \leq h_1 \leq h} = \eta_M \, L \left(\frac{D_c}{D} \right)^2 \qquad (7\text{-}8)$$

where $\eta_M(D)$ represents the measured value of η for droplet diameter D. With equation (7-6) the matching $t_c(D)$ can be calculated. This has been done for Q = 0.5, 1.0 and 1.5 m³/hr. The resulting values of $t_c(D,Q)$ and $t_c(D)$ are shown graphically in figure (7-2). From the figure it appears on the one hand that t_c decreases with increasing D (line: $t_c(D,Q)$), on the other that t_c increases with increasing D (lines: $t_c(D)$). If the first statement is correct, then it means that for a certain D, t_c decreases with increasing Q. This phenomenon is unlikely to occur, because the angular velocity of a particular droplet is proportional to Q (see: section 2.6), which may possibly

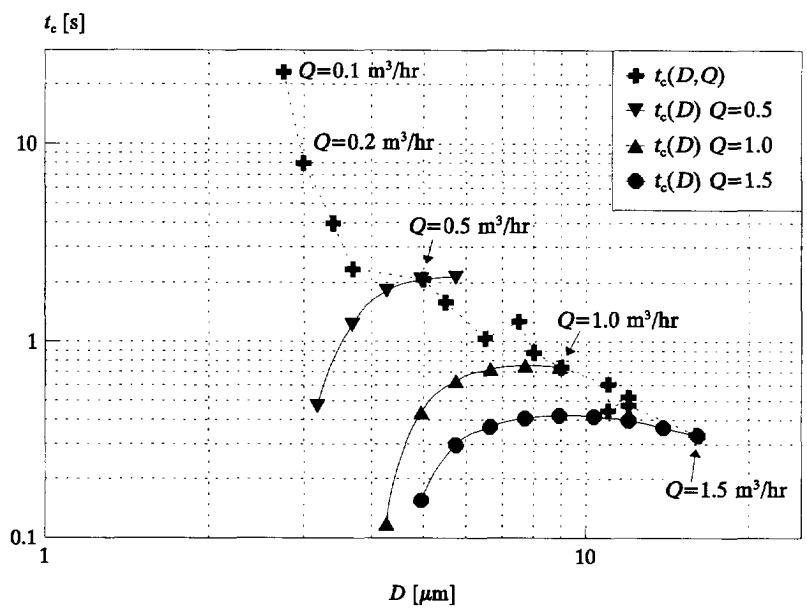

Figure (7-2) Relationship between coalescence time and droplet size.

result in aquaplaning of the droplet and hence, in the slowing down of the process of coalescence. Consequently, it has not been proved by this method that significant coalescence times of oil droplets exist in the CPS.

Particle-particle coalescence times
If coalescence of two droplets D_1 and D_2 occurs, the measured separation efficiencies $\eta(D_1)$ and $\eta(D_2)$ will be higher than if no coalescence occurred. The resulting droplet, D_3 , can either be separated or not. In the former case $\eta(D_3)$ will remain unchanged, while in the latter case a lower value of $\eta(D_3)$ will be measured than expected. If $D_1 < D_c$ and/or $D_2 < D_c$, then results could be obtained as have been measured with the experimental GPS and CPS (see figures (4-17) to (4-25) and (6-8) to (6-14)). In spite of the fact that some inter-droplet coalescence could have taken place during the experiments, it is uncertain to what extent this happened and for which droplet sizes, or where: in the inlet part, the plate pack or the outlet part of the separator.

Break-up
Break-up of droplets did practically not occur in the GPS. In the CPS break-up of relatively large droplets and the formation of secondary droplets has probably taken place. If so, and if the secondary droplets are sized within the critical range of the centrifuge, a lower total separation efficiency in that range would be measured than the predicted one. However, this has only been measured for droplets smaller than approximately 1.5 μm and for droplets sized around D_c. Droplets sized in the range between those values showed higher separation efficiencies. To prove that break-up of droplets has had a significant influence on the separation performance, more research is necessary.

7.1.2 Plate pack dimensions

From equations (3-2-27) and (3-5-2) it can be determined that if either the length L, or the width W of the separator deviates with factor ϵ, then the critical droplet diameter D_c and the total separation efficiency will change with factor $\epsilon^{-½}$. Generally, the construction tolerances for L and W of the plate pack are smaller than 1%, which results in: $0{,}99 < \epsilon < 1.01$ or $0.995 < \epsilon^{-½} < 1.005$, which can be ignored. Variations of the plate thickness can be neglected but variations of plate distances due to displaced or inadvertently curved plates may result in a significant decrease of separation efficiencies. This is explained by the following example:

Imagine a plate separator with dimensions as shown in figure (3-12). If all plate distances are identical, then its critical droplet diameter D_c is given by equation (3-4-2), and the pressure drop caused by the flow by [1]:

$$\Delta P_1 = \frac{12\ \mu\ L\ Q}{h^3\ n\ W} \qquad (7\text{-}9)$$

Each channel has the same flow rate: Q/n. If the plate distance varies between the channels, then the pressure drop is given by:

$$\Delta P_2 = \frac{12\ \mu\ L \sum_{i=1}^{n} Q_i}{W \sum_{i=1}^{n} h_i^3} \tag{7-10}$$

where:

$$\sum_{i=1}^{n} Q_i = Q \tag{7-11}$$

Assume, for example, that $n/2$ channels have a height $h(1+\epsilon)$, while the remaining channels have a height: $h(1-\epsilon)$, where: $0 \leq \epsilon < 1$. Consequently:

$$\Delta P_2 = \frac{24\ \mu\ L\ Q}{n\ h^3\ W\left((1+\epsilon)^3 + (1-\epsilon)^3\right)} \tag{7-12}$$

and the flow rate in each set of equivalent channels is then:

$$Q_{+\epsilon} = \frac{\Delta P_2\ h^3(1+\epsilon)^3\ n\ W}{24\ \mu\ L} \tag{7-13}$$

and:

$$Q_{-\epsilon} = \frac{\Delta P_2\ h^3(1-\epsilon)^3\ n\ W}{24\ \mu\ L} \tag{7-14}$$

After some calculations the critical droplet diameter of each set follows from:

$$D_{c,+\epsilon} = D_c \sqrt{\frac{2}{1 + \frac{(1-\epsilon)^3}{(1+\epsilon)^3}}} \tag{7-15}$$

and:

$$D_{c,-\epsilon} = D_c \sqrt{\frac{2}{1 + \frac{(1+\epsilon)^3}{(1-\epsilon)^3}}} \tag{7-16}$$

The corresponding separation efficiencies are then given by:

$$D \le D_{c,+\epsilon}: \quad \eta_{+\epsilon} = \left(\frac{D}{D_{c,+\epsilon}}\right)^2 \qquad D \ge D_{c,+\epsilon}: \quad \eta_{+\epsilon} = 1 \tag{7-17}$$

and:

$$D \le D_{c,-\epsilon}: \quad \eta_{-\epsilon} = \left(\frac{D}{D_{c,-\epsilon}}\right)^2 \qquad D \ge D_{c,-\epsilon}: \quad \eta_{-\epsilon} = 1 \tag{7-18}$$

Finally, the resulting total separation efficiency of the separator is given by:

$$\eta_{tot} = \eta_{+\epsilon}\frac{Q_{+\epsilon}}{Q} + \eta_{-\epsilon}\frac{Q_{-\epsilon}}{Q} \tag{7-19}$$

Figure (7-3) shows $D_{c,-\epsilon}/D_c$ and $D_{c,+\epsilon}/D_c$ for $0 \le \epsilon \le 1$. Note that for $\epsilon=1$: $D_{c,+\epsilon}=\sqrt{2}\cdot D_c$ and $D_{c,+\epsilon}=0$. In fact, this situation coincides with a plate pack of which half the channels have equal heights.

Figure (7-4) shows η_{tot} for $\epsilon=0$, $\epsilon=0.1$, $\epsilon=0.2$ and $\epsilon=0.3$, respectively. Note that η_{tot} remains unchanged for $D < D_{c,-\epsilon}$, while $D_{c,+\epsilon}=D_{c,tot} > D_c$.

Apart from vertical movement, one or more plates can be inclined relative to the each other. This results in similar deviations of $D_{c,tot}$ and η_{tot}.

Examining the results of the experiments, it can be concluded that this phenomenon may have caused the disagreements between the outcome of the simulations and the experiments for droplets sized around D_c.

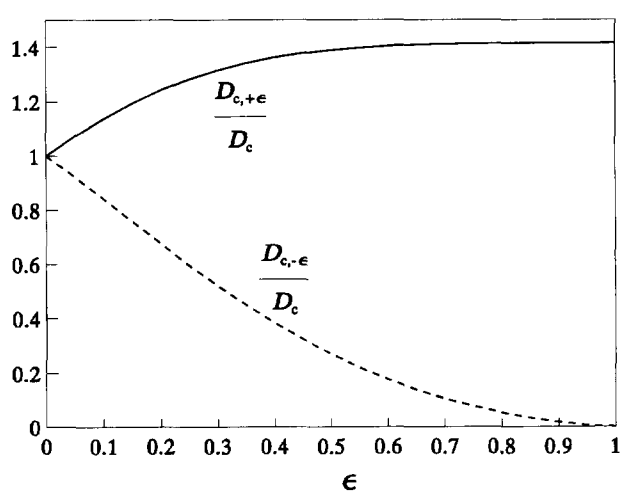

Figure (7-3) Relation between ϵ and the resulting deviations of D_c.

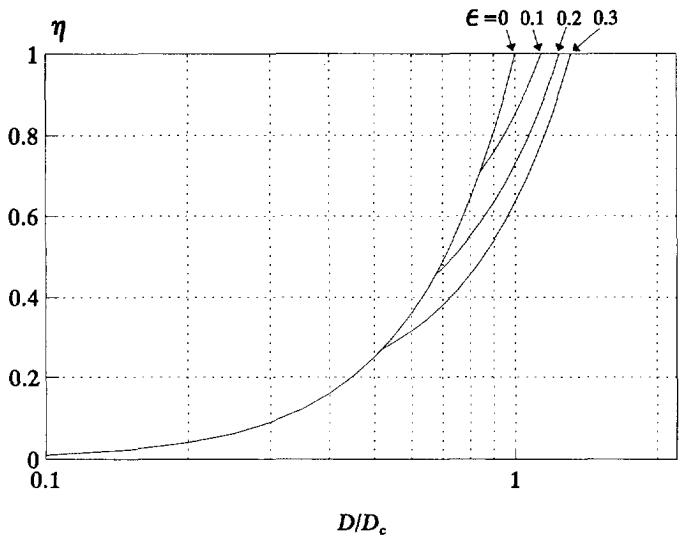

Figure (7-4) Relation between $\eta(D)$ and ϵ.

7.1.3 Uneven flow distribution

If the flow towards and from the plate pack has different restrictions, the flow rate in each channel may differ. This results in identical deviations of $D_{c,tot}$ and η_{tot} as derived in section 7.1.2. However, in this case variations of ΔP over each channel cause changes in flow rates. Thus, uneven flow distribution also may have caused the disagreements between the outcomes of simulations and experiments for droplets sized around D_c.

7.1.4 Separation outside the pack of plates

Rising oil droplets may reach some surface, such as the inner wall of a conduit-pipe or in- or outlet section of the separator. A film of oil may build up on these walls. This film could be separated, or dispersed into the flow again. Generally, a significant part of the droplets sized much larger than D_c will be separated this way. If separation outside the pack of plates takes place for droplets sized around and below D_c, this will result in increased separation efficiencies for all of these droplet sizes. However, this has not been observed in any of the experiments.

7.1.5 Measurement inaccuracies

Droplet size measurements were carried out with a Malvern Particle Sizer, model 3600E, the principle of which is based on diffraction (or scattering) of light by a particle (droplet). Under this principle droplets of a given size diffract light through a given angle, which increases with decreasing droplet size. According to the manufacturer, the measuring accuracy of the 3600E is $\pm 4\%$ on the volume median diameter [4]. Syvitsky [5] investigated the state of the art in particle size characterization and found that the Malvern Particle Sizer does not give a good indication of the amount of material below the analytical range. Furthermore it was found that the amount indicated between 0.5 μm and 2 μm was 16%-20% of the amount < 2 μm actually present. These results were obtained by using an older version (6.0) of the software than we have used (SB.0A). The latter one is claimed to be more accurate for droplets sizes below 7 μm. Because no exact figures were given, the accuracy of the measured number of droplets sized below 2 μm is still uncertain.

In connection with the use of the Malvern Particle Sizer, the experimental curves as shown for both gravity plate separation and centrifugal plate separation will be briefly discussed. General characteristics of the gravity plate separation curves (Figures (4-13) to (4-21)) are that the experimentally measured efficiencies are somewhat larger than the theoretical efficiencies (except for the region near D_c) and that for very small diameters the experimental curves have an irregular, almost sinusoidal shape. Concerning the first effect, the most logical explanation is that the occurrence of some oil droplet coalescence has a favourable influence on the efficiency. Concerning the second effect it is more difficult to provide a suitable explanation. It is highly improbable that the effect is caused by an accidental error in the experiments itself, because the effect occurs for all experiments. A second possibility is that the curves are irregular as a result of variations in the respective concentrations. It is noted that the efficiency is a ratio of two concentrations, and in case one of the concentrations is small, a substantial variation of this concentration can lead to a large error in the efficiency. Again, it can be argued that this supposition is not valid, because in all figures the same tendency can be observed: there is a regularity in the irregularity. Where it is not probable that the mentioned effect is a result of experimental procedures, it is concluded that the effect has an instrumental origin. The results achieved with the Malvern Particle Sizer near its lower diameter limit must be regarded with caution, see also above. In connection with this conclusion we mention research activities on other subjects, where also inconsistent results were obtained for measurements with the Malvern Particle Sizer for small diameters [2].

Essentially the same tendencies are observed for the experiments concerning the efficiency of the plate packed centrifuge (Figures (6-15) to (6-22)). For small diameters even negative efficiencies appear. Also here the conclusion is defensible that the irregularity of the curves for small diameters is mainly due to errors connected with the performance of the Malvern Particle Sizer.

7.2 Conclusions

For gravity plate separators and centrifugal plate separators the terminal rising velocity (or: terminal settling velocity) of small oil droplets can be predicted fairly well by Stokes' law, because the droplets may be assumed to be rigid spheres. Gravity in a GPS, and centrifugal forces in a CPS, are the dominant forces determining the rising velocity.

The separation efficiency is determined by the critical droplet diameter, for which the separation efficiency is 100%, and by the particle size distribution. Droplets smaller than the critical droplet diameter are only partially separated. The separation efficiency for all droplet sizes below the critical diameter is determined by the general separation efficiency function. This function is **un**affected by the shape of the flow profile in a plate pack (GPS as well as CPS), as long as the flow regime is laminar.

An overview of the effects of various mechanisms and phenomena affecting the separation efficiency is given in table (7-1). The Coriolis force can generally be neglected in centrifuges. However, if the density difference between the dispersed and continuous phase is much larger than in our system, this statement must be reconsidered, especially when heavy particles have to be separated. The influence of coalescence times and break-up in a

Mechanism/phenomenon		GPS	CPS
Droplet deformation		-	-
Forces	Gravity	+	-
	Centrifugal		+
	Coriolis		-*
	Shear	-	-
	Molecular (Brownian motion)	-	-
Coalescence times		-*	?
Break-up		-*	?
Deviations of the plate pack dimensions	Width	-	-
	Length	-	-
	Plate distance	+	+

+	large effect
-	negligible
*	not generally

Table (7-1) The effect of various mechanisms and phenomena on the separation efficiency of GPS's and CPS's as found in this thesis. Some are not generally applicable, e.g. coalescence times may have a significant effect in systems where additives such as surface contaminants delay the process of coalescence.

CPS is still uncertain. In our systems there were no clear indications that they have played a role, but in other systems where additives such as surface contaminants delay the process of coalescence or promote break-up, these phenomena may have a significant effect on the separation efficiency.

More practically, when constructing a plate pack for either a GPS or a CPS, deviations of the plate distance must be kept relatively small, because slight deviations will cause a substantial decrease in separation efficiency.

To check the design of prototypes and existing plate separators (both GPS and CPS), the general separation efficiency function can be used as a reference. Namely, if the separator in question is connected to a set-up similar to the one described in this thesis, the separation efficiency as function of droplet size can be measured. Comparing the results with the general separation efficiency function gives insight into the quality of the plate pack and/or the stream divider.

In gravity plate separators the plates should be flat to obtain optimal separation efficiency. However, practical considerations may lead to a choice for corrugated plates which are mechanically more stable. Corrugations have an insignificant effect on the separation efficiency. In practice, the shape of the plates is determined by constructional and maintenance considerations, the latter being very real because plugging of plate packs by scale is often a problem in the oil field. Moreover, cleanability plays a significant role in the food industry because of hygienic aspects. Finally, economic considerations will have an influence, too.

The model of the PPC and PCC gives a satisfactory prediction of the critical droplet diameter as well as of the separation efficiency as function of the oil droplet diameter. The simulation program -based on this model- proved to be a valuable tool for design purposes. The simulation program shows one optimum configuration for each of the four plate pack types. In plate packed centrifuges the use of curved plates or curved channels is recommended, because -for both the PPC and the PCC- the optimum configurations for curved plates/ channels perform roughly twice as well as the optimum configurations for flat plates/straight channels. However, which of the two will be selected depends also on economical considerations.

Comparison of the plate centrifuges and the disc stacked centrifuge shows that the latter has a different response to flow-rate changes. Plate centrifuges show a practically unlimited operating range with respect to flow rate, while disc stacked centrifuges feature a relatively restricted tolerance for flow rate variations, lest water comes out of the oil outlet or the separation efficiency decreases excessively. Models which are provided with a system to regulate the outlet pressure (back pressure) can handle a wider flow rate range.

In a DSC the flow distribution over the separation channels is strongly determined by the disc stack dimensions and the flow rate. In the PPC/PCC the flow distribution is determined by a separate device upstream of the plate pack. In addition, there are no hydrodynamic restrictions to the length of the PPC/PCC. The separation efficiency improves by a factor two

if the length increases fourfold; the length is only restricted by mechanical limitations. The length-diameter ratio of the DSC is limited due to increased flow distribution deviation with increasing length-diameter ratio.

References

[1] Bird, R.B. et. al.: Transport phenomena, John Wiley & Sons, New York, 1960.
[2] Boxman, A., Particle size measurement for the control of industrial crystallizers, Thesis, Delft Univerity of Technology, Delft, 1992.
[3] Clift, R. et. al.: Bubbles, drops, and particles, Academic Press, New York, 1978.
[4] Reference Manual: Malvern instruments particle sizer, model 3600E.
[5] Syvitski, J.P.M.: Principles, methods, and application of particle size analysis, Cambridge University Press, Cambridge, 1991.

Appendices and List of symbols

Appendix A

Derivation of the terminal rising velocity

A free droplet will move in water by a buoyant force:

$$F_b = \frac{\pi}{6} D^3 (\rho_w - \rho_o) g \tag{A-1}$$

This motion gives rise to a resistance force. For $Re < 0.3$ [9] this force is, according to Stokes' law:

$$F_S = 3 \pi \mu v D \tag{A-2}$$

The droplet accelerates due to F_b. Hence, v increases until F_S balances F_b. Thus, the equation of motion of the droplet is:

$$m \frac{dv}{dt} = F_b - F_S \tag{A-3}$$

so that:

$$\frac{dv}{dt} = -\frac{18\mu}{D^2 \rho_o} \left(v - \frac{(\rho_w - \rho_o) g D^2}{18\mu} \right) \tag{A-4}$$

and:

$$\int \frac{dv}{v - (\Delta\rho\, g D^2/[18\mu])} = -\frac{18\mu}{D^2 \rho_o} \int dt \tag{A-5}$$

This yields:

$$v = \frac{(\rho_w - \rho_o) g D^2}{18\ \mu} + constant \cdot e^{-\frac{18\mu t}{D^2 \rho_o}} \tag{A-6}$$

with boundary condition $v=0$ for $t=0$ we find:

$$v = \frac{(\rho_w - \rho_o) g D^2}{18\ \mu} \left(1 - e^{-\frac{18\mu t}{D^2 \rho_o}} \right) \tag{A-7}$$

This yields for the terminal rising velocity v_t:

$$v_t = \lim_{t \to \infty} v = \frac{(\rho_w - \rho_o) g D^2}{18\mu} \tag{A-8}$$

Appendix B

Derivation of the general separation efficiency function

Theorem:

$$\forall v_x(x,y), \int_0^h v_x(x,y)\,dy = \frac{Q}{nW} \;:\; D_c = \sqrt{\frac{18\,Q\,\mu}{nLW(\rho_w-\rho_o)g}} \;\wedge\; \eta = \left(\frac{D}{D_c}\right)^2 \qquad \begin{matrix}(0\le x\le L)\\(0\le y\le h)\\(D\le D_c)\end{matrix}$$

Consider a channel between two flat plates as sketched in figure (B-1).

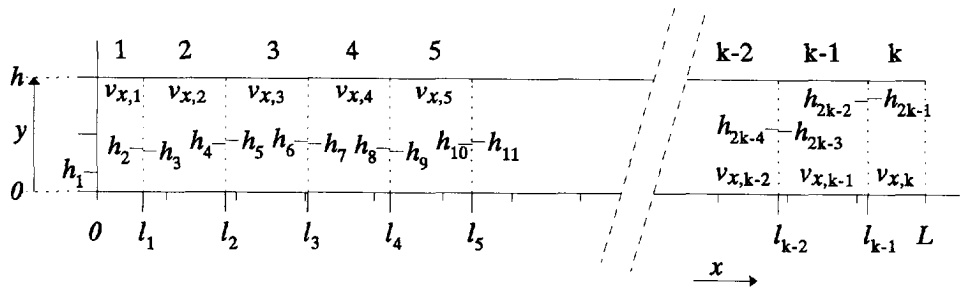

Figure (B-1) Channel between two flat plates divided into **k** sections, each with its specific flow velocity profile.

For all velocity distributions is valid:

$$\int_0^h v_{x,1}(y)\,dy = \int_0^h v_{x,2}(y)\,dy = \ldots\ldots = \int_0^h v_{x,k-1}(y)\,dy = \int_0^h v_{x,k}(y)\,dy = \frac{Q}{nW} \qquad \textbf{(B-1)}$$

Assume a droplet with diameter D, entering the channel at height h_1, and rising with velocity v_t according to equation (2-6). The droplet will have a horizontal velocity v_x. Assume the droplet reaches the end of the first part at (l_1,h_2), and enters the second part of the channel at (l_1,h_3), and so on. Assume also that the droplet reaches the surface of the upper plate at (L,h). Then the time t_1 to travel from $(0,h_1)$ to (l_1,h_2) is:

$$t_1 = \frac{h_2-h_1}{v_t} = \frac{l_1}{\overline{v_{x,1}}} = \frac{l_1(h_2-h_1)}{\int_{h_1}^{h_2} v_{x,1}\,dy} \qquad \textbf{(B-2)}$$

and the time t_2 to travel from (l_1,h_3) to (l_2,h_4) is:

$$t_2 = \frac{h_4 - h_3}{v_t} = \frac{l_2 - l_1}{\overline{v_{x,2}}} = \frac{(l_2 - l_1)(h_4 - h_3)}{\int_{h_3}^{h_4} v_{x,2}\,dy} \qquad \textbf{(B-3)}$$

and the time t_{k-1} to travel from (l_{k-2},h_{2k-3}) to (l_{k-1},h_{2k-2}) is:

$$t_{k-1} = \frac{h_{2k-2} - h_{2k-3}}{v_t} = \frac{l_{k-1} - l_{k-2}}{\overline{v_{x,k-1}}} = \frac{(l_{k-1} - l_{k-2})(h_{2k-2} - h_{2k-3})}{\int_{h_{2k-3}}^{h_{2k-2}} v_{x,k-1}\,dy} \qquad \textbf{(B-4)}$$

and the time t_k to travel from (l_{k-1},h_{2k-1}) to (L,h) is:

$$t_k = \frac{h - h_{2k-1}}{v_t} = \frac{L - l_{k-1}}{\overline{v_{x,k}}} = \frac{(L - l_{k-1})(h - h_{2k-1})}{\int_{h_{2k-1}}^{h} v_{x,k}\,dy} \qquad \textbf{(B-5)}$$

Combination of the equations given above yields:

$$v_t = \frac{\int_{h_1}^{h_2} v_{x,1}\,dy}{l_1} = \frac{\int_{h_3}^{h_4} v_{x,2}\,dy}{l_2 - l_1} = \ldots\ldots = \frac{\int_{h_{2k-3}}^{h_{2k-2}} v_{x,k-1}\,dy}{l_{k-1} - l_{k-2}} = \frac{\int_{h_{2k-1}}^{h} v_{x,k}\,dy}{L - l_{k-1}} \qquad \textbf{(B-6)}$$

Further we know that:

$$\forall p \in \mathbb{N} | 1 \le p \le k : \int_0^{h_{2p-1}} v_{x,p}\,dy + \int_{h_{2p-1}}^{h_{2p}} v_{x,p}\,dy + \int_{h_{2p}}^{h} v_{x,p}\,dy = \int_0^{h} v_{x,p}\,dy = \frac{Q}{nW} \qquad \textbf{(B-7)}$$

In addition, the following relation is also valid:

$$\forall p \in \mathbb{N} | 1 \le p \le k-1 : Q_{p;0 \uparrow h_{2p}} = Q_{p+1;0 \uparrow h_{2p+1}} \rightarrow \int_0^{h_{2p}} v_{x,p}\,dy = \int_0^{h_{2p+1}} v_{x,p+1}\,dy \qquad \textbf{(B-8)}$$

Combination of the equations above yields:

$$\int_0^{h_1} v_{x,1}\,dy + \int_{h_1}^{h_2} v_{x,1}\,dy + \int_{h_3}^{h_4} v_{x,2}\,dy + \ldots\ldots + \int_{h_{2k-3}}^{h_{2k-2}} v_{x,k-1}\,dy + \int_{h_{2k-1}}^{h} v_{x,k}\,dy = \int_0^{h} v_{x,1}\,dy \qquad \textbf{(B-9)}$$

Combination of equations (B-6) and (B-9) yields:

$$\int_0^{h_1} v_{x,1}\,dy + v_t l_1 + v_t(l_2 - l_1) + \ldots\ldots + v_t(l_{k-1} - l_{k-2}) + v_t(L - l_{k-1}) = \int_0^{h} v_{x,1}\,dy \qquad \textbf{(B-10)}$$

Hence:

$$v_t = \frac{\int_{h_1}^{h} v_{x,1}\,dy}{L} \qquad \textbf{(B-11)}$$

Combination of equations (2-6) and (B-11) gives the expression for the diameter D of the droplet:

$$D = \sqrt{\frac{18\ \mu \int_{h_1}^{h} v_{x,1}\,dy}{L\ (\rho_w - \rho_o)\ g}} \qquad \textbf{(B-12)}$$

The critical droplet diameter D_c is:

$$D_c = \sqrt{\frac{18\ \mu \int_{0}^{h} v_{x,1}\,dy}{L\ (\rho_w - \rho_o)\ g}} = \sqrt{\frac{18\ Q\ \mu}{nWL(\rho_w - \rho_o)g}} \qquad \textbf{(B-13)}$$

This gives for the ratio D/D_c:

$$\frac{D}{D_c} = \sqrt{\frac{\int_{h_1}^{h} v_{x,1}\,dy}{\int_{0}^{h} v_{x,1}\,dy}} \qquad \textbf{(B-14)}$$

Droplets with diameter D entering the plate pack at positions between h_1 and h will reach the plate surface when $l < L$, while droplets with diameter D entering the plate pack below h_1 will not reach the plate surface. Consequently, if we define the separation efficiency η as the fraction of the total amount of droplets with diameter D reaching the plate surface then:

$$\eta = \frac{Q_{1;h_1 \uparrow h}}{Q} = \frac{\int_{h_1}^{h} v_{x,1}\,dy}{\int_{0}^{h} v_{x,1}\,dy} \qquad \textbf{(B-15)}$$

Hence

$$\eta = \left(\frac{D}{D_c}\right)^2 \qquad \textbf{(B-16)}$$

Appendix C

Experimental set-up

C.1 In-line oil-water mixing

Several methods of oil-water mixing were considered and tested. Ideally, the mixer should be capable of producing a mixture of which the droplets are within a small size-range, and the mean droplet size should be adjustable between at least 1 μm and 50 μm. Such a mixer would facilitate observation of break-up of droplets of a certain size, because then the influx would contain essentially only droplets of that specific size. However, the results of tests on the prototypes were quite unfavourable. Eventually, a mixer was constructed which produces oil droplets with diameters of 0.5 to 500 μm.

Figure (C-1) gives the scheme of the mixer which was used. By means of a four-way junction a part of the water stream is by-passed and led through a needle valve by a gear pump (Make: Verder, type: 2030, pump head: V108.05). The oil is displaced from a tank by a plunger pump (Make: Gilson, type: 305, pump head: 10SC) and injected into the by-pass line through the adjustable needle valve. The needle is adjusted in such a way that the pressure gauge reads about 100 bar. This procedure leads to a very constant and reproducible mixture. For a given setting of gear pump, plunger pump and needle valve, the oil-droplet size distribution stays constant for any flow rate of the main stream, as long as the latter is

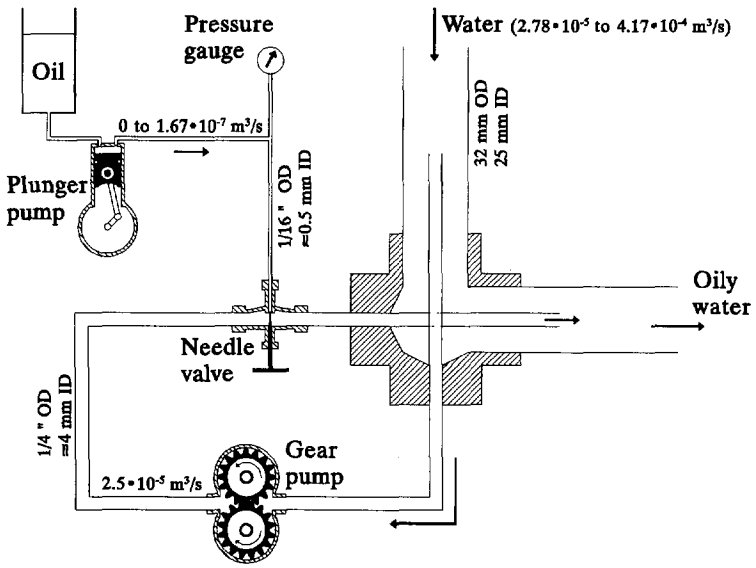

Figure (C-1) The in-line oil-water mixer.

kept larger than the rate of the by-pass stream. If not, the mixture leaving the by-pass will flow back through the main flow line and re-enter the by-pass, which leads to an unstable droplet size distribution.

C.2 In-line droplet size measurement

Oil-droplet size distributions are measured with a Malvern 3600E particle size analyzer. This apparatus is based on the principle that particles of a certain size diffract light through a specific angle, which increases with decreasing particle size. A parallel beam of monochromatic light is passed through the mixture (see figure (C-2)), and the diffracted light is focused onto the multi-element ring detector. This detector senses the angular distribution of scattered light intensity. A lens, placed behind the illuminated sample with the ring detector at its focal point, focuses the undiffracted light on the central detector. The surrounding diffraction pattern, which does not vary with particle movement, is separately detected by the ring detector. Thus, a stream of particles can be passed through the beam to generate a stable diffraction pattern. For the Malvern, three lenses are available with focal lengths of 63, 100 and 300 mm, the length determining the size range that is analyzed (1.2-118 μm, 1.9-188 μm and 5.6-564 μm, respectively).

The standard Malvern particle size analyzers are provided with only a small sample cell and a small flow-through cell. Using the sample cell was not convenient, and the flow-through cell could not handle large volumes of water. Initially, the flow-through cell was used in combination with a by-pass, but this led to problems such as complex and time-consuming

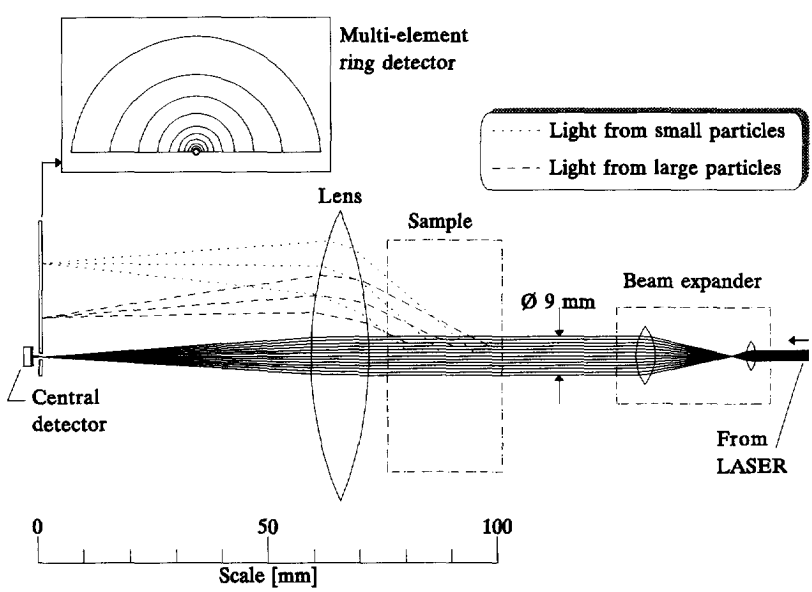

Figure (C-2) Schematic diagram of the Malvern 3600E laser particle size analyzer showing the primary components.

cleaning procedures. Another serious problem was that the windows of these cells have fixed distances which can hardly be altered. Being able to alter the window distance is essential to obtain reliable results, because the number of droplets intercepted by the laser beam determines the amount of light registered by the detector. To keep the output of the detector within its operating range when analyzing different oil-droplet concentrations, the path length of the laser beam through the mixture must be adjustable. This led to the design of a new measuring cell.

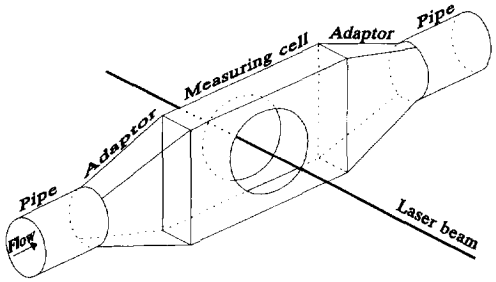

Figure (C-3) Basic diagram of the in-line measuring cell for particle size analysis.

A sketch of the new in-line measuring cell is given in figure (C-3). The cell is part of the main flow line to avoid problems with by-pass lines. Figure (C-4) shows the section drawing of the new cell. The amount of diffracted laser light can be decreased by screwing the movable holder with window further inside. This will shorten the distance which the laser beam has to travel through the mixture. Other advantages of this cell are that the windows can be cleaned and their distance altered without interrupting the process of separation.

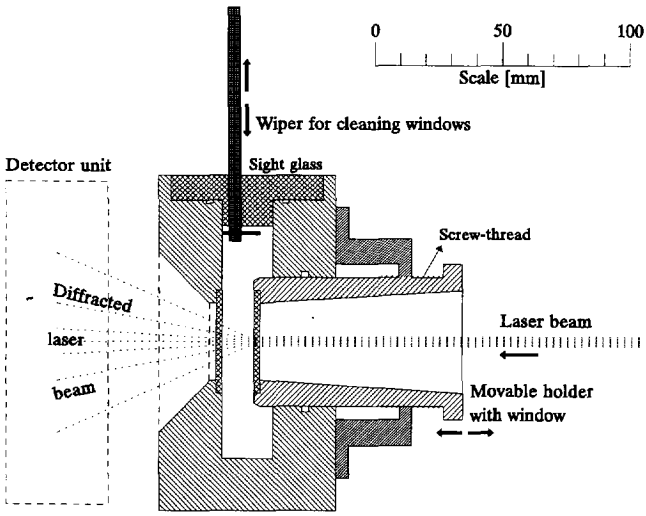

Figure (C-4) Section drawing of the in-line measuring cell.

Appendix D

The disc stacked centrifuge

D.1 Principles

To reduce the settling distance for oil droplets, in many cases a stack of conical discs is mounted inside the rotating bowl of a centrifuge. The function of the discs is to divide the separation zone into thin layers, so that the particles to be separated need to travel only a very short distance before they collide with the disc surface and are separated from the continuous phase. The distance between two discs is determined by radially orientated spacers or caulks. A minimum distance between two plates is required to prevent clogging.

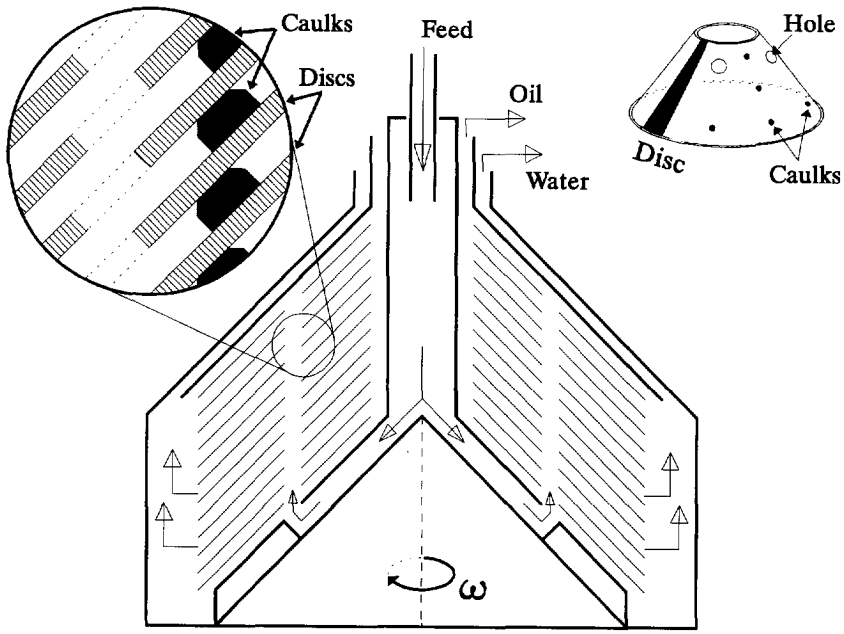

Figure (D-1) The interior of a disc stacked centrifuge.

Each disc is provided with holes (usually: 4 or 6) at a specific distance from the centrifuge axis. The discs (quantity: 50 to 200) are placed on top of each other in such a way that the holes in the discs form vertical distribution channels (see figure (D-1)). Because the discs are conically shaped, two discs form a channel that has an angle with the axis. The denser phase is thrown radially outward along the underside of the discs by centrifugal forces. The lighter

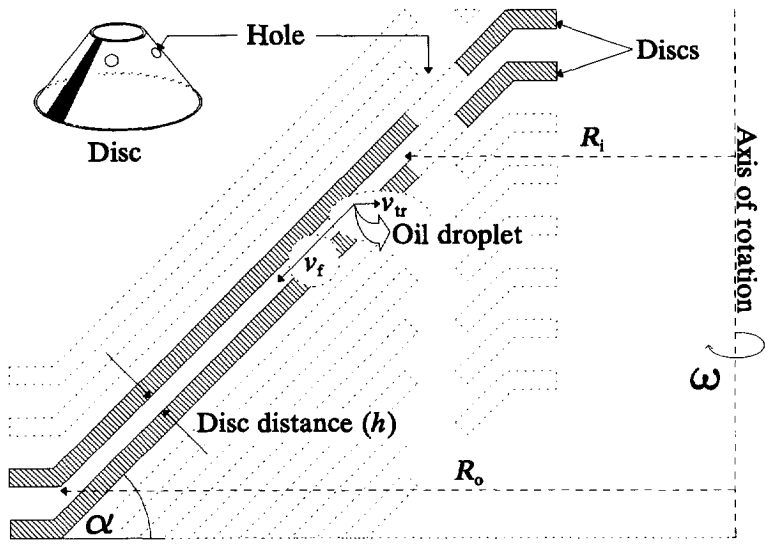

Figure (D-2) A channel between two discs of a disc stacked centrifuge, where separation takes place.

phase will, as a result of its lower density, be forced to flow upwards along the discs towards the axis where it will be collected in vertical channels and will leave the centrifuge through the light phase outlet.

Oily water enters the channel between two successive discs at radius R_i (see figure (D-2)). It flows through this channel with velocity v_f. Here separation will take place. Oil droplets dragged along with the water, will have a velocity component v_f and a velocity component v_{tr}, where the last is the radial settling velocity according to equation (2-9). Hence, oil droplets are forced towards the upper surface of the lowest of the two consecutive discs. If v_{tr} is large enough with respect to v_f, the oil droplet will collide at this surface before it reaches the end of the channel. Droplets colliding at the disc surface will coalesce and form a thin layer which is forced to flow along the surface towards the centre of rotation. Finally, de-oiled water leaves at the periphery of the stack of discs, at radius R_o. In an ideal situation, with equal flow rate in each channel, v_f is given by:

$$v_f = \frac{Q}{2\pi R h n} \qquad \text{(D-1)}$$

The position of the interface between the heavy and the light phase is dependent on the hydrostatic balance in the outlet channels and can be adjusted by altering the diameter of a special ring. This ring, the gravity disc, determines the diameter of the heavy phase outlet. Van der Linden [1] carried out theoretical and experimental studies on the separation performance as a function of the position of the oil-water interface. He found that optimum separation is achieved when the oil-water interface is located in such a way that the distribution channels are entirely within the continuous phase.

Some unfavourable aspects of the flow behaviour in a disc stack are:

- As a result of the presence of flow restrictions, a variation of the flow rate will lead to a shift of the interface position. Because this position is important for the centrifuge performance, the flow rate is allowed to vary only within a restricted range. In practice some centrifuge models are provided with a system to regulate the outlet pressure (back pressure). These can handle a wider flow rate range.
- Because of the presence of counter-current flow between the water and the oil stream re-entrance of oil droplets in the main water stream may occur.
- The flow distribution in each separation channel is strongly determined by the disc stack dimensions. It is also dependent on the flow rate of the influx.

Figure (D-3) shows the difference between the flow patterns in the disc stacked centrifuge (left part of the figure) and in the plate packed centrifuge (right side of the figure).

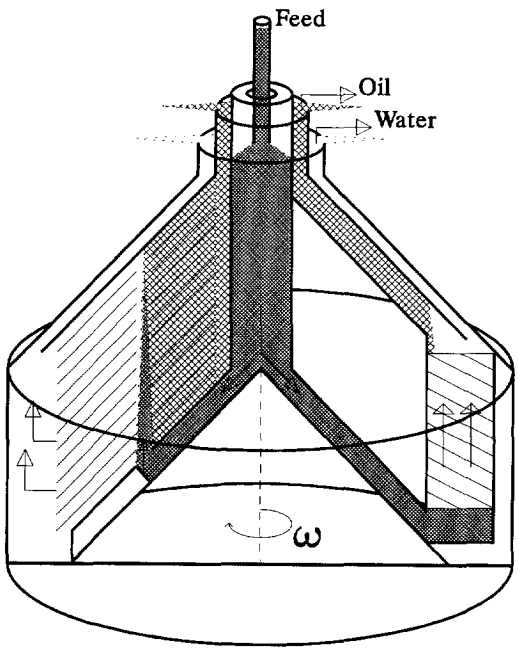

Figure (D-3) Difference between the flow patterns in a disc stacked and a parallel plate centrifuge.

D.2 Experimental

A number of experiments on the disc stacked centrifuge have been carried out. The results are shown in figure (D-4). The figure also shows a curved line which is the outcome of the simulation program, based on equations (D-1) and (2-9). To cover a flow rate range from 400 to 1500 l/hr it was necessary to change the gravity disc size at about 900 l/hr. Below this

flow rate the large gravity disc leads to less favourable results than those obtained with the small gravity disc. At flow rates above 900 l/hr, with the smaller gravity disc present, not only oil but also water appeared in the oil effluent outlet. Theoretically, the D_{90}-points should be below the curved line, which represents D_c obtained from simulations. Especially for the lower flow rates the D_{90}-points have higher values than the corresponding results of the simulation program.

The parameters of the used oil-water mixture were:

- Temperature	T:	286 K
- Density of water	ρ_w:	1000 kg/m^3
- Density of oil	ρ_o:	899 kg/m^3 (Shell Omala 220)
- Flow rate (water)	Q:	0.4 to 1.5 m^3/hr (in steps of 0.1 m^3/hr), (1.11 10^{-4} to 4.17 10^{-4} m^3/s)
- Flow rate (oil)	Q_{oil}:	0.18 10^{-3} m^3/hr (5 10^{-8} m^3/s)

The characteristics of the experimental centrifuge were:

- Manufacturer and type:		Alfa Laval Industries, MAB 104
- Angular velocity	ω:	785 rad/s (7500 rpm)
- Inner radius	R_i:	46 mm
- Outer radius	R_o:	76 mm
- Cone angle	α:	60 degrees
- Disc distance	h:	0.35 mm
- Number of discs	n:	72

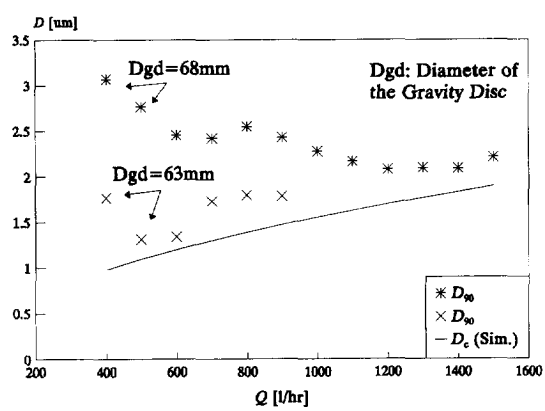

Figure (D-4) Results of the experiments and the simulations.

References

[1] Linden, J.P. van der: Liquid-liquid separation in disc-stack centrifuges, Thesis, Delft University of Technology, 1987.

Appendix E

Results of the simulations with plate packed centrifuges

PPC

Fig. No.:	R_i^*	d^*	R_p^*	β / h_{min}^*	n
E-1	0.5 - 1	0.002	1000	20 / var	500
E-2	0.5 - 1	0.002	1000	var / 0.003	500
E-3	0.5 - 1	0.002	0.85	20 / var	500
E-4	0.5 - 1	0.002	0.85	var / 0.003	500
E-5	0.7	0 - 0.005	1000	20 / var	500
E-6	0.7	0 - 0.005	1000	var / 0.003	500
E-7	0.7	0 - 0.005	0.85	20 / var	500
E-8	0.7	0 - 0.005	0.85	var / 0.003	500
E-9	0.7	0.002	0.4 - 1.5	20 / var	500
E-10	0.7	0.002	0.4 - 1.5	var / 0.003	500
E-11	0.7	0.002	1000	−30 - +50 /var	500
E-12	0.7	0.002	0.85	−30 - +50 /var	500
E-13	0.7	0.002	1000	20 / var	100 - 1100
E-14	0.7	0.002	1000	var / 0.003	100 - 1100
E-15	0.7	0.002	0.85	20 / var	100 - 1100
E-16	0.7	0.002	0.85	var / 0.003	100 - 1100

PCC

Fig. No.:	R_i^*	h^*	R_c^*	β / d_{min}^*	n
E-17	0.5 - 1	0.002	1000	20 / var	500
E-18	0.5 - 1	0.002	1000	var / 0.003	500
E-19	0.5 - 1	0.002	0.85	20 / var	500
E-20	0.5 - 1	0.002	0.85	var / 0.003	500
E-21	0.7	0 - 0.005	1000	20 / var	500
E-22	0.7	0 - 0.005	1000	var / 0.003	500
E-23	0.7	0 - 0.005	0.85	20 / var	500
E-24	0.7	0 - 0.005	0.85	var / 0.003	500
E-25	0.7	0.002	0.4 - 1.5	20 / var	500
E-26	0.7	0.002	0.4 - 1.5	var / 0.003	500
E-27	0.7	0.002	1000	−30 - +50 /var	500
E-28	0.7	0.002	0.85	−30 - +50 /var	500
E-29	0.7	0.002	1000	20 / var	100 - 1100
E-30	0.7	0.002	1000	var / 0.003	100 - 1100
E-31	0.7	0.002	0.85	20 / var	100 - 1100
E-32	0.7	0.002	0.85	var / 0.003	100 - 1100

Table E-1 Parameter values of the **PPC** and **PCC** as chosen for the simulations.

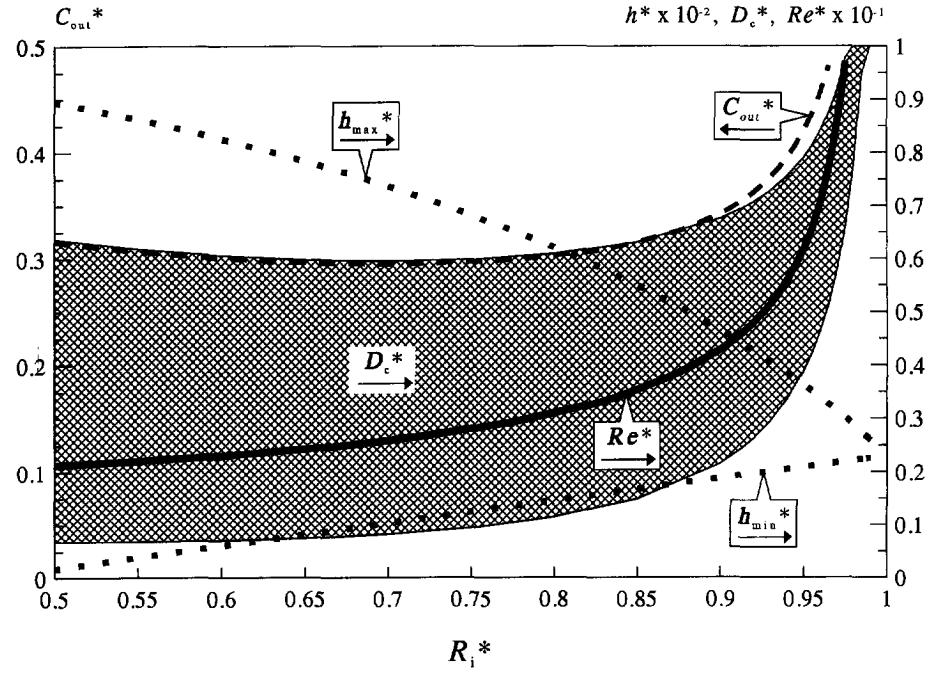

Figure (E-1) Flat plates. β=20 degrees, h_{min}^*=variable.

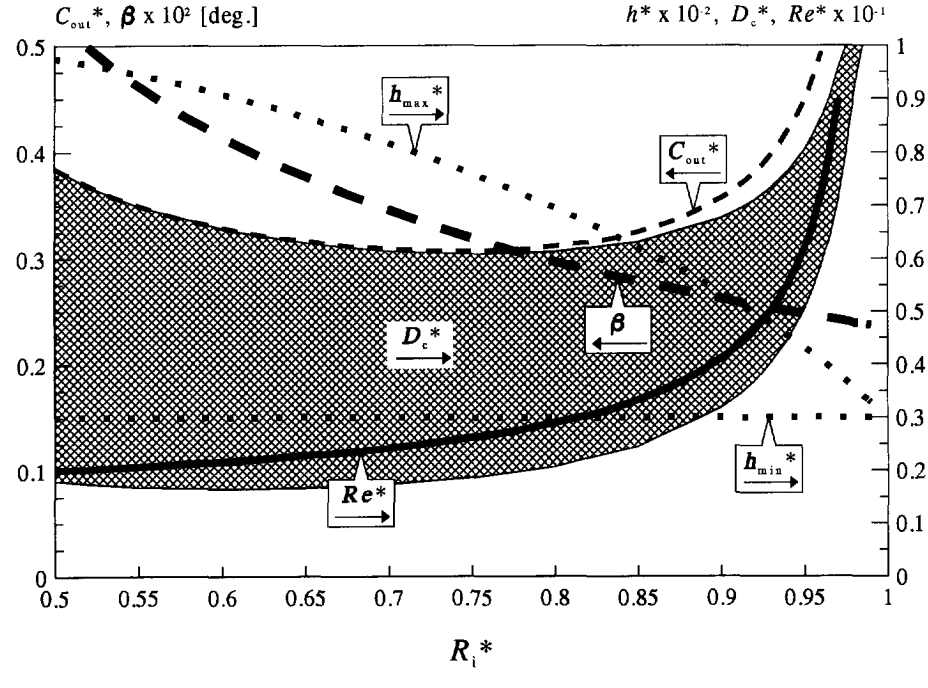

Figure (E-2) Flat plates. β=variable, h_{min}^*=0.003.

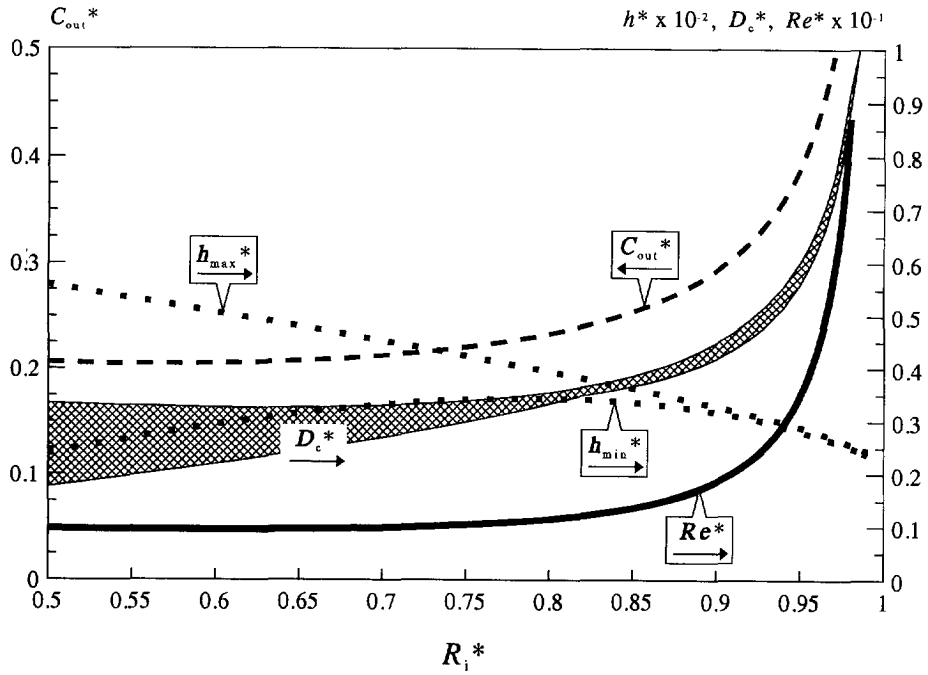

Figure (E-3) Curved plates. β=20 degrees, h_{min}^*=variable.

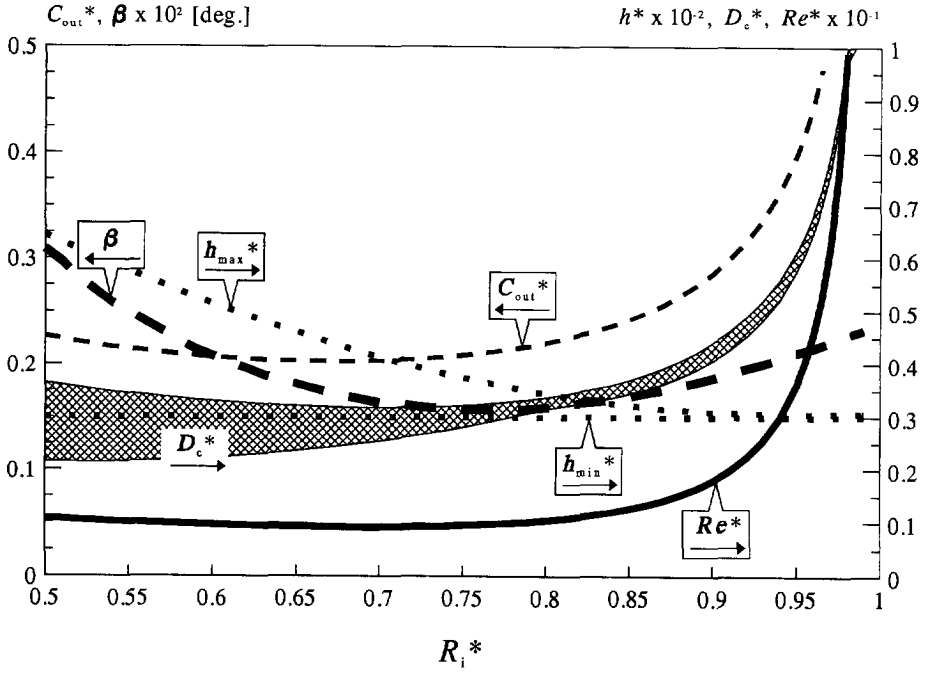

Figure (E-4) Curved plates. β=variable, h_{min}^*=0.003.

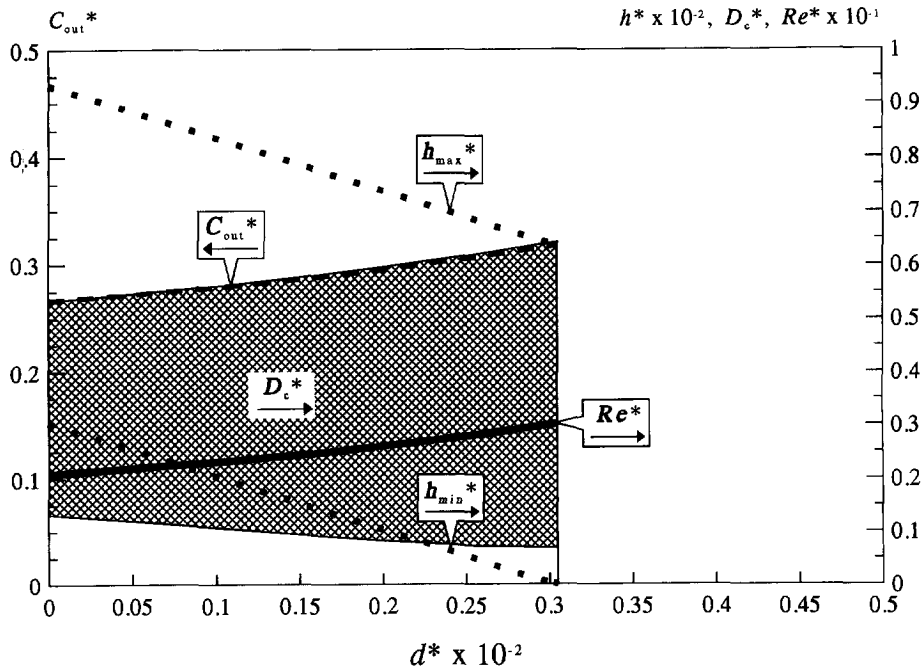

Figure (E-5) Flat plates. β=20 degrees, h_{min}*=variable.

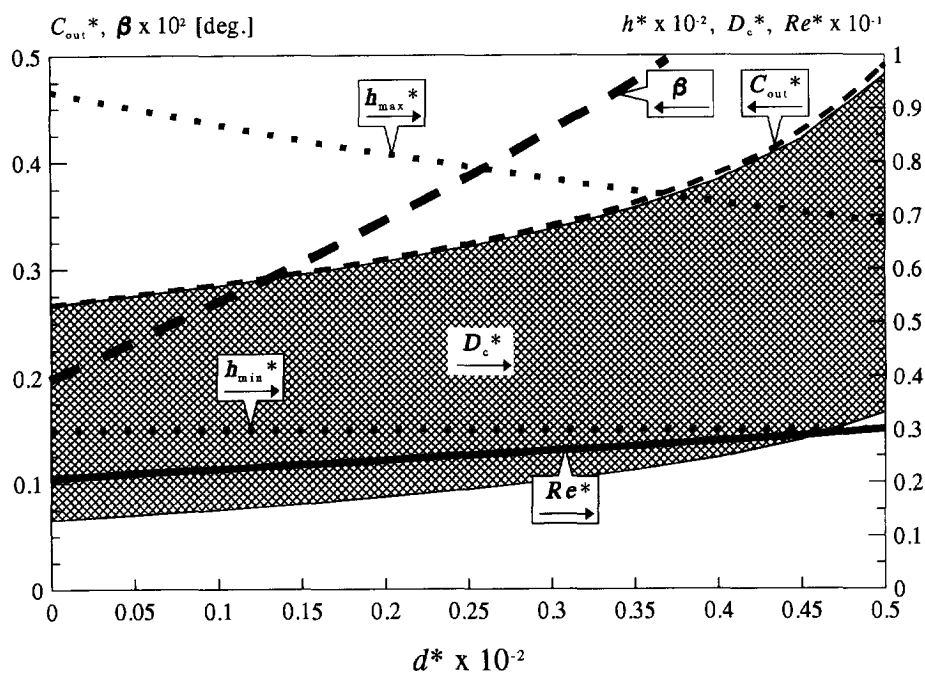

Figure (E-6) Flat plates. β=variable, h_{min}*=0.003.

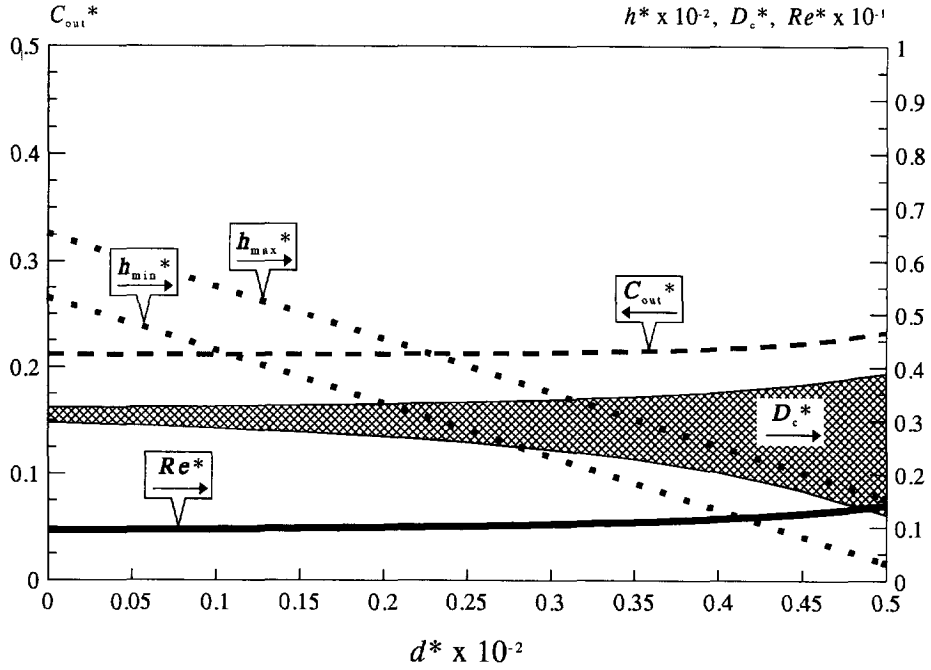

Figure (E-7) Curved plates. β=20 degrees, h_{min}^*=variable.

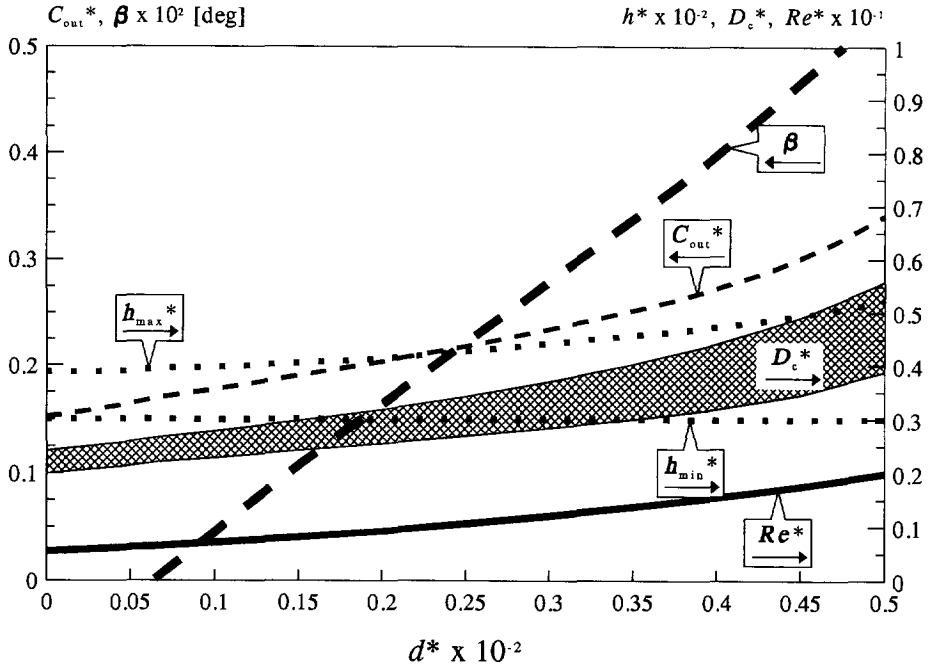

Figure (E-8) Curved plates. β=variable, h_{min}^*=0.003.

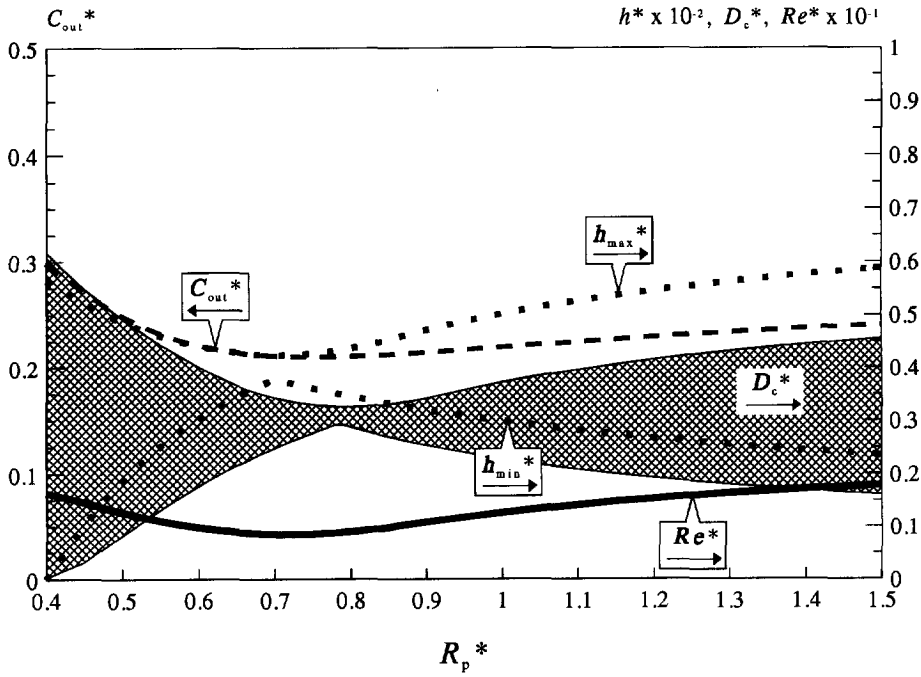

Figure (E-9) Curved plates. β=20 degrees, h_{min}^*=variable.

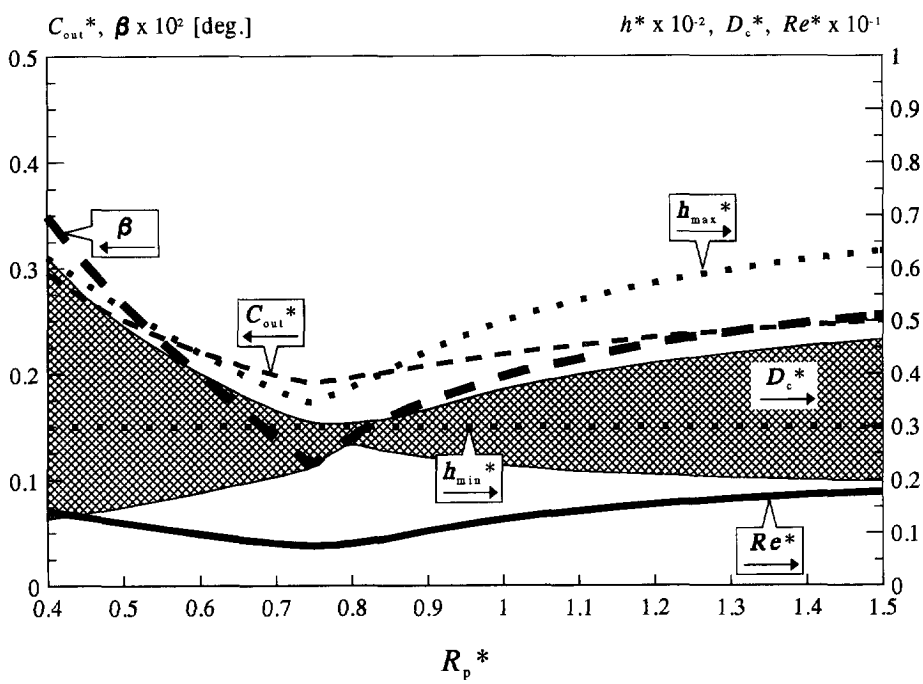

Figure (E-10) Curved plates. β=variable, h_{min}^*=0.003.

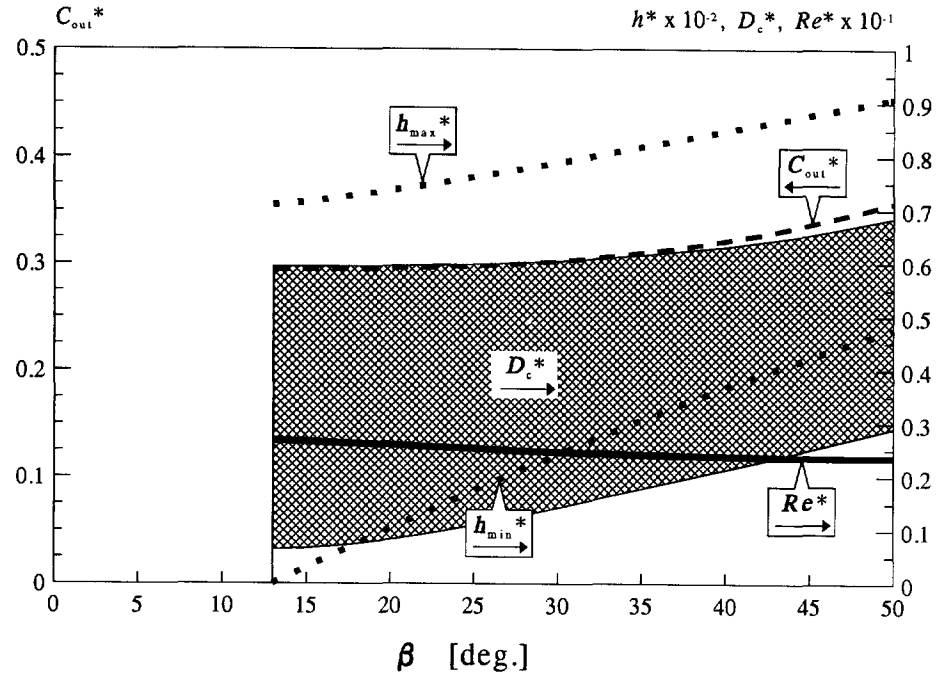

Figure (E-11) Flat plates.

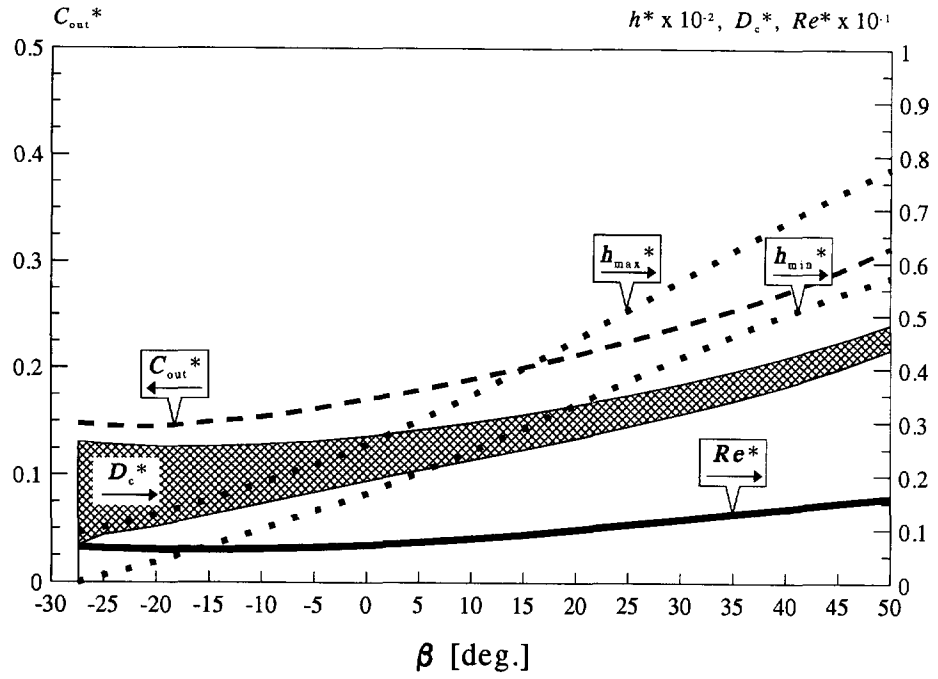

Figure (E-12) Curved plates.

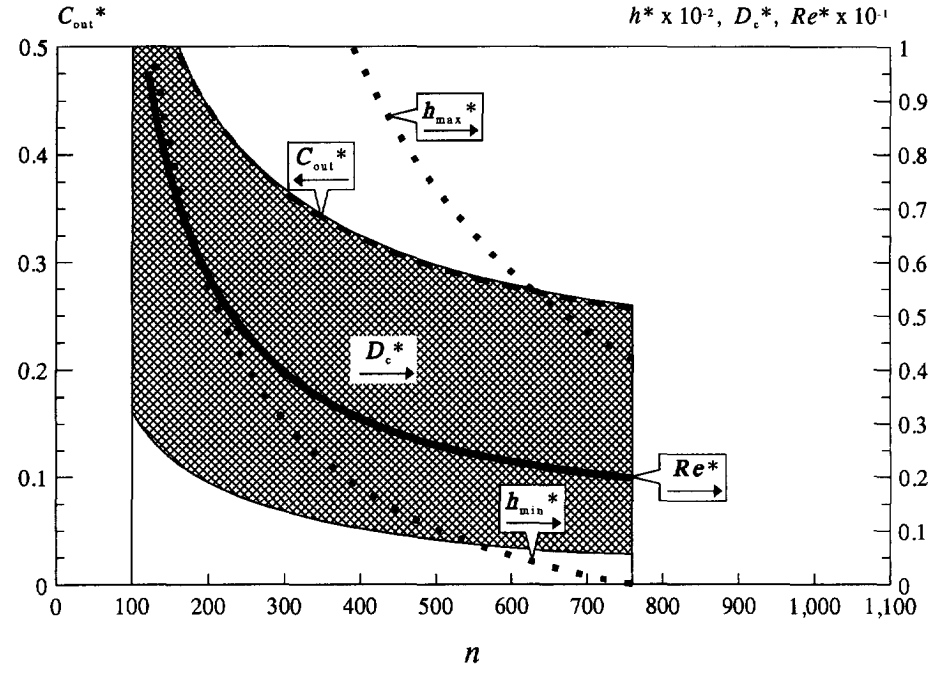

Figure (E-13) Flat plates. β=20 degrees, h_{min}^*=variable.

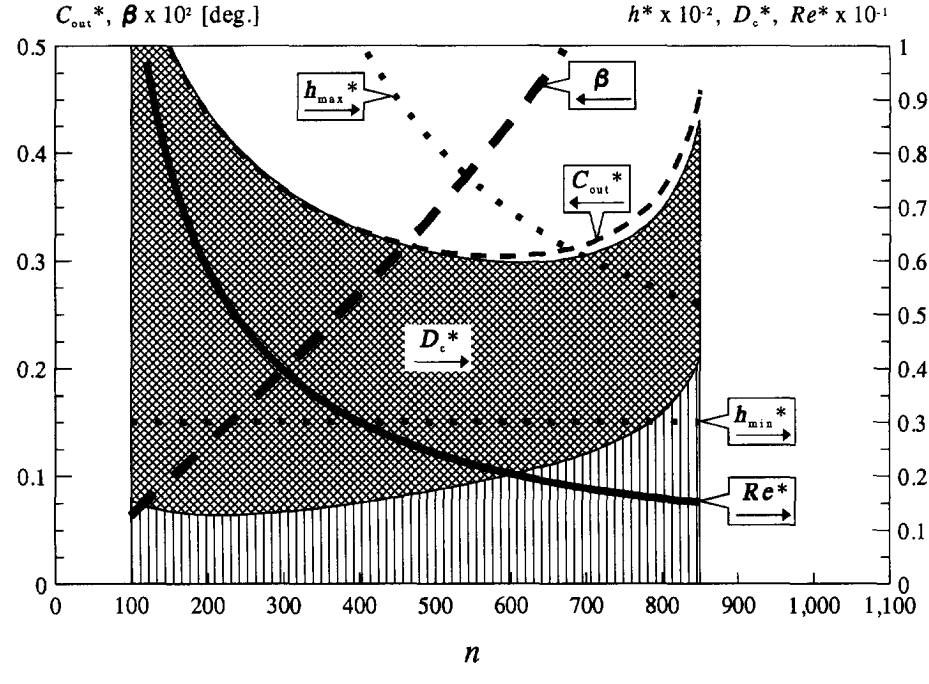

Figure (E-14) Flat plates. β=variable, h_{min}^*=0.003.

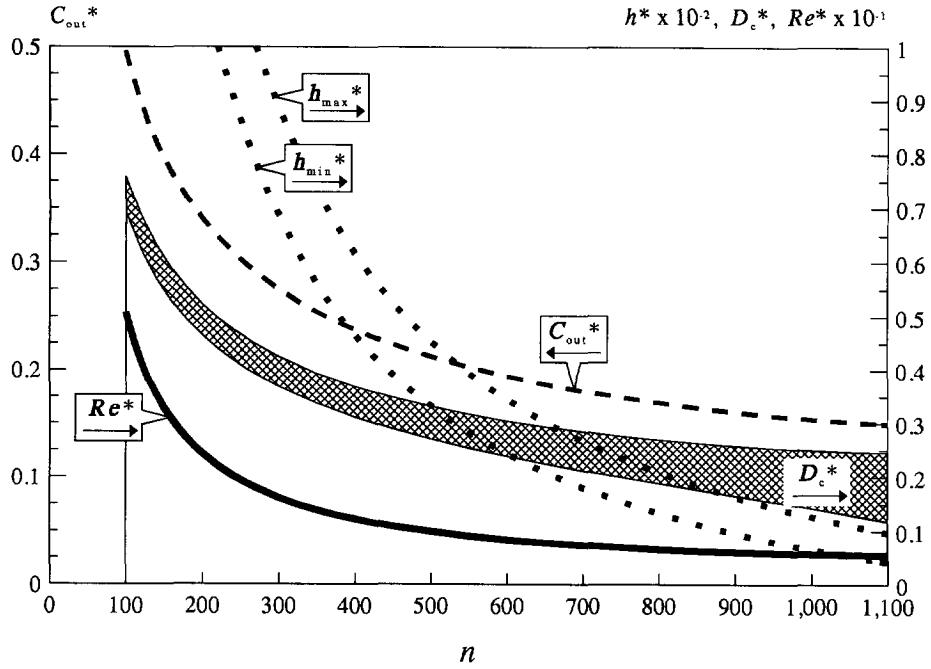

Figure (E-15) Curved plates. β=20 degrees, h_{min}^*=variable.

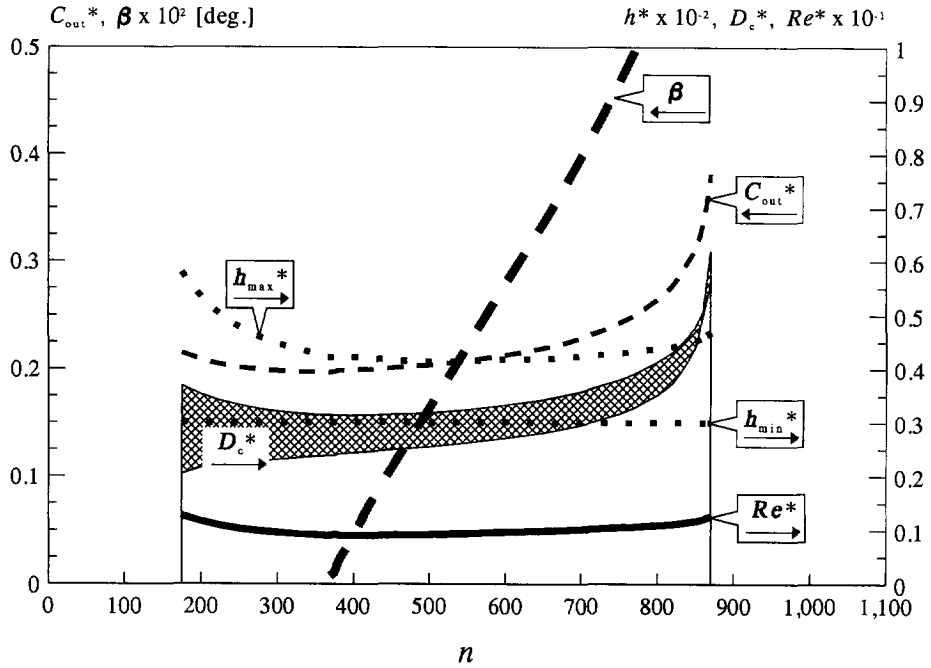

Figure (E-16) Curved plates. β=variable, h_{min}^*=0.003.

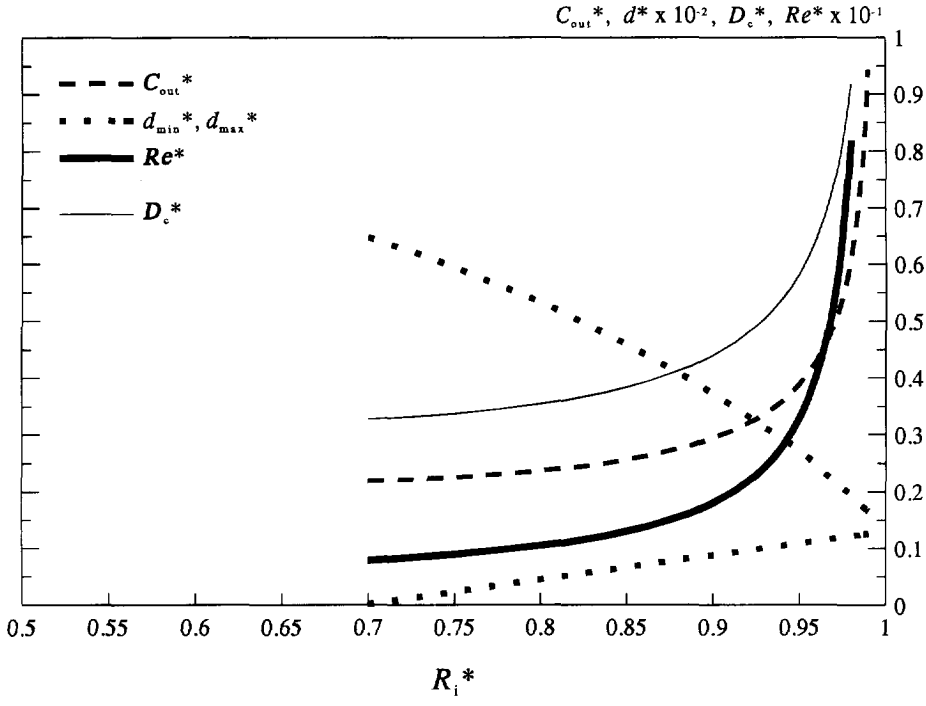

Figure (E-17) Flat channels. β=20 degrees, d_{min}^*=variable.

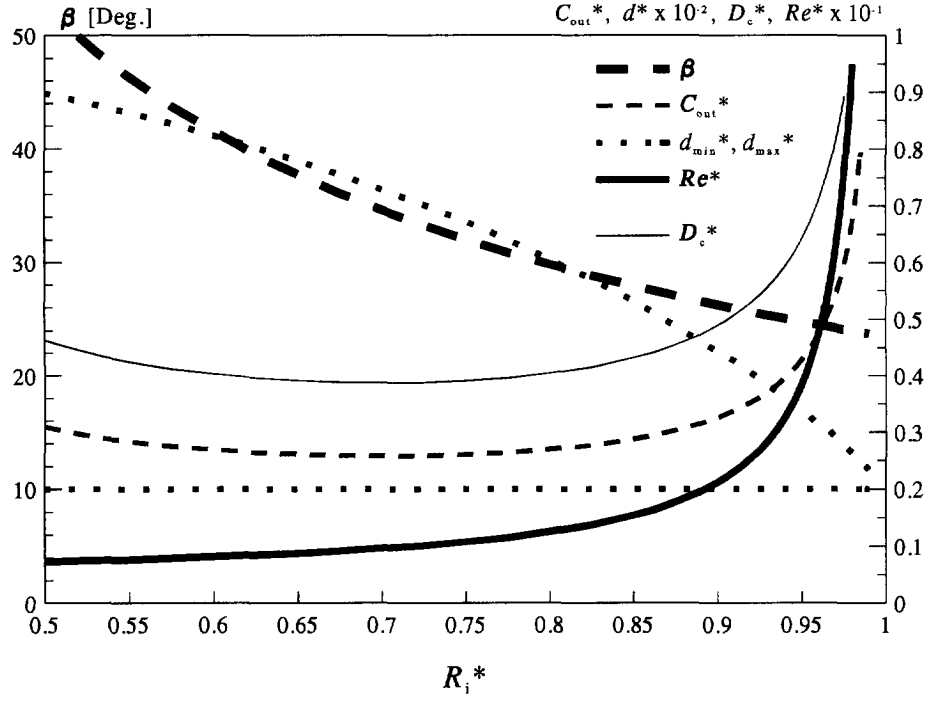

Figure (E-18) Flat channels. β=variable, d_{min}^*=0.003.

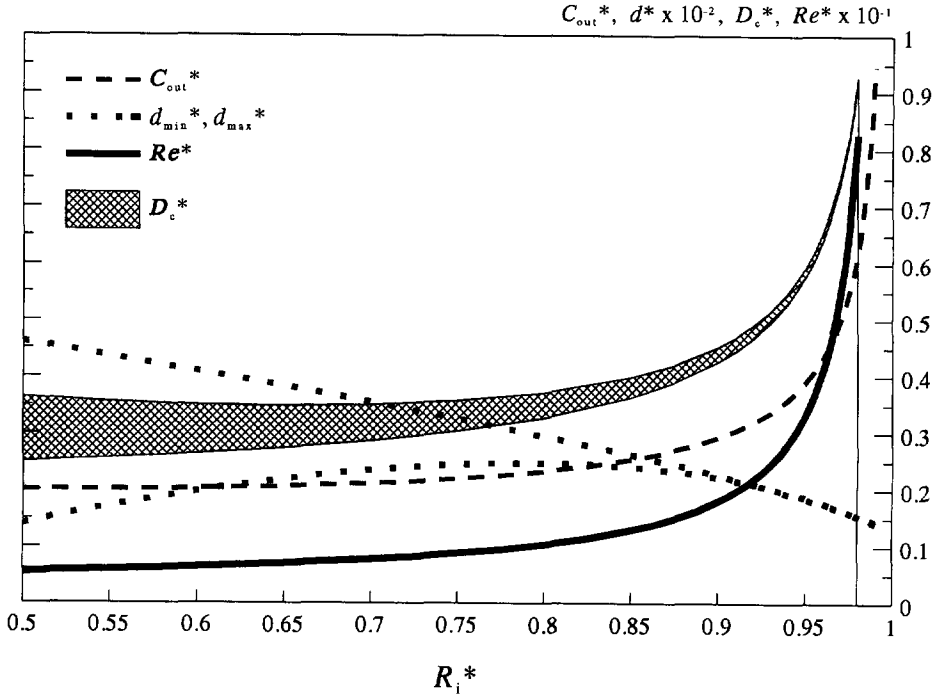

Figure (E-19) Curved channels. β=20 degrees, d_{min}^*=variable.

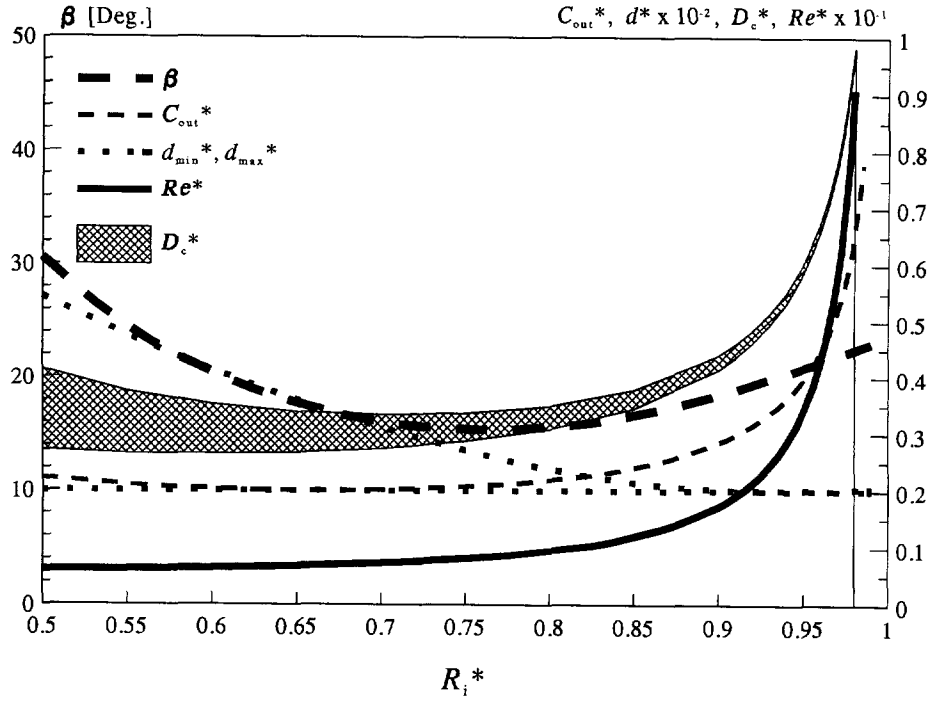

Figure (E-20) Curved channels. β=variable, d_{min}^*=0.003.

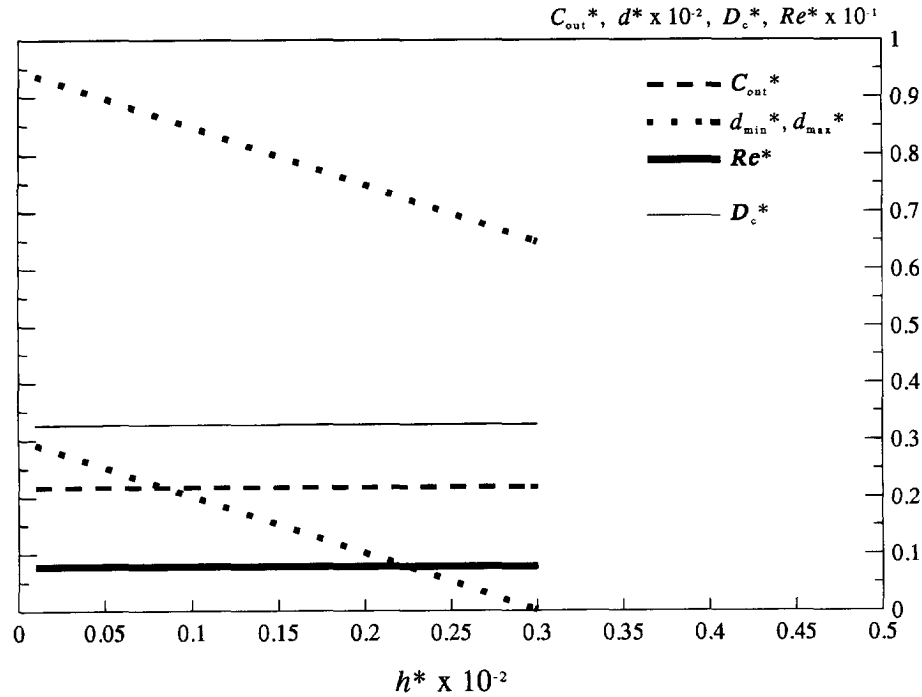

Figure (E-21) Flat channels. β=20 degrees, d_{min}^*=variable.

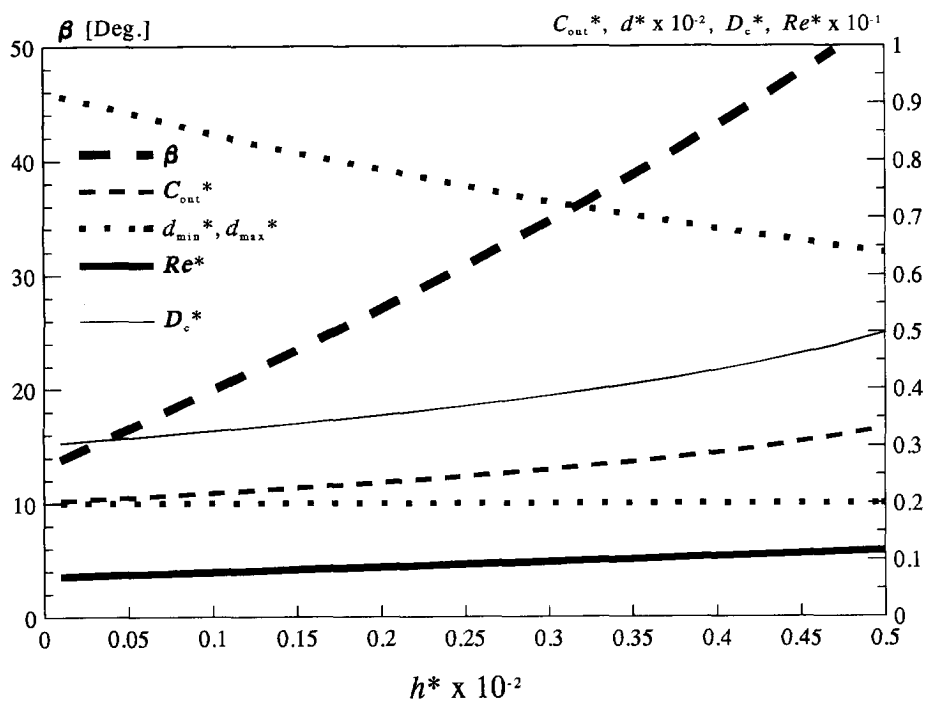

Figure (E-22) Flat channels. β=variable, d_{min}^*=0.003.

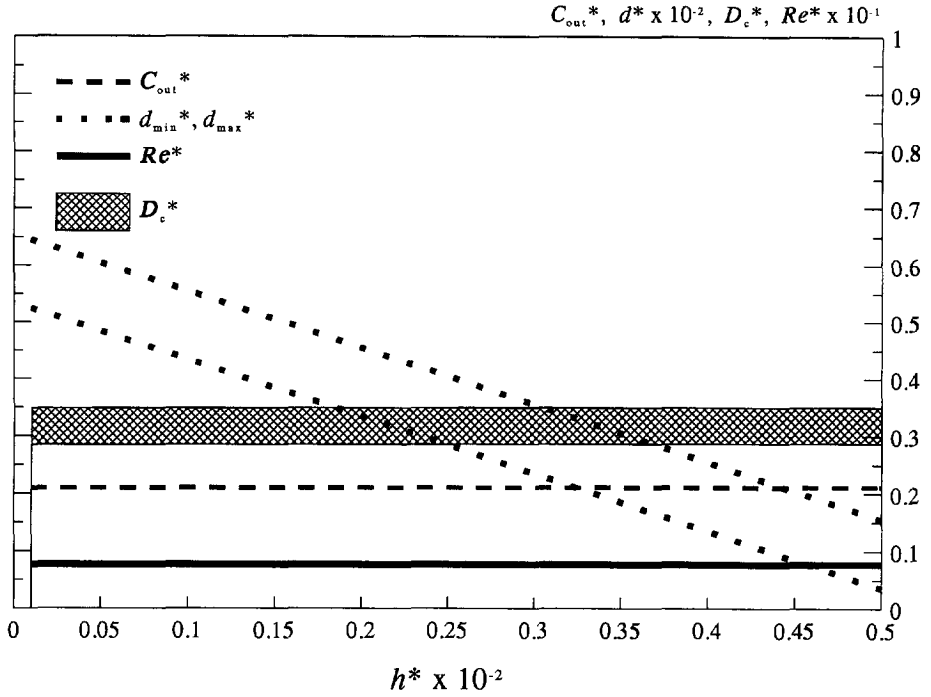

Figure (E-23) Curved channels. β=20 degrees, d_{min}^*=variable.

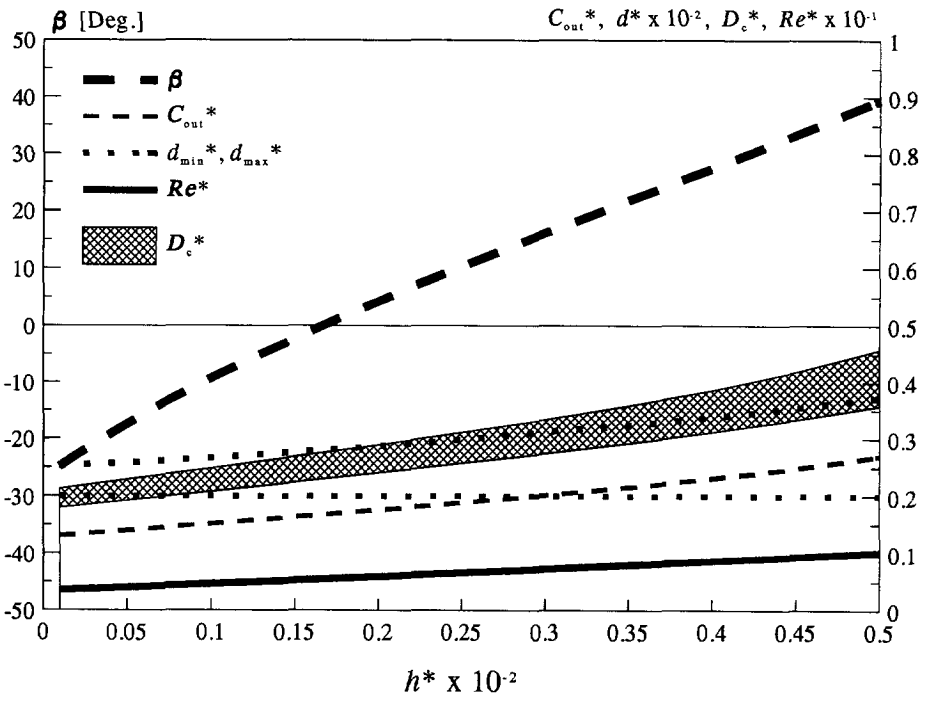

Figure (E-24) Curved channels. β=variable, d_{min}^*=0.003.

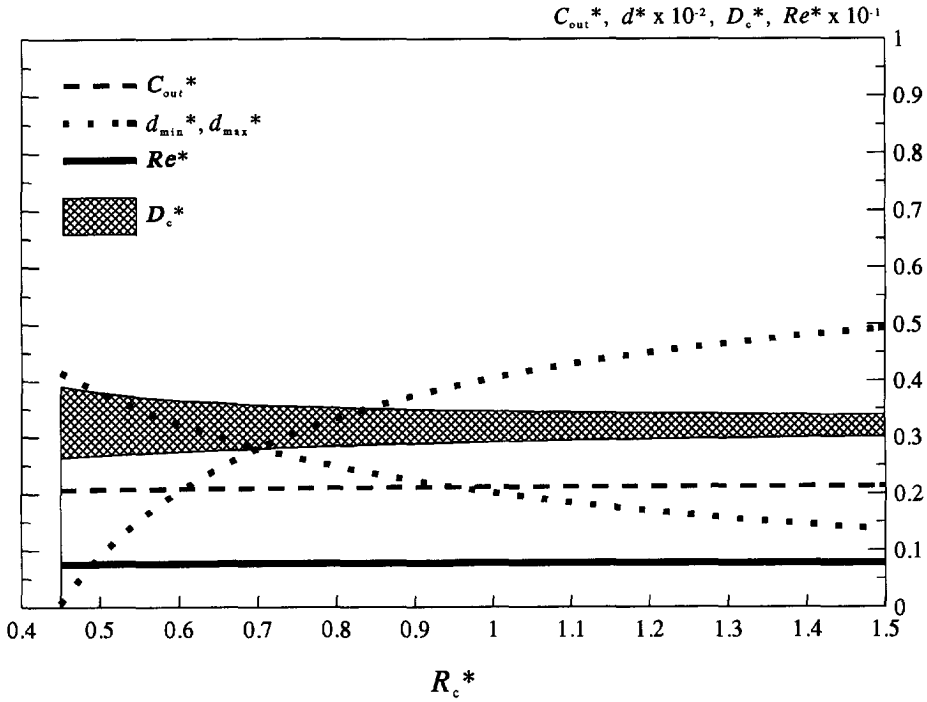

Figure (E-25) Curved channels. β=20 degrees, d_{min}*=variable.

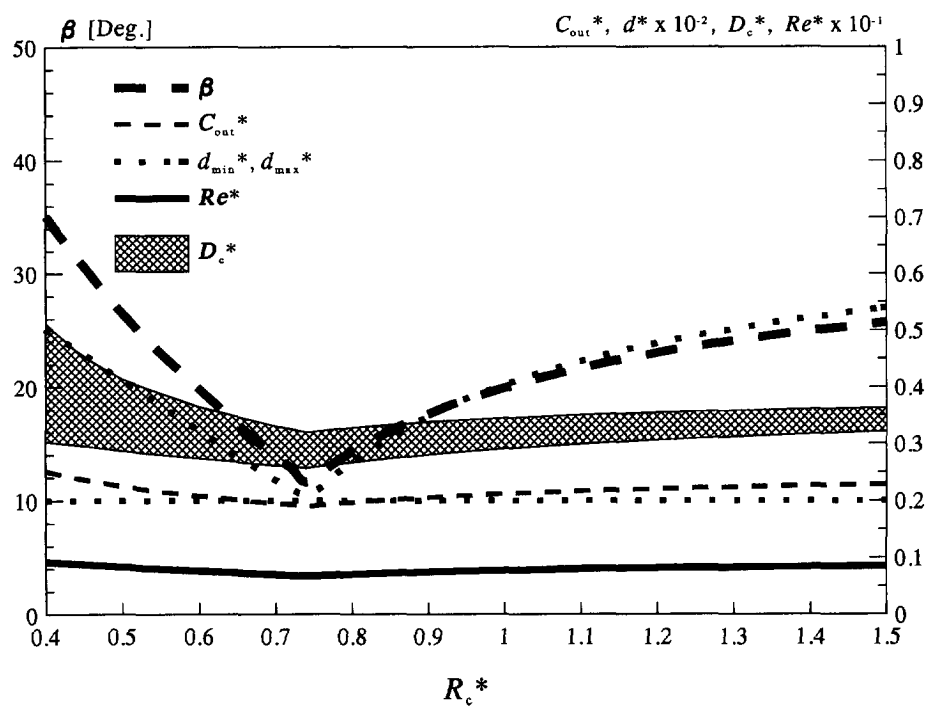

Figure (E-26) Curved channels. β=variable, d_{min}*=0.003.

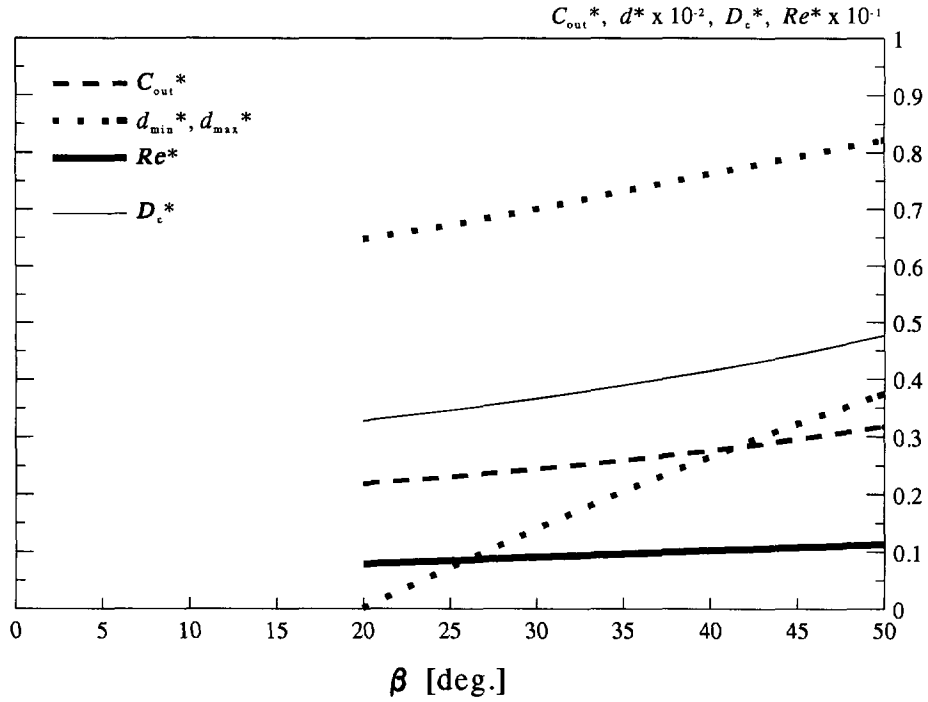

Figure (E-27) Flat channels.

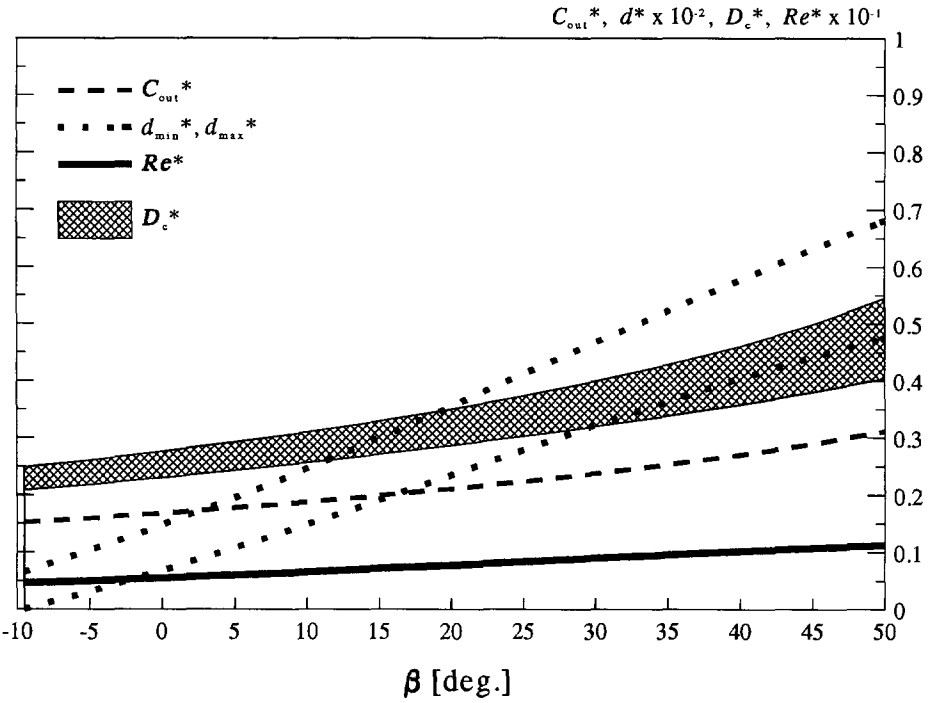

Figure (E-28) Curved channels.

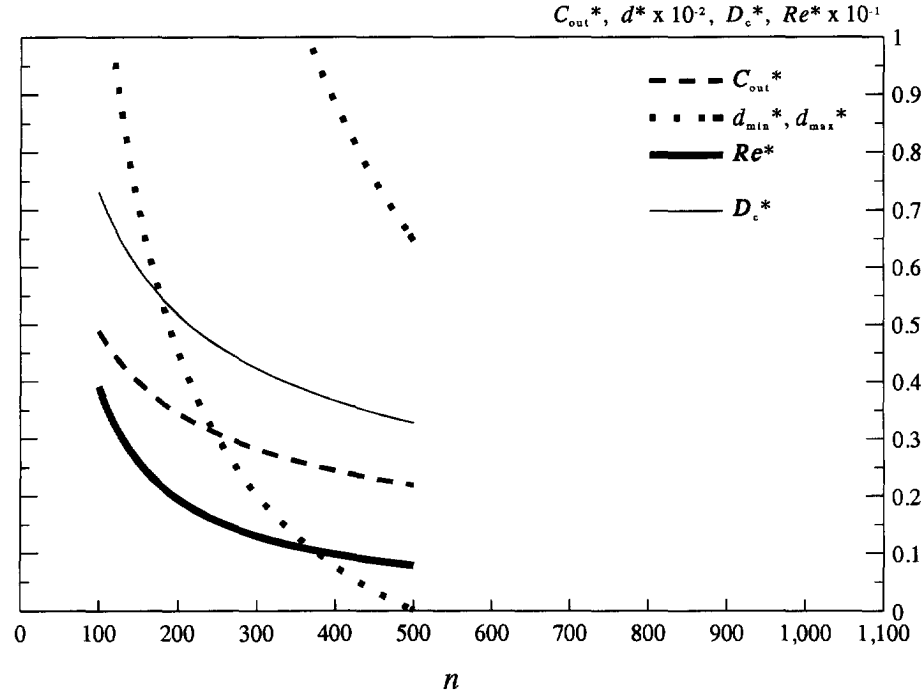

Figure (E-29) Flat channels. β=20 degrees, d_{min}^*=variable.

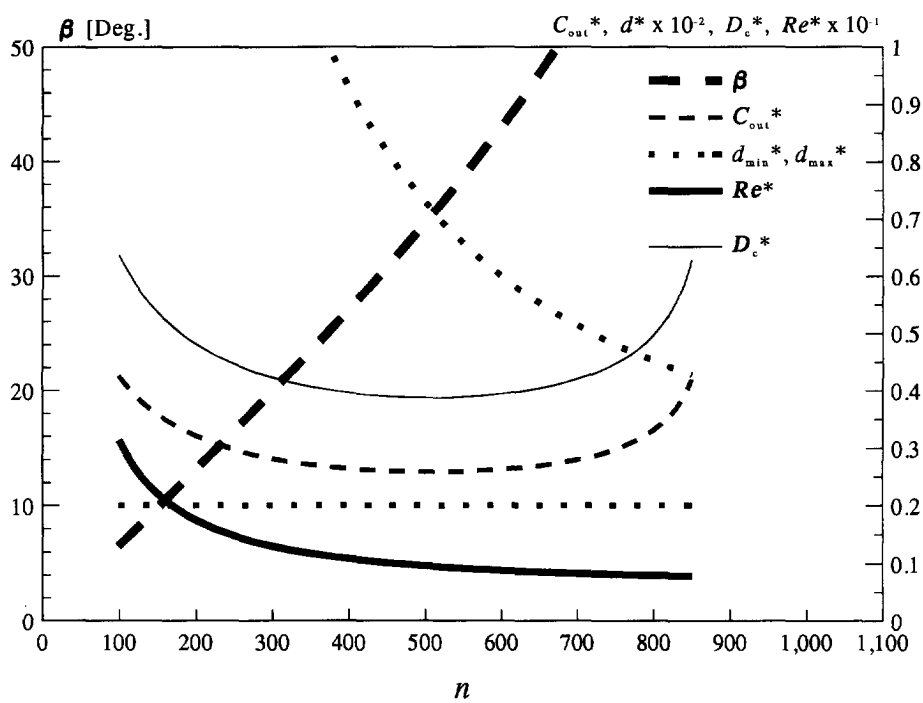

Figure (E-30) Flat channels. β=variable, d_{min}^*=0.003.

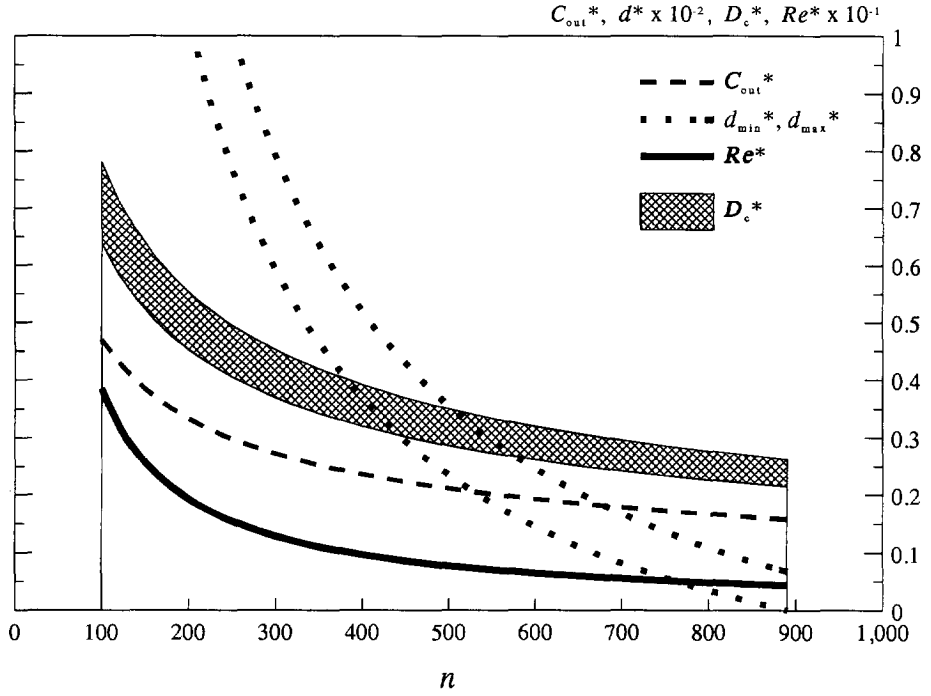

Figure (E-31) Curved channels. β=20 degrees, d_{min}^*=variable.

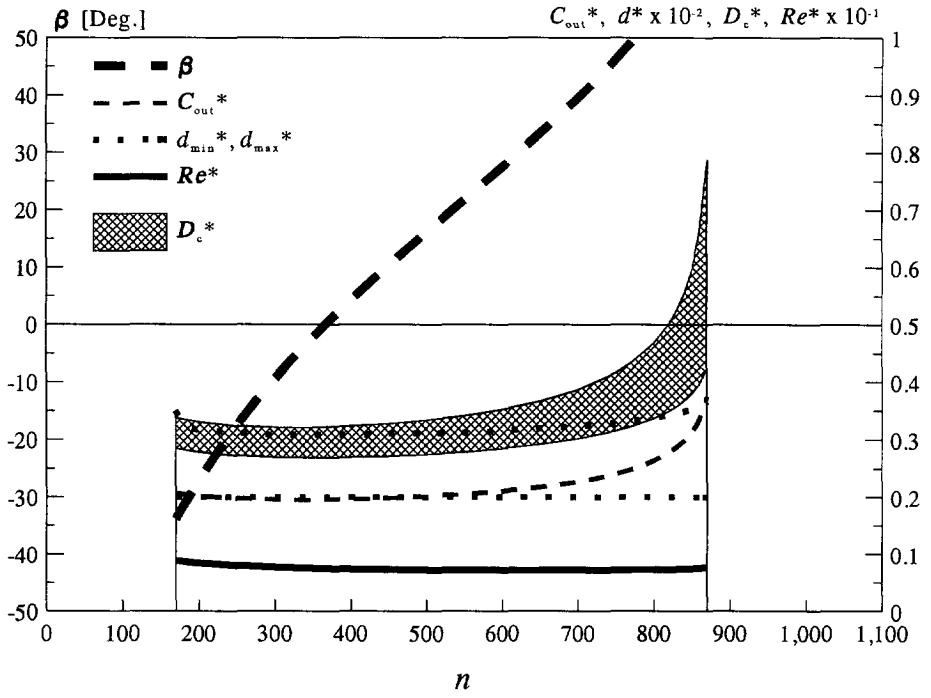

Figure (E-32) Curved channels. β=variable, d_{min}^*=0.003.

List of symbols

a	acceleration	[m/s^2]
A	amplitude of a cyclic function	[m]
C	constant	[m^{-1}s^{-1}]
C_D	oil concentration distribution constant	[ppm/m]
$C_{in,cum}$	cumulative oil concentration of the influx	[ppm]
C_{out}	total oil concentration of the water effluent	[ppm]
C_1	experimentally determined constant	[-]
d	plate thickness	[m]
D	droplet diameter	[m]
D_c	critical droplet diameter	[m]
$D_{c,M}$	measured critical droplet diameter	[m]
D_e	volume-equivalent diameter $(6V/\pi)^{1/3}$	[m]
D_h	hydraulic diameter	[m]
D_i	diameter of impeller	[m]
D_{max}	maximum stable droplet diameter	[m]
D_{90}	oil droplet diameter for which is valid: 90 volume % of the oil consists of droplets with a diameter smaller than D_{90}	[m]
e	energy dissipation per unit mass	[W/kg]
Eo	Eötvös number	[-]
F_b	buoyant force	[N]
F_{cor}	Coriolis force	[N]
F_L	lift force	[N]
F_S	drag force	[N]
g	acceleration of gravity	[m/s^2]
G	g-factor $(\omega^2 r)/g$	[-]
G_S	shear rate (flow-velocity gradient)	[s^{-1}]
h_θ	vertical plate distance	[m]
h	plate distance	[m]
h_{av}	average plate distance	[m]
h_0	thickness of film when droplet initially comes to rest	[m]
h_R	thickness of film the moment it ruptures	[m]
H	height of plate pack	[m]
k	number of sections	[-]
k	Boltzmann constant ($\approx 1.38 \cdot 10^{-23}$)	[J/K]
l	travelled distance (in x-direction)	[m]
L	length of plate (pack)	[m]
m	mass	[kg]
M	Morton number	[-]
n	number of channels	[-]
N	impeller speed	[rev/s]
q	average travelled distance	[m]
Q	oily-water flow rate	[m^3/s]

$Q_{k;a\Phi b}$	flow rate in section number k between height **a** and **b**	[m³/s]
r,R	radius	[m]
R_c	radius of channel curvature	[m]
R_i	inner radius	[m]
R_o	outer radius	[m]
R_p	radius of plate curvature	[m]
Re	Reynolds number	[-]
Re_{Gs}	shear Reynolds number	[-]
s	travelled distance	[m]
t	time	[s]
t_c	coalescence time	[s]
t_r	residence time	[s]
T	temperature	[K]
v	velocity	[m/s]
v_{cor}	terminal Coriolis velocity	[m/s]
v_f	average flow velocity	[m/s]
v_F	local flow velocity	[m/s]
v_R	velocity relative to the fluid velocity v_F	[m/s]
v_S	droplet velocity due to the fluid velocity v_F	[m/s]
v_t	terminal velocity	[m/s]
v_{tr}	terminal radial velocity	[m/s]
v_x	flow velocity (x-direction)	[m/s]
v_y	flow velocity (y-dir.) caused by variation of the flow profile	[m/s]
v_Y	flow velocity (y-dir.) caused by γ	[m/s]
$\overline{v_{x,a-b}}$	average velocity from $y=a$ to $y=b$	[m/s]
v_∞	flow velocity outside the boundary layer	[m/s]
V	volume	[m³]
W	width of the plate pack	[m]
We_i	impeller Weber number	[-]
x,y,z	coordinates	[m]
x	position in horizontal direction	[m]
x_e	end of transition zone	[m]
x_s	beginning of transition zone	[m]
y	position in vertical direction (y=0 at lower plate surface)	[m]
Y	position in vertical direction (Y=0 at flat horizontal surface crossing the lowest point(s) of the lower plate)	[m]

Greek symbols:

α	cone angle	[rad]
β	plate angle	[rad]
γ	local angle of inclination of the plate	[rad]
δ	thickness of the boundary layer	[m]
ϵ	deviation factor	[-]

η	separation efficiency	[-]
θ	tilt angle	[rad]
λ	wavelength	[m]
Λ	distance from where t_c is measured	[m]
μ	dynamic viscosity (of continuous phase)	[Ns/m^2]
ξ	system constant	[m^{-1}s^{-1}]
ρ	density (of continuous phase)	[kg/m^3]
ρ_w	density of water	[kg/m^3]
ρ_o	density of oil	[kg/m^3]
σ	interfacial tension	[N/m]
ϕ	angle between two consecutive plates	[rad]
ψ	angle [of space coordinate (r,ψ)]	[rad]
ω,Ω	angular velocity (centrifuge, droplet)	[rad/s]

Subscripts:

$_{max}$	maximal
$_{min}$	minimal

Superscripts:

^{ref}	reference
*	specific

Abbreviations:

CPS	centrifugal plate separator
DSC	disc stacked centrifuge
FP	flow profile
GPS	gravity plate separator
LDA	laser doppler anemometer
LPS	laser-diffraction particle sizer
PCC	parallel channel centrifuge
PPC	parallel plate centrifuge

Summary

After some stages of treatment, most production water and other oily waste water is discharged into the sea or onto other surface water. To protect the environment, the total amount of oil discharged must be kept to a minimum. Legislation with regard to the discharge of oil into the sea is being pursued in an international context. One of these is the Paris Convention, covering regulations for discharges from both offshore and onshore operations in and around the North Sea; a limit of 40 ppm monthly average has been agreed.

Concerning gravity and centrifugal separators, theoretical studies have been carried out with respect to oil-droplet shape, forces acting on oil droplets and interaction of oil droplets with oil-water interfaces. For these types of separators, oil-droplet diameters within the critical range may be assumed to be rigid spheres; Stokes' law is valid. A generally applicable separation efficiency function has been derived analytically, which is valid for gravity separators as well as centrifuges. Computer simulations and laboratory experiments support the predictions of this function.

Gravity plate separators are among the most frequently applied separator types in the oil-industry. The gravity plate separator is relatively cheap compared to other types of separators, but it is heavy and bulky and cannot always reach the target effluent oil concentration of 40 ppm. A number of different plate shapes are available, from simply flat to complicated corrugated designs. Theoretical and experimental research demonstrates that a pack of corrugated plates does not give a better performance than a comparable pack of flat plates. Corrugated plates may promote coalescence of oil droplets due to flow velocity fluctuations. Coalescence will only occur when the oil droplets are close together; thus, when the oil concentration exceeds a certain value.

The centrifuge is one of the best separators. It can meet the Paris Convention requirements and gives good performance in relation to required deck space and weight. The main disadvantage of the centrifuge is its high cost.

Centrifuges are usually provided with internals. These internals have the same function as the plate packs in a gravity plate separator and consist in most cases of a stack of conical discs. Investigations on gravity plate separators prompted the idea for the development of an analogous plate pack for rotating separators. The plates are installed parallel to the axis of rotation, like fan blades, and can be either flat or curved. There are two basic configurations: the Parallel Plate Centrifuge with plates of uniform thickness, and the Parallel Channel Centrifuge with uniform distance between the plates.

The theoretical model of these centrifuges gives a satisfactory prediction of the critical droplet diameter as well as of the separation efficiency as a function of the oil droplet diameter. The simulation program -based on this model- is a valuable tool for design purposes. It shows one optimum configuration for each of four plate pack types considered. For both types the optimum configurations with curved plates or channels is twice as

effective as the optimum configurations with flat plates or straight channels.

Comparison of the plate centrifuges and the disc stacked centrifuge shows that the latter has a different response to flow-rate changes. Plate centrifuges show a practically unlimited operating range with respect to flow rate, while disc stacked centrifuges features a relatively restricted tolerance for flow rate variations, lest water comes out of the oil outlet or the separation efficiency decreases excessively. Models which are provided with a system to regulate the outlet pressure (back pressure) can handle a wider flow rate range.

Samenvatting

Na het doorlopen van één of meerdere scheiders wordt het meeste produktiewater en ander oliehoudend afvalwater geloosd in zee of op oppervlaktewater. De hoeveelheid olie die geloosd wordt, moet tot een minimum beperkt worden om aantasting van het milieu zoveel mogelijk te beperken. De wetgeving aangaande olielozingen wordt geregeld op internationaal niveau. De Conventie van Parijs restringeert de maximale olieconcentratie van het te lozen water tot 40 ppm. Deze limiet geldt voor mijnbouwinstallaties op de Noordzee en in de landen rond de Noordzee.

Met betrekking tot zwaartekracht- en centrifugaalscheiders is theoretisch onderzoek verricht naar de vorm van de oliedruppel, de krachten die op oliedruppels werken en de interactie van een oliedruppel met een olie-watergrensvlak. In beide soorten scheiders gedraagt de oliedruppel zich als een star bolletje, waarvoor de wet van Stokes geldt. Een algemeen toepasbare vergelijking is analytisch afgeleid. Met deze vergelijking kan het scheidingsrendement worden bepaald voor iedere oliedruppeldiameter kleiner dan de kritische diameter. Computersimulaties en laboratoriumexperimenten bevestigen de validiteit van deze algemene vergelijking.

De gravitatie-plaatscheider is de meest gebruikte scheider in de olie-industrie. Hij is goedkoop in vergelijking met andere soorten. Hij is echter erg groot en zwaar en niet altijd in staat voldoende olie af te scheiden om de 40 ppm-norm voor het behandelde water te bereiken. Voor deze scheider zijn al vele plaatvormen beschikbaar, van eenvoudige rechte platen tot gecompliceerde golfvormen. Theoretisch en experimenteel onderzoek heeft aangetoond dat de golfvorm niet van invloed is op het scheidingsrendement. Stromingsfluctuaties die optreden bij het gebruik van gegolfde platen, kunnen coalescentie van oliedruppels bevorderen, wat in een verbeterd scheidingsrendement resulteert. Dit fenomeen kan alleen in voldoende mate optreden als de gemiddelde afstand tussen de oliedruppels klein genoeg is, d.w.z. als de olieconcentratie hoog genoeg is.

De centrifuge is één van de betere scheiders. De 40 ppm norm wordt hiermee gemakkelijk gehaald en hij geeft goede prestaties in verhouding tot grootte en gewicht. Een bezwaar is echter de hoge kostprijs.

Centrifuges zijn intern veelal voorzien van een platenpakket. Dit pakket heeft dezelfde functie als het platenpakket in een gravitatie-plaatscheider en bestaat in de meeste gevallen uit kegelvormige schotels. Dit type staat bekend als de schotelcentrifuge (Eng: disc stacked centrifuge). Onderzoek aan platenpakketten voor de gravitatie-plaatscheider leidde tot de ontwikkeling van een analoog platenpakket voor een centrifuge: de centrifugaal-plaatscheider. Hierin zijn de platen als de schoepbladen van een centrifugaalpomp parallel aan de as van rotatie gemonteerd. De platen kunnen recht of gebogen zijn. Er zijn twee soorten pakketten te onderscheiden: de parallelle platen centrifuge met platen van gelijke dikte en de parallelle kanalen centrifuge met uniforme kanaalbreedte.

Het theoretisch model van de centrifugaal-plaatscheider geeft een goed beeld van het te verwachten scheidingsrendement als functie van de druppelgrootte. Het op het model gebaseerde computersimulatie programma is een waardevol instrument voor het maken van ontwerpen. Dit programma kan iedere mogelijke configuratie doorrekenen en is in staat een configuratie te bepalen waarbij het hoogste scheidingsrendement wordt behaald. Deze optimum configuratie is bepaald voor beide types centrifugaal-plaatscheiders, voor zowel rechte als gebogen platen, waarbij voor de laatste ook de optimale kromtestraal wordt bepaald. Voor beide soorten is het scheidingsrendement van de optimum configuratie met gebogen platen ongeveer twee maal beter dan die met rechte platen.

Vergelijking van de centrifugaal-plaatscheider met de schotelcentrifuge laat zien dat laatstgenoemde een ander gedrag vertoont ten aanzien van debietfluctuaties. De centrifugaal-plaatscheider heeft een vrijwel onbeperkt debietbereik, terwijl bij de schotelcentrifuge een verandering in debiet een snel dalend rendement tot gevolg heeft of resulteert in een ongewenste waterstroom door de olie-uitlaat. Uitvoeringen van de schotelcentrifuge waarbij de druk in de uitlaten geregeld kan worden, hebben evenwel een aanzienlijk verbeterd debietbereik.

Nawoord

Dit proefschrift is zeker niet de verdienste van één persoon. Vele discussies heb ik gevoerd met mijn begeleider en toegevoegd promotor Dr.ir. W.M.G.T van den Broek, die ik veel dank verschuldigd ben voor de vele nuttige suggesties en voor het vrijmaken van tijd om alle versies van dit proefschrift te lezen en van kritische opmerkingen te voorzien.

Zeer erkentelijk ben ik mijn beide promotoren Prof.ir. J.J. van der Vuurst de Vries en Prof.dr.ir. J. de Graauw, aan wie de duidelijkheid van dit proefschrift voor een belangrijk deel te danken is.

Ir. J.C. van Muiswinkel, Peter Sänger en Marc Hettema waren bereid de afleidingen en berekeningen in dit proefschrift te verifiëren.

Het uiteindelijke onderzoekswerk is verricht in samenwerking met de technische staf van het Dietz Laboratorium. Met name Bert Meijer, Gerard Sigon, Henny van der Meulen en Jan Steiger hebben zich ingezet bij het opbouwen van de verschillende proefopstellingen. Andre Hoving, als tekenaar-constructeur, wist al mijn ambitieuze ideeën te vertalen naar een werkbaar en betaalbaar ontwerp.

Peter Holtkamp en de medewerkers van de Alfa Laval/ Oilfield Division hebben het mogelijk gemaakt dat het werk een industriële dimensie kreeg. Enerzijds door een centrifuge met alle randapparatuur voor het onderzoek ter beschikking te stellen, anderzijds door mij in de gelegenheid te stellen metingen in het veld uit te voeren en congressen en onderzoekscentra te bezoeken.

Ook het ter beschikking stellen van twee plaatscheiders door Frits Koene van Burgess-Manning Europe heeft mij in staat gesteld een deel van het onderzoek te verrichten.

De afstudeerders Martijn Groenendijk, Izaak Dekker, Yvonne van den Berg, Marc Martens, Jan Robert Huisman, Edgar van Asperen, Berend Jan Potter, Eric Ham en Kolya Natakusuma hebben met hun werk en enthousiasme bijgedragen aan het onderzoek.

Paul van Lingen heeft zich ingezet bij het streven naar een errata-vrij proefschrift.

Alle genoemde, en niet genoemde personen die aan dit werk hebben bijgedragen, dank ik van harte.

Curriculum vitae

19 april 1960 geboren te Bergen op Zoom

1977	Diploma MAVO Rijksscholengemeenschap, Harderwijk
1980	Diploma HAVO Norbertus college, Roosendaal
1986	Diploma leraar Natuurkunde en Wiskunde (2e graad) Nieuwe lerarenopleiding "Mollerinstituut", Tilburg
1989	Diploma Petroleum- en gastechnologie Hogeschool voor Petroleum- en gastechnologie "Noorderhaaks", Den Helder
1988 - 1994	Promotieonderzoek in de petroleumwinning: Technische Universiteit Delft, Faculteit der Mijnbouwkunde en Petroleumwinning